

Cyclic Polyolefins via Ring-Expansion Metathesis Polymerization

Thesis by
Julian Peter Edwards

In Partial Fulfillment of the Requirements
for the Degree of
Doctor of Philosophy

CALIFORNIA INSTITUTE OF TECHNOLOGY

Pasadena, California

2018

(Defended 4 May 2018)

dedicated to my family and friends, to whom I owe everything

Abstract

Chapter 1 introduces cyclic polymers and olefin metathesis. Synthetic methods for cyclic polymer synthesis, and methods for the determination of cyclic polymer purity are also discussed.

Chapter 2 describes previous efforts in our group towards cyclic polymers via ring-expansion metathesis polymerization and highlights its deficiencies. A new catalyst design is proposed to rectify these deficiencies, and its synthesis is reported.

Chapter 3 recalls early efforts to produce cyclic polymers via ring-expansion metathesis polymerization using a supported molecular cyclic catalyst. The topological purity of cyclic poly(cyclopentene) is established using interaction chromatography.

Chapter 4 expands ring-expansion metathesis polymerization methodology to provide for the large scale synthesis of cyclic polybutadiene, an important commercial material. Interaction chromatography is used to verify its highly pure cyclic topology, and an unexpected *cis*-selective property of our supported cyclic polymer catalysts is reported.

Chapter 5 details efforts to understand the selectivity in the ring-expansion metathesis polymerization of cyclododecatriene and cyclooctadiene. Progress towards controlling the molecular weight and *cis/trans* isomerism of cyclic polybutadiene is discussed.

Table of Contents

Abstract		iv
Table of Contents		v
Chapter 1	<i>Introduction</i>	1
	Cyclic Polymers	2
	Synthetic Strategies for Cyclic Polymers	4
	Determining Cyclic Polymer Purity	7
	Olefin Metathesis	8
	References	15
Chapter 2	<i>Design and Synthesis of Supported Molecular REMP Catalysts</i>	16
	Abstract	17
	Introduction	18
	Results and Discussion	23
	Conclusions and Future Outlook	30
	Experimental	31
	References	60
Chapter 3	<i>Initial Investigations with Supported Molecular REMP Catalysts</i>	61
	Abstract	62
	Introduction	63
	Results and Discussion	65
	Conclusions and Future Outlook	78
	Experimental	79
	References	84
Chapter 4	<i>Large-Scale Cyclic Polybutadiene Synthesis</i>	85
	Abstract	86
	Introduction	87
	Results and Discussion	89
	Conclusions and Future Outlook	103
	Experimental	104
	References	106
Chapter 5	<i>Selectivity in Cyclic Polybutadiene Synthesis</i>	107
	Abstract	108
	Introduction	109
	Results and Discussion	111
	Conclusions and Future Outlook	141
	Experimental	142
	References	144
Appendix 1	<i>Spectra Relevant to Chapter 2</i>	145
Appendix 2	<i>ICP-MS Characterization of REMP Catalysts</i>	165

Chapter 1

Introduction to Cyclic Polymers and Olefin Metathesis

Cyclic Polymers

Cyclic polymers have drawn considerable interest for their distinct physical properties relative to analogous linear polymers, despite their equivalent chemistries. This divergence in material properties originates entirely from their divergent topologies. The mobility of chain-ends in linear polymers determines their propensity for chain-entanglement, whereas the absence of chain-ends in cyclic polymers engenders comparatively lower propensities for chain-entanglement. Additionally, the inherent restriction of cyclic polymer elongation produces densities, conformations, and viscoelastic properties unique to their topologies in all physical states. Exploitation of these fundamental differences through a cyclic topology-selective synthetic methodology affords distinct material properties from an analogous linear synthetic methodology, but without modification of monomer composition or MW distribution¹⁻⁶ (Table 1).

Table 1 | The discrepancies in physical properties of cyclic versus linear polymers. (R_h = hydrodynamic radius, T_g = glass transition temperature).

Property	Linear Polymer	Cyclic Polymer
Intrinsic Viscosity	higher	lower
Melt Viscosity	higher	lower
Solution Conformation	random coil	discotic
R_h	higher	lower
T_g	lower	higher

The most common methods for the synthesis of cyclic polymers are a) ring-closure of a telechelic linear polymer and b) ring-expansion, where the cyclic topology of the growing polymer chain is preserved throughout (Figure 1).¹⁻³ Significant limitations and advantages exist for both methods. The requisite high dilution for ring-closure methods foments a number of fundamental problems: gram-scale quantities are infeasible, high MWs are inaccessible, and ring concatenation is inevitable. However, since ring-closing reactions are often carried out with telechelic polymers prepared by living methods, the resulting cycles can have low \bar{D} .^{4,5} Additionally, there are many more ring-closure synthetic strategies, so diversity in monomer scope is common.

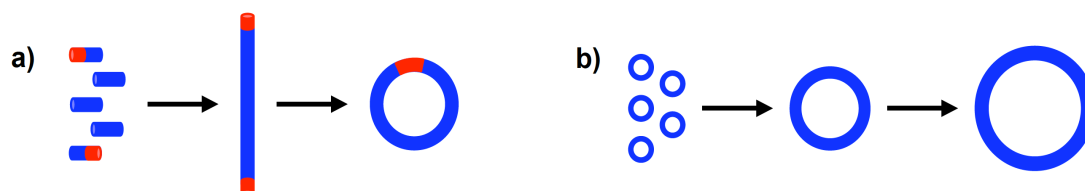


Figure 1.1 | Ring-closure (a) and ring-expansion (b) routes to cyclic polymers.

Ring-expansion of cyclic polymers is a newer method that is being explored by a number of groups. Ring-expansion polymerizations can be conducted on a more useful scale because they do not require high dilution, though they typically suffer from broad \bar{D} . Additionally, ring-expansion produces polymers with uniform chemical composition, unlike the cycles formed using ring-closure of telechelic chains that possess at least one condensed telechelic moiety per chain.^{5,7} Larger quantities of cyclic material than are generally accessible

through ring-closure methods are required to study melt-state properties because of the sample sizes required — e.g., differential scanning calorimetry (DSC), and especially rheology.

Existing studies on the rheological properties of cyclic polymers have not been in complete agreement. This is generally thought to be a result of both broad dispersity of the bulk material and the presence of linear polymer impurities. These undesirable features negatively impact analysis of melt-state material due to irreproducibility and convoluted data interpretation.⁸ A method to synthesize cyclic polymers free of linear impurity at scale and with MW control (including MWs above 100 kg/mol), low \bar{D} , and functional-group-tolerance of diverse monomer compositions remains elusive, but would dramatically increase our understanding of cyclic polymer material properties and synthetic strategies.

The lack of agreement among the polymer synthesis and polymer physics communities in regards to the properties of cyclic polymers comes, in large part, from linear polymers present in cyclic samples. Rheology of cyclic polymers is particularly challenging, because even minuscule levels of linear impurity nullify their peculiar viscoelastic properties. Using common rheology techniques, samples of cyclic polymers containing less than 0.07 wt.% linear impurity leads to inadequate data.⁹

Recent developments in cyclic polymer synthesis

Cyclic polymer synthetic methodology has been continually expanding and improving, particularly in the past 5 years. One notable example of a ring-closing

technique was reported for the ROP of γ -butyrolactone. Through judicious control of catalyst design and conditions, both cyclic and linear poly(γ -butyrolactone) with MWs exceeding 30 kDa were accessible. Notably, they found the cyclic polymer to be considerably more stable than its linear analog during the thermal depolymerization process used to recycle the monomer (Fig 1.2).¹⁰

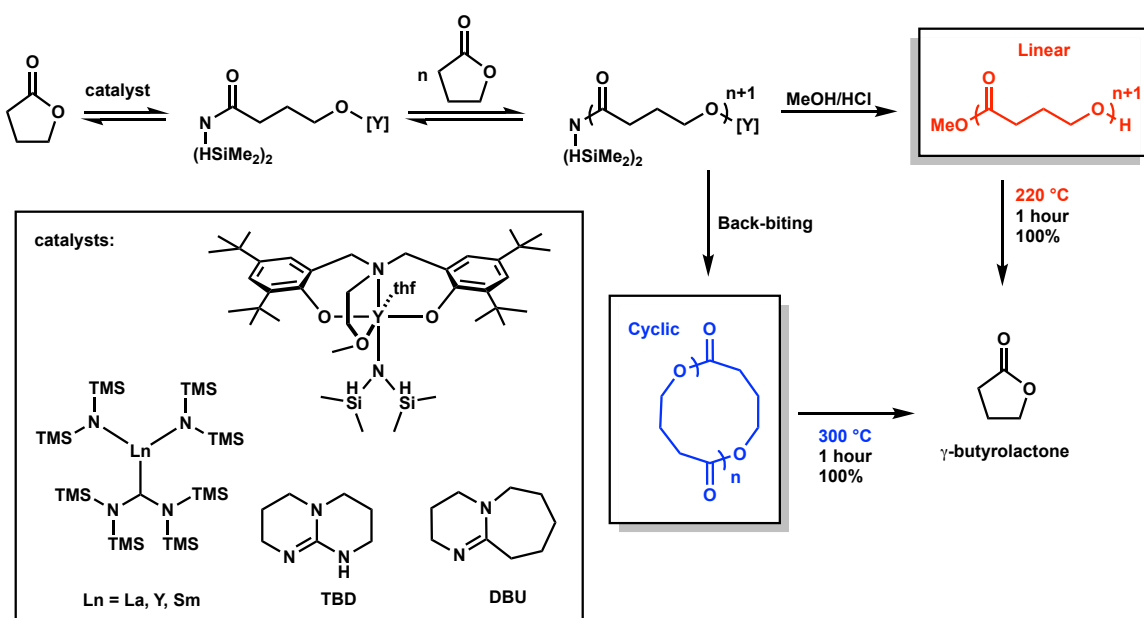


Figure 1.2 | Cyclic poly(γ -butyrolactone) synthesis and depolymerization recycling process.

Some work using zwitterionic ring-opening polymerization (ZROP) has also garnered attention. In ZROP, an N-heterocyclic carbene (NHC) is used to ring-open a lactone or lactide monomer and the electrostatic attraction between the two chain ends provides a cyclic topology upon release of the NHC (Fig 1.3).^{1,7,11}

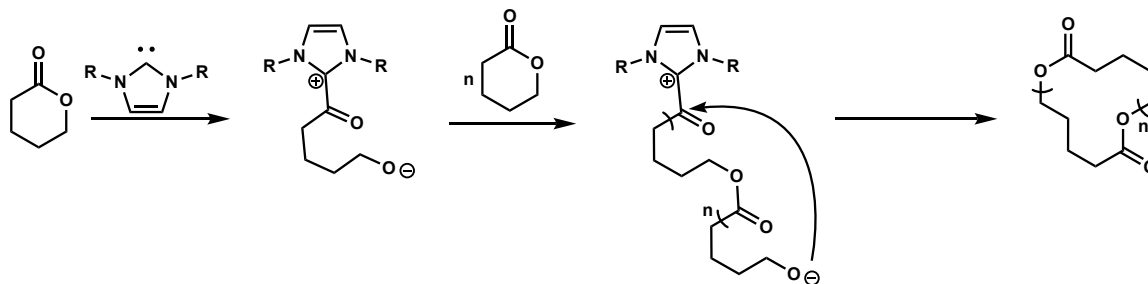


Figure 1.3 | Zwitterionic ring-opening polymerization (ZROP) of δ -valerolactone.

Radical addition-fragmentation polymerization (RAFT) is a powerful method to prepare polymers in a living fashion. It has also been used to prepare cyclic polymers from monomers such as N-vinyl carbazole using a cyclic RAFT initiator (Fig 1.4).¹²

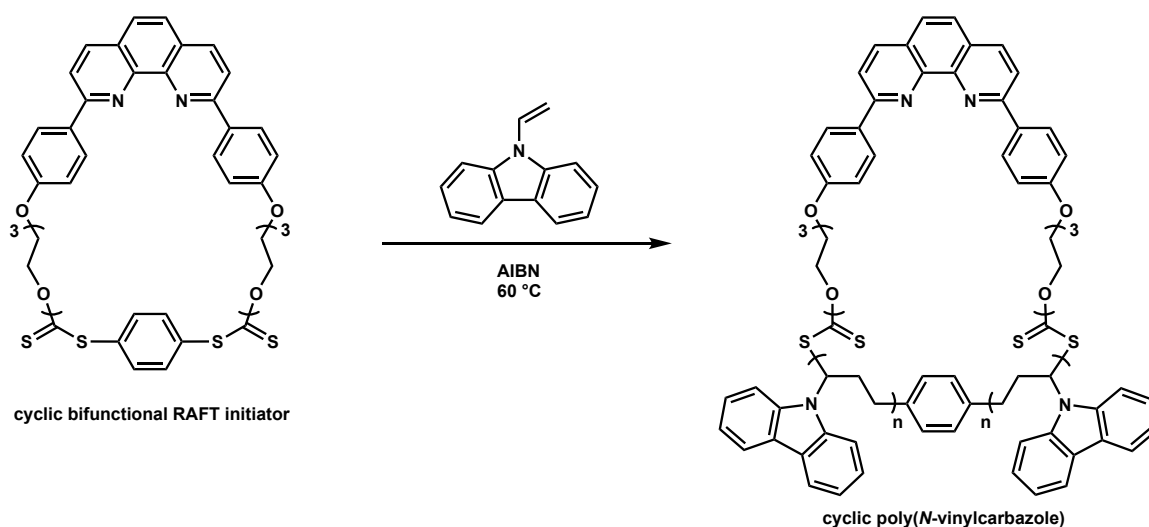


Figure 1.4 | Cyclic poly(N-vinylcarbazole) using a bifunctional RAFT initiator.

Determining cyclic polymer purity

Assessing the purity of cyclic polymers presents a challenge equal to the synthesis itself. The only compositional discrepancy between cyclic and linear is the latter's end-groups, but the concentration of end-groups in linear polymer chains often falls below the detection limit of conventional spectroscopic methods. However, a few powerful techniques for measurement of cyclic purity do exist: viscometry for intrinsic viscosity, rheology for melt-state viscoelasticity, and interaction chromatography (IC) for molecular homogeneity.¹³

The different intrinsic viscosities of cyclic and linear chains with equivalent MW can be useful to qualitatively assign a cyclic topology, but this method cannot quantify linear impurity. Rheology is the most sensitive analytical technique: 0.07% (w/w) linear impurity can be reliably detected. Kapnistos et al. observed significant differences in the stress relaxation modulus between linear poly(styrene) (PS), cyclic PS made by a ring-closure method, and the same cyclic PS after purification by IC (Fig 1.5, left).⁹ They observed the characteristic entanglement plateau at intermediate relaxation times ($10^{-3} < t \text{ (s)} < 10^0$) for linear PS. However, during the same intermediate relaxation time, an "extended relaxation regime" was observed for cyclic PS. The intermediate curve for unpurified rings (red, Fig 1.5) corroborates the suspicion that cyclic polymers free of linear impurity are exceptionally rare. They also intentionally mixed linear chains with cycles and studied the relaxation behavior based on the weight fraction of added linear chains (Fig 1.5, right). This demonstrated the incredible power of

rheology to assess purity of cyclic polymers, but also revealed the vital importance of IC in the field of cyclic polymers—these findings would not have been possible without cyclic PS purified through preparative IC.

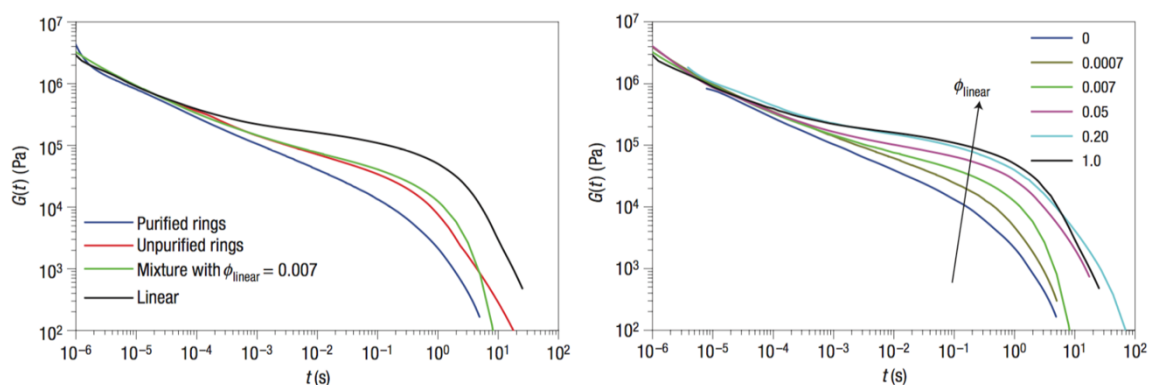


Figure 1.5 | Stress-relaxation modulus for cyclic and linear PS (left) and the effect of linear impurity on the stress-relaxation dynamics of cyclic PS (right). Reproduced from Kapnistos et al.⁹

Macromolecules with distinct molecular compositions, but otherwise similar physical properties, can be separated, quantified, and purified with IC. The success of IC with cyclic polymers has been well demonstrated, although there is disagreement as to the thermodynamic parameters underlying this success. Nevertheless, separation of macromolecules by topology can be achieved with IC, so direct measurement of cyclic and linear chains can be made.

Olefin Metathesis

Olefin metathesis emerged as one of the most powerful carbon-carbon bond forming reactions available in chemical synthesis in the 1980's and 1990's when R.H. Grubbs (Caltech) and R.R. Schrock (MIT) developed the first well-defined olefin metathesis catalysts. Their work confirmed the mechanism

originally proposed by Y. Chauvin (IFP) decades prior. The three shared the Nobel Prize in Chemistry in 2005 for their contributions to the olefin metathesis reaction.

Schrock developed many types of metathesis catalysts based on tungsten (W) and molybdenum (Mo)(**1.0–1.2**, Fig 1.6). Grubbs then followed with a number of catalysts based on ruthenium (Ru)(**1.3–1.8**, Fig 1.6). Grubbs-type catalysts are generally more stable, whereas Schrock-type catalysts are generally more active. This maxim was particularly accurate in the early days of metathesis, although the Grubbs-type catalysts are still more bench-stable and rarely require storage in inert atmosphere or reduced temperature, unlike the Schrock-type catalysts.

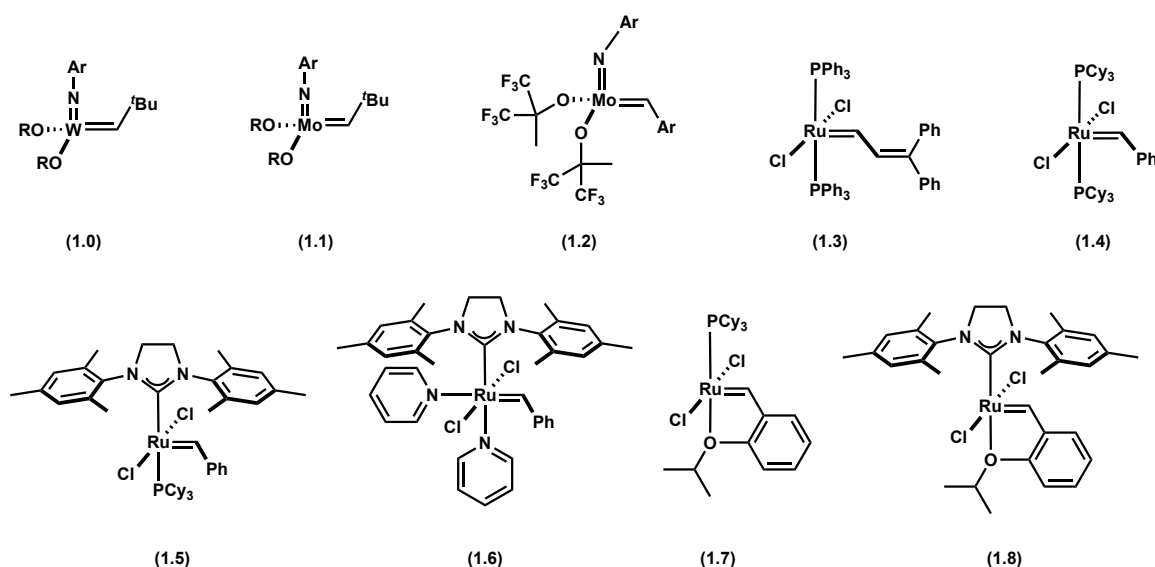


Figure 1.6 | Common olefin metathesis catalysts based on W (**1.0**), Mo (**1.1–1.2**), and Ru (**1.3–1.8**).

A carbene—a metal-carbon double bond—is the unifying feature of olefin metathesis catalysts (Fig 1.7, **1.9**). The metathesis catalytic cycle begins when an olefin (**1.10**) coordinates to the metal center (**1.11**) and undergoes a [2+2]

cycloaddition to form a metallocyclobutane intermediate (**1.12**). The subsequent cycloreversion rearranges the carbon-carbon bonds to form an olefinic product (**1.13**) bearing the functional group previously bound to the metal center (R). This forms a ruthenium-carbon double bond with new substituents (**1.14**). The metathesis reaction continues with substrates bearing different substituents (**1.15**) which undergo the [2+2] cycloaddition and cycloreversion step (**1.16**) which ultimately leads to the metathesis product (**1.17**), which is an olefin substituted with a combination of the original substrates' substituents (**1.10** and **1.15**).

The metathesis activity of early catalysts was generally verified by their ability to ring-open norbornene, a reactive bicyclic olefin with high ring-strain (28 kcal/mol). Metathesis catalysts gradually improved, becoming more stable and more active, such that many other types of olefin metathesis reactions for small-molecule synthesis (Fig 1.8, left) and polymerization (Fig 1.8, right) became viable.

The scope of transformations that metathesis catalysts were able to perform became expansive (Fig 1.3): ring-closing metathesis (RCM), cross metathesis (CM), ring-opening cross metathesis (ROCM), alkyne metathesis (AM), enyne metathesis (EYM), ring-opening metathesis polymerization (ROMP), acyclic diene metathesis (ADMET), ring-closing enyne metathesis polymerization (RECEYMP), and ring-expansion metathesis polymerization (REMP). These

reactions have contributed tremendously to the fields of organic synthesis and polymer synthesis, both academically and commercially.

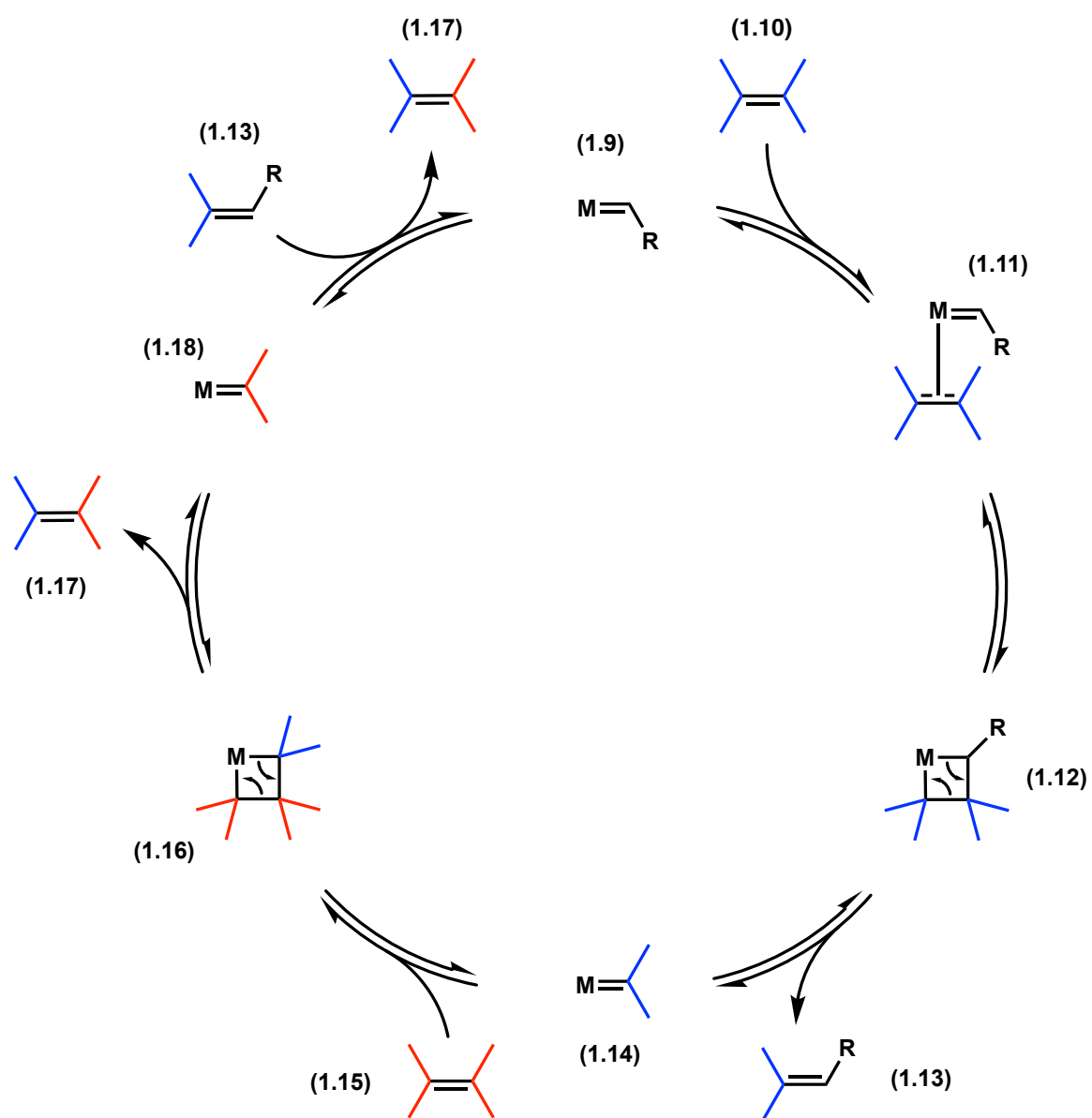


Figure 1.7 | The olefin metathesis reaction catalyzed by a metal carbene complex. $\text{M} = \text{Ru}, \text{W}, \text{Mo}$

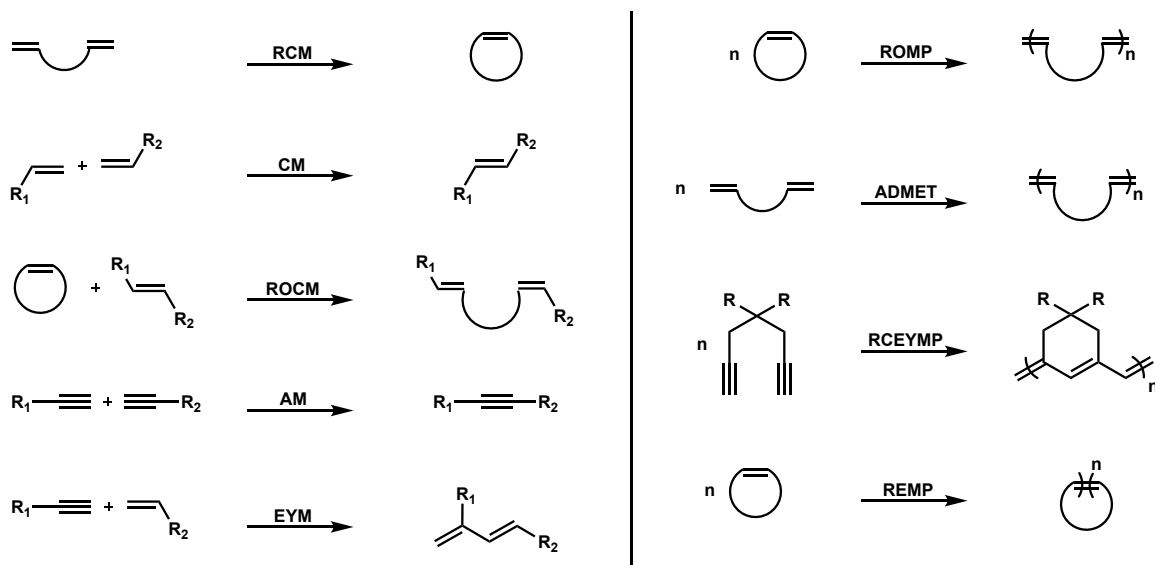


Figure 1.8 | Common types of olefin metathesis reactions for small-molecule synthesis (left) and polymer synthesis (right).

The utility of ROMP in polymer chemistry cannot be overstated. ROMP provides functional group tolerance, MW control, low \bar{D} , and architectural control, particularly when using Grubbs-type ruthenium-based catalysts.¹⁴ The mechanism of ROMP (Fig 1.5) is consistent with its living nature and ability to control MW through $[\text{monomer}]_0:[\text{catalyst}]_0$ loadings, whereby each catalyst produces one chain by chain-growth.

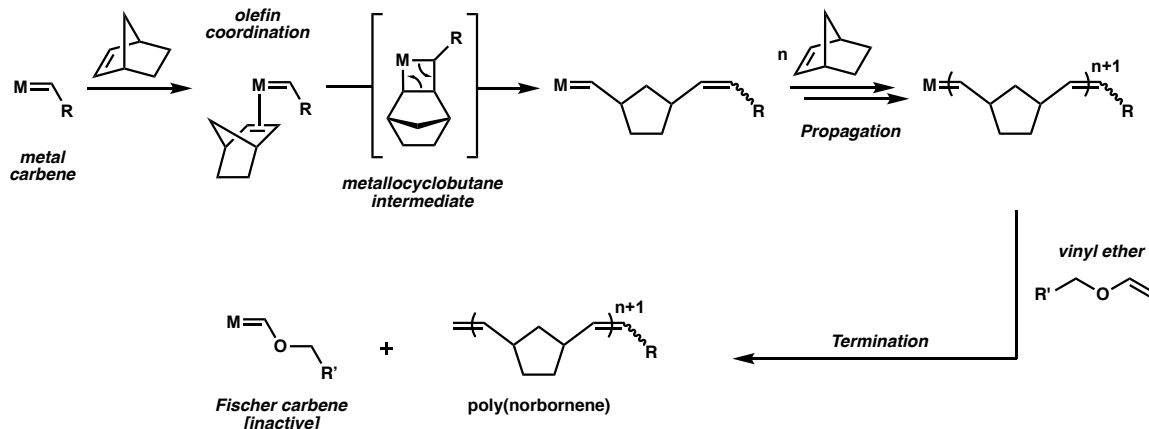


Figure 1.9 | The mechanism of ROMP for norbornene.

These desirable features do require, however, a cyclic olefin monomer with high ring-strain. High ring-strain monomers provide ROMP polymers with the best MW control and \bar{D} because secondary metathesis events which increase \bar{D} through back-biting and chain-transfer cannot occur. Although low ring-strain monomers can be polymerized, they are generally more difficult to polymerize in a controlled fashion (Fig 1.10). The ring-strain necessary for ROMP is approximately 5 kcal/mol because the entropic penalty is approximately 5 kcal/mol. That is, the enthalpy of ring-opening the monomer must compensate for the entropic cost of polymerization. A consequence of these basic thermodynamic principles is that the critical monomer concentration (CMC) must be exceeded for ROMP to be spontaneous, so for low- and intermediate- ring-strain monomers, concentrations above 1.0 M are generally required. The CMC for high ring-strain monomers, such as norbornene, is negligibly small.

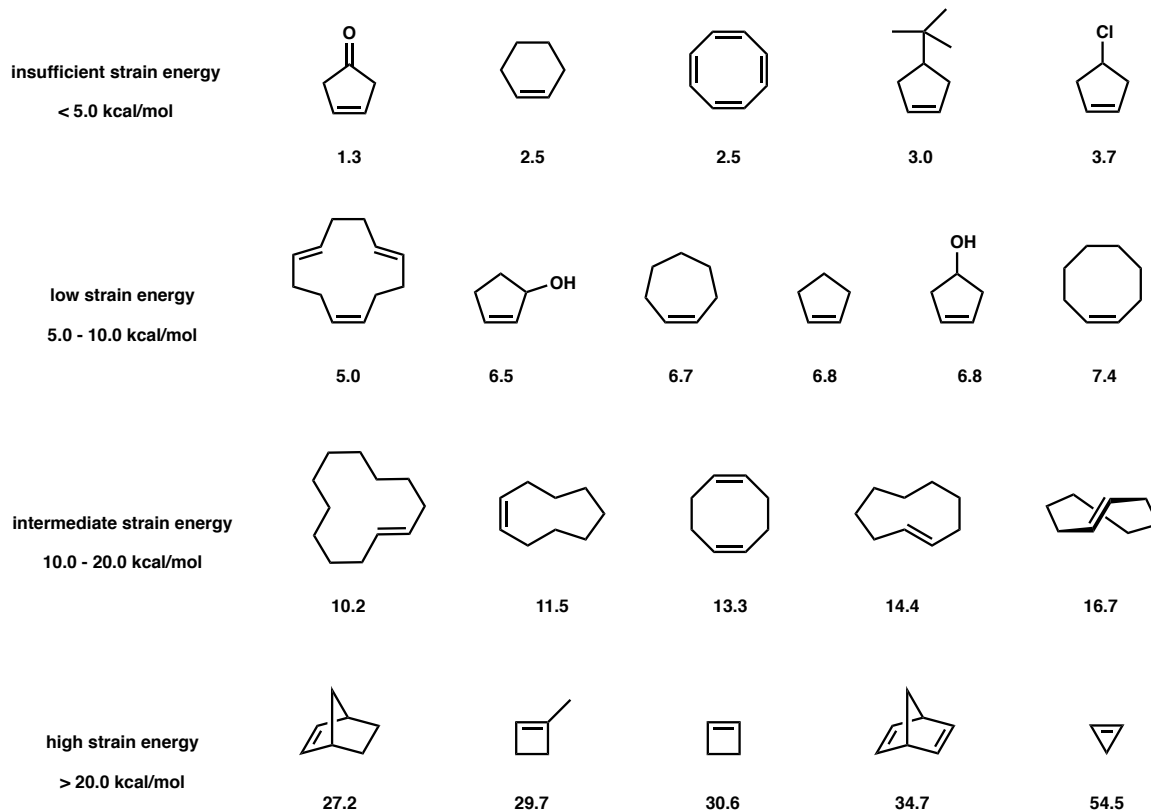


Figure 1.10 | Monomers unsuitable for ROMP (top row) and monomers with ring-strain sufficient for ROMP (bottom rows).

References

- (1) Brown, H. A.; Waymouth, R. M. *Acc. Chem. Res.* **2013**, *46* (11), 2585–2596.
- (2) Zhu, Y.; Hosmane, N. S. *ChemistryOpen* **2015**, *4* (4), 408–417.
- (3) Kricheldorf, H. R. *Journal of Polymer Science Part A: Polymer Chemistry* **2009**, *48*, 251–284.
- (4) Xia, Y.; Boydston, A. J.; Yao, Y.; Kornfield, J. A.; Gorodetskaya, I. A.; Spiess, H. W.; Grubbs, R. H. *J. Am. Chem. Soc.* **2009**, *131* (7), 2670–2677.
- (5) Laurent, B. A.; Grayson, S. M. *Chem. Soc. Rev.* **2009**, *38* (8), 2202–2213.
- (6) Nasongkla, N.; Chen, B.; Macaraeg, N.; Fox, M. E.; Fréchet, J. M. J.; Szoka, F. C. *J. Am. Chem. Soc.* **2009**, *131* (11), 3842–3843.
- (7) Chang, Y. A.; Waymouth, R. M. *Journal of Polymer Science Part A: Polymer Chemistry* **2017**, *55* (18), 2892–2902.
- (8) McKenna, G. B.; Hostetter, B. J.; Hadjichristidis, N.; Fetters, L. J.; Plazek, D. J. *Macromolecules* **1989**, *22* (4), 1834–1852.
- (9) Kapnistos, M.; Lang, M.; Vlassopoulos, D.; Pyckhout-Hintzen, W.; Richter, D.; Cho, D.; Chang, T.; Rubinstein, M. *Nat Mater* **2008**, *7* (12), 997–1002.
- (10) Hong, M.; Chen, E. Y. X. *Nature Chemistry* **2016**, *8* (1), 42–49.
- (11) Culkun, D. A.; Jeong, W.; Csihony, S.; Gomez, E. D.; Balsara, N. P.; Hedrick, J. L.; Waymouth, R. M. *Angew. Chem. Int. Ed.* **2007**, *46* (15), 2627–2630.
- (12) Bunha, A.; Cao, P.-F.; Mangadlao, J. D.; Advincula, R. C. *Reactive and Functional Polymers* **2014**, *80*, 33–39.
- (13) Lee, H. C.; Lee, H.; Lee, W.; Chang, T.; Roovers, J. *Macromolecules* **2000**, *33* (22), 8119–8121.
- (14) Trnka, T. M.; Grubbs, R. H. *Acc. Chem. Res.* **2001**.

Chapter 2

Design and Synthesis of Supported Molecular REMP Catalysts

2.0 – Abstract

The history and applications of ring-expansion metathesis polymerization (REMP) for the synthesis of cyclic polymers is discussed. Although ruthenium-based REMP catalysts have been explored and developed, significant limitations prompted the design and synthesis of a new family of REMP catalysts. The new supported molecular REMP catalyst was devised and its synthesis discussed. Despite challenging synthetic steps with low yields, multi gram quantities of the supported REMP catalysts were prepared. The synthesis reported may be adapted for future catalyst design.

Chapter 2 Acknowledgments

Bob Grubbs, Steve Diver (SUNY Buffalo), Patrick Montgomery, Willie Wolf, Tonia Ahmed, Allegra Liberman-Martin, Sankar Krishnamoorthy, Eric Welin, Adam Johns (Materia Inc.), Choonwoo Lee, Scott Virgil, Dave VanderVelde

2.1 – Introduction

The first ring-expansion metathesis polymerization (REMP)(Fig 2.1) catalyst (**2.1**), developed in our group in 2002, provided the first strategy for the preparation of all-hydrocarbon cyclic polyolefins via ring-expansion (Fig 2.1).¹ The distinguishing design feature of REMP catalyst **2.1** was the alkyl tether between the two carbene ligands which was designed to selectively produce cyclic polyolefins from cyclic olefin monomers.¹ Catalyst **2.1** also provided a novel strategy for the preparation of cyclic polyethylene (PE) using a living polymerization strategy: hydrogenation of any cyclic polyalkenamer (e.g., cyclic PCOE) prepared with **2.1** could be hydrogenated to PE (Fig 2.1, right). This early report also supposed a REMP catalytic cycle to rationalize the selective formation of cyclic polymers (Fig 2.2).

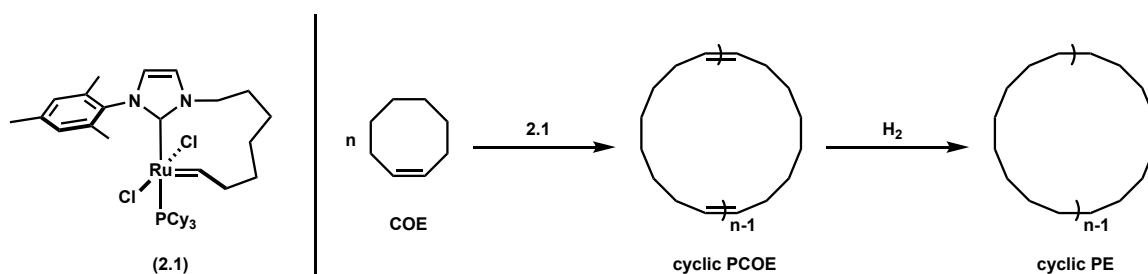


Figure 2.1 | REMP catalyst (**2.1**) (left) and the REMP of COE by **2.1** to produce cyclic PCOE and subsequent hydrogenation to cyclic PE (right).

The importance of monomer purity in the REMP of cyclododecatriene (CDT) using **2.1** was established.² Our group reported the synthetic strategy for a family of REMP catalysts similar to **2.1**, but with varying tether lengths between

NHC ligand and alkylidene, and the degree of saturation of the NHC ligand backbone (Fig 2.3).⁴ Subsequently, the catalyst-dependent polymerization profiles⁵ for **2.1-2.6** were studied and structure-property relationships were established. As with common ROMP catalysts, saturation of the NHC ligand increased the activity of **2.5** and **2.6** relative to **2.3** and **2.4**. Additionally, the tether length dictated relative rates of intra- and intermolecular chain transfer: longer tethers produced higher M_w chains due to reduced intramolecular chain transfer. Our group also expanded the monomer scope so that ultra-high MW brush and dendritic cyclic polymers could be prepared from norbornene-based monomers (Fig 2.4)

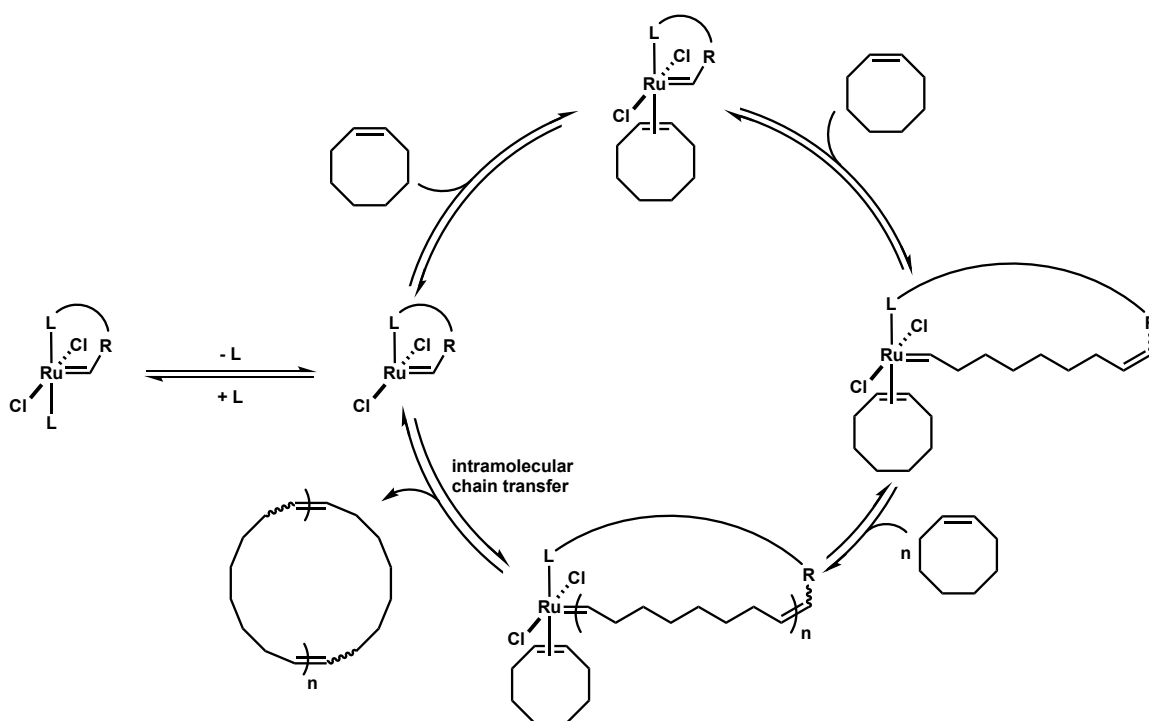
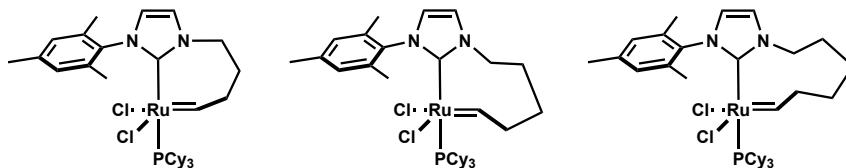


Figure 2.2 | The REMP catalytic cycle.

Unsaturated NHC ligand

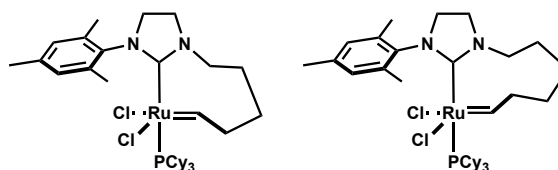


2.2

2.3

2.4

Saturated NHC ligand



2.5

2.6

Figure 2.3 | Homogeneous REMP catalysts with unsaturated NHC ligand (top) and saturated NHC ligand (bottom).

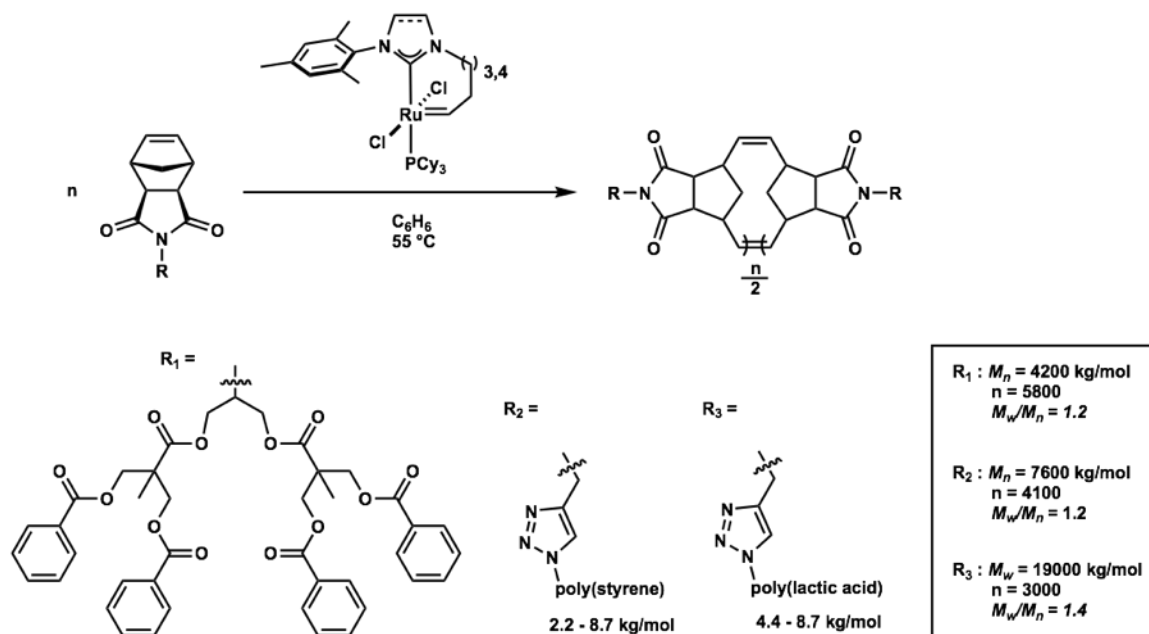


Figure 2.4 | Cyclic brush and dendritic polymers.

Efficient ROMP methodology, often utilizing common commercially available ruthenium-based catalysts (Fig 2.5), is characterized by the linear relationship between M_n and monomer conversion—this equates to a controlled, living polymerization which provides low dispersity (\mathcal{D}) material in high yield. The goal of similarly improving REMP methodology ca. 2003 – 2011 in our group focused on catalyst development,^{4,5} mechanistic studies,^{4,6} and expansion of monomer scope.⁷⁻⁹ The unifying obstacle in these efforts was the poor performance of all REMP catalysts we pursued.

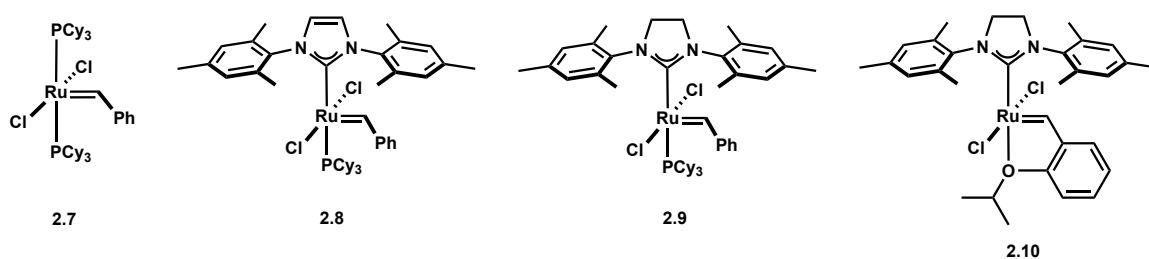


Figure 2.5 | Ruthenium-based olefin metathesis catalysts commonly used in ROMP.

The problems with catalysts **2.1** - **2.6** were three-fold: 1) poor activity; 2) poor scalability; 3) ineffective separation from the bulk material. Although the activity of unsaturated catalysts **2.1** - **2.4** was improved through saturation of the NHC backbone in **2.5** and **2.6**, these catalysts still performed poorly in comparison to **2.7** - **2.10**. The dual-chelating ligand—the alkyl tether from the NHC ligand to the alkylidene (**2.1** - **2.6**)—is the critical design feature which

produces cyclic polymers, but the concomitant electronic effects from these modifications are well-known to lower the stability and activity in olefin metathesis catalysts. This is why almost all commercially available ruthenium-based olefin metathesis catalysts with NHC ligands have aryl groups at both N1 and N3, and bear a benzylidene as opposed to an alkylidene. Attempts to incorporate the structural features unique to **2.1 – 2.6** into catalysts with similar electronics to **2.7 – 2.10** were unsuccessful.

Additionally, the poor activity of **2.1 – 2.6** necessitated high catalyst loading for REMP reactions. Synthesis of these catalysts was non-trivial, so the scale-up necessary to produce large quantities of material was highly impractical. Ironically, the final step in the syntheses of REMP catalysts **2.1 – 2.6** was a ring-closing metathesis (RCM) reaction that required prohibitively high dilution for scale up—REMP was originally conceived to circumvent this exact problem in cyclic polymer synthesis (see intro).

The aforementioned concerns with activity and scalability were compounded by another fundamental problem. Highly pure cyclic polymers could only be isolated if the REMP catalyst was completely removed from the bulk material. No such isolation procedure could be developed because **2.1 – 2.6** were invariably still incorporated into a cyclic polymer backbone, even when all monomer was consumed. The best isolation procedure developed was to rapidly precipitate the polymer under air, leaving the ruthenium catalyst in solution. This involved transferring the REMP reaction from an inert environment to atmospheric

O₂ and adventitious compounds potentially detrimental to polymerization and topological fidelity. Based on NMR experiments, the REMP catalyst was invariably still active and bound to the growing polymer chain at all times due to its living nature. We believe that the linear contaminants in the cyclic polymers isolated with this strategy arose from oxidative decomposition and subsequent chain cleavage localized at the catalyst active site. That is, decomposition at the metal center was thought to induce chain cleavage, resulting in linear chains. We were unable to envision a superior strategy for polymer isolation.

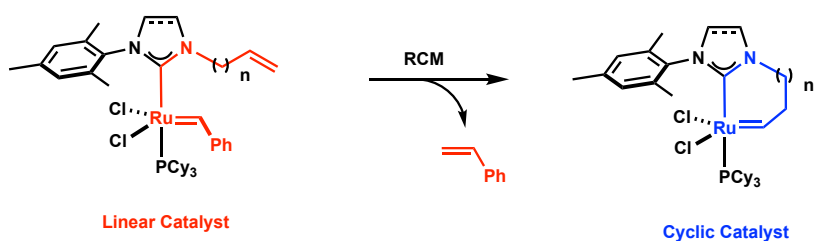
Despite earnest efforts to develop REMP methodology sufficiently to reliably produce large quantities of highly pure cyclic polymer, these problems proved insurmountable. We recognized that to overcome these challenges, a new approach was necessary. Our acceptance of this fact led us to design a radically different REMP catalyst and synthetic methodology. *The path toward, and realization of, a superior REMP strategy began in 2013 and is the subject of this dissertation.*

2.2 – Results and Discussion

The inadequacy of homogeneous REMP catalysts prompted us to investigate a catalyst with minimal structural differences from an existing ROMP catalyst already proven to perform well with common cycloolefin monomers and in a variety of chemical environments. The 2nd Generation Hoveyda-Grubbs catalyst (Fig. 2.3, **2.10**) fulfilled this requirement and was chosen as the template for a new REMP catalyst.

We proposed that as a key design feature, tethering both the NHC ligand and the benzylidene ligand to a solid support would produce catalysts with similar electronic and steric parameters to catalyst **2.10**, but that would lead exclusively to cyclic products. Condensation of these tethers in a ring-closing reaction would then impart the catalyst with the requisite cyclic topology of a REMP catalyst. Additionally, a molecular REMP catalyst covalently bound to a solid surface could be easily separated by filtration, a key advantage over previous catalysts.

Previous Work: Homogeneous REMP Catalysts



This Work: Supported Molecular REMP Catalysts

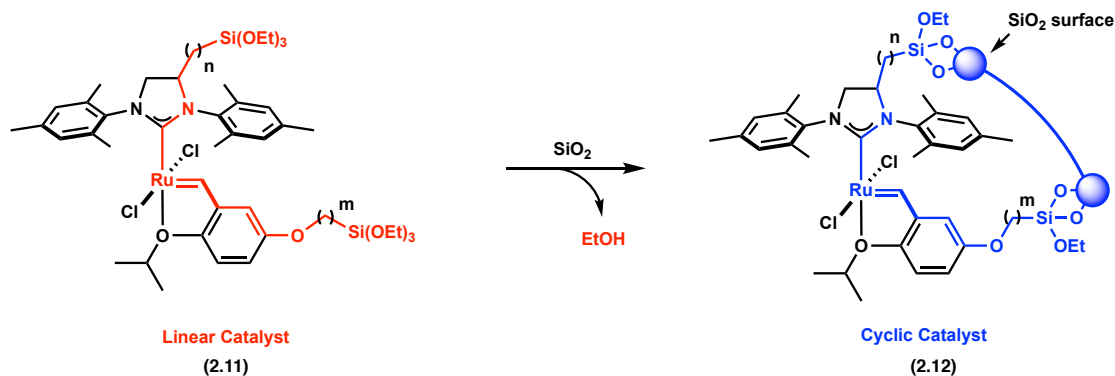


Figure 2.6 | The final ring-closure step to create a new family of REMP catalysts (top), and the analogous final ring-closure step for the previous family of homogeneous REMP catalysts (bottom).

We proposed that catalyst **2.11**, bearing triethoxysilyl-terminated alkyl chains from both NHC ligand and benzylidene ligand, would minimize structural

and electronic distinctions from **2.10** and could easily be attached to silica gel by the displacement of ethanol via Si-OH surface functionality. Ring-closing of **2.11** via condensation of both tethers to the SiO₂ surface would furnish **2.12** (Fig 2.6). Coincidentally and fortuitously, catalyst **2.12** had been reported already in the patent literature,¹⁰ although it had been developed for use in flow reactors for traditional small molecule cross metathesis and ring-closing metathesis reactions. There were also a few examples in the literature describing other types of mono-tethered supported metathesis catalysts.¹¹⁻¹⁴¹¹⁻¹⁴

The polymerization profiles of the first generation of homogeneous REMP catalysts **2.1** – **2.6** showed a strong dependence on the tether length between NHC and alkylidene ligands,⁵ so a modular approach to catalysts of the type **2.12** with varying tether lengths was targeted. The following describes the synthesis of these catalysts, beginning with the synthesis of triethoxysilyl-functionalized NHC and benzylidene ligands.

The NHC ligands were synthesized over 4 steps beginning with the commercially available starting materials 2,4,6-trimethylaniline and glyoxal to create the diimine **2.13** (Fig 2.7). The synthesis of NHCs with different tether lengths then diverges to form **2.14** and **2.15** using a 3-carbon or 11-carbon Grignard reagent, respectively. Formation of the imidazolidinium chloride salts **2.16** and **2.17** proved facile using HC(OEt)₃. A hydrosilylation reaction using Karstedt's Pt⁰ catalyst was used to prepare the final NHC-precursors **2.18** and

2.19; indeed, it was this step that introduced the greatest synthetic challenges of any discussed in this chapter. The hydrosilylated NHC-precursors were extremely hygroscopic and surfactant-like during the arduous purification procedure which involved multiple precipitations, aqueous work ups, and rounds of chromatographic purification. In addition, the products were simultaneously acid- and base-sensitive and could not be heated above room temperature without decomposition.

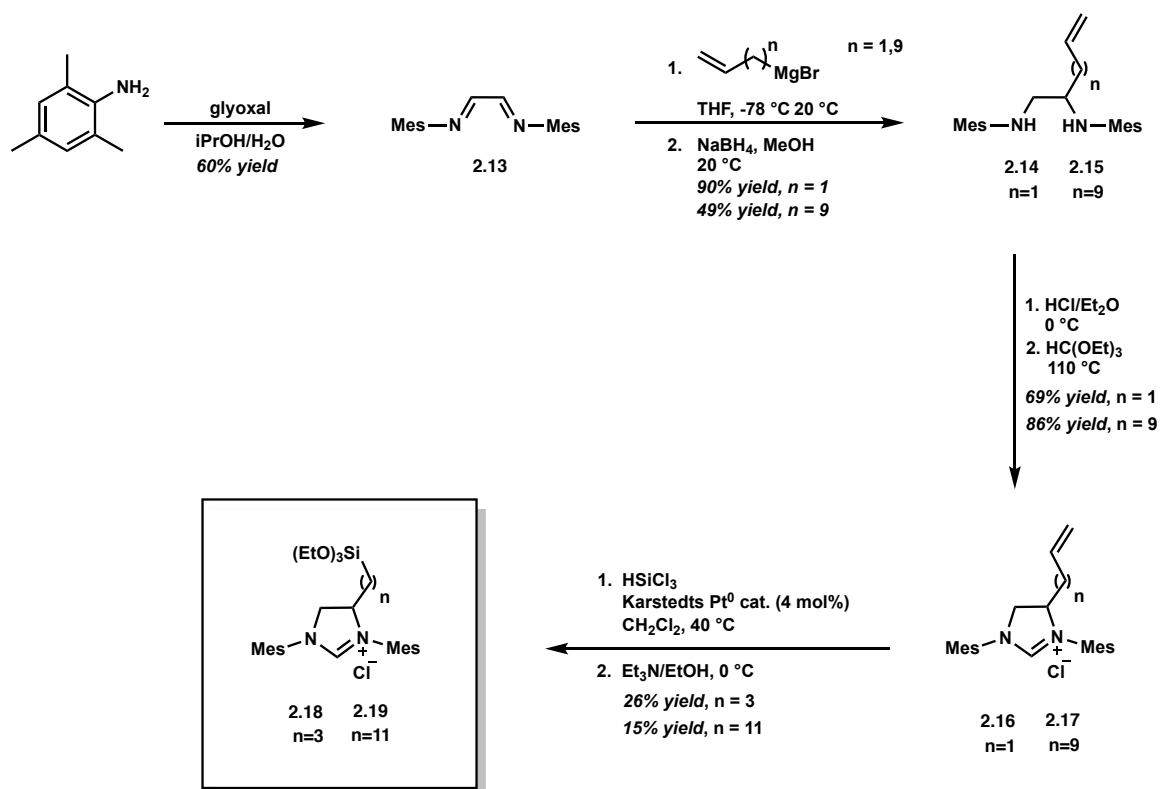


Figure 2.7 | Synthetic scheme for triethoxysilyl-functionalized NHCs **2.18** - **2.19**.

The relatively poor yields for **2.18** and **2.19** (Fig 2.5), 26% and 11%, respectively, were hard fought and ultimately sufficient for the purpose of

preparing REMP catalysts. Nonetheless, the method for their preparation described herein admittedly precludes synthesis at gram-scale at the present time, so the pursuit of an alternative strategy for **2.18** and **2.19** might eventually be required.

The synthetic strategy for the benzylidene ligands was straightforward (Fig 2.8) and began with 2,5-dihydroxybenzaldehyde (**2.20**). Following selective pivalate protection of the hydroxyl group at the 5-position of **2.20**, an alkylation with isopropyl iodide produced the benzaldehyde **2.22** in good yield. Wittig olefination of **2.22** led to an 80% yield with an inconsequential 70:30 *cis:trans* mixture of **2.23**, as the vinyl group would ultimately undergo a cross-metathesis reaction in the final step of the REMP catalyst synthesis, thus ablating the olefin geometry upon attachment of the catalyst.

Deprotection of **2.23** provided the key phenol intermediate **2.24** in excellent yield. Alkylation of phenol **2.24** with a triethoxysilyl-terminated alkyl iodide or bromide (chlorides were unreactive) was a straightforward and modular strategy to provide access to benzylidene ligands with any tether length desired. Triethoxysilyl-functionalized alkyl bromides can be easily accessed from hydrosilylation of the appropriate commercially-available olefin (Fig 2.9, left) and triethoxysilyl-functionalized alkyl iodides can be easily accessed via a Finkelstein reaction of the appropriate commercially-available triethoxysilyl-terminated alkyl chloride (Fig 2.9, right). This strategy was used for benzylidene ligands **2.25** and

2.26 with 3-carbon and 11-carbon tethers, respectively. We envision that future catalyst development will exploit this modularity to explore structure-property relationships of other REMP catalysts with different tether lengths.

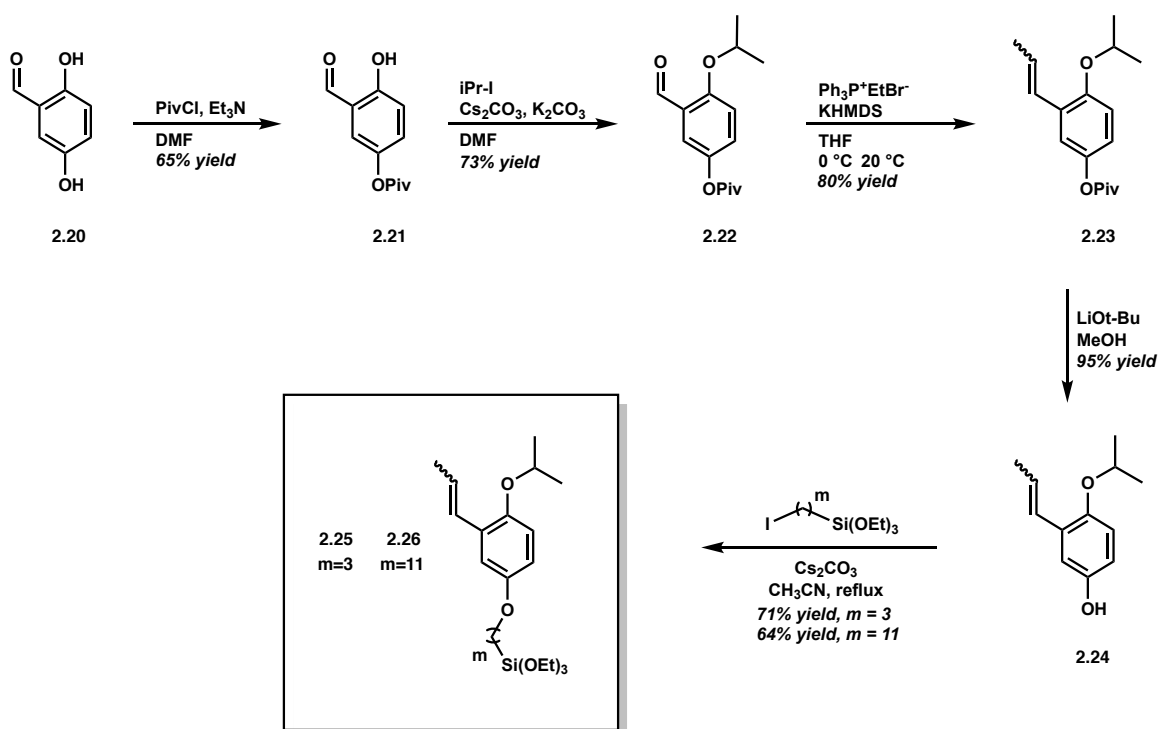


Figure 2.8 | Synthetic scheme for triethoxysilyl-functionalized benzylidene ligands **2.25** - **2.26**.

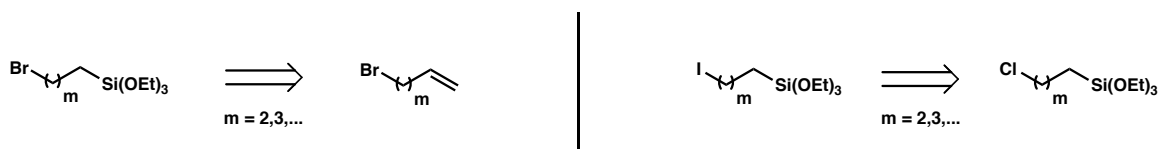


Figure 2.9 | Simple access to triethoxysilyl-terminated alkyl bromides (left) and triethoxysilyl-terminated alkyl iodides (right).

The NHC ligand precursors **2.18** and **2.19**, and benzylidene ligand precursors **2.25** and **2.26**, were successfully isolated in sufficient quantity to begin

the final phase of the molecular REMP catalyst synthesis (Fig 2.10). Metalation of **2.7** (the 1st generation Grubbs catalyst) with **2.18** or **2.19** provided the mono-tethered catalysts **2.27** and **2.28**, with 3- and 11-carbon tethers, respectively, in acceptable yields. Molecular REMP catalysts **2.29** – **2.32** (Fig 2.8, bottom right) were then accessed by the four combinations of cross-metathesis reactions of benzylidene precursors **2.25** and **2.26** with catalysts **2.27** and **2.28**.

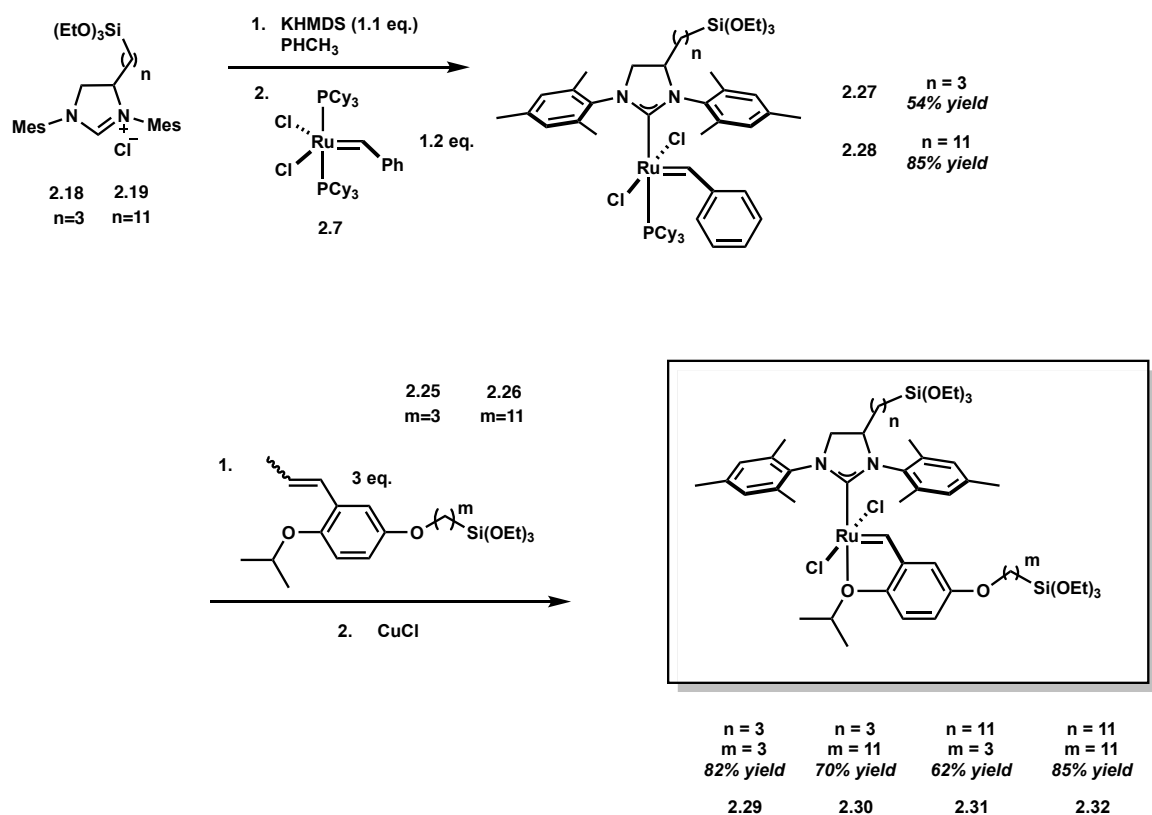


Figure 2.10 | The synthesis of catalysts **2.29** – **2.32**.

The final step in preparing the supported molecular REMP catalysts **2.33** - **2.36** was the ring-closure reaction with the surface of particulate SiO₂ (Fig 2.11),

which is a well-known strategy for surface functionalization. Trialkoxysilyl moieties are commonly chosen to attach organic molecules to hydroxyl-terminated surfaces, such as ZrO_2 , Fe_2O_3 , and SiO_2 .¹⁵⁻¹⁷ Simply stirring **2.33** – **2.36** in a $\text{SiO}_2/\text{PhCH}_3$ slurry successfully tethered them to the surface, although a Soxhlet extraction of the SiO_2 using CH_2Cl_2 for at least 9 days was necessary to remove residual homogeneous catalyst (**2.29** – **2.32**). To verify that all homogeneous catalyst had been washed away, aliquots of the extraction solvent were periodically added to neat COD until its polymerization could not be observed by GPC.

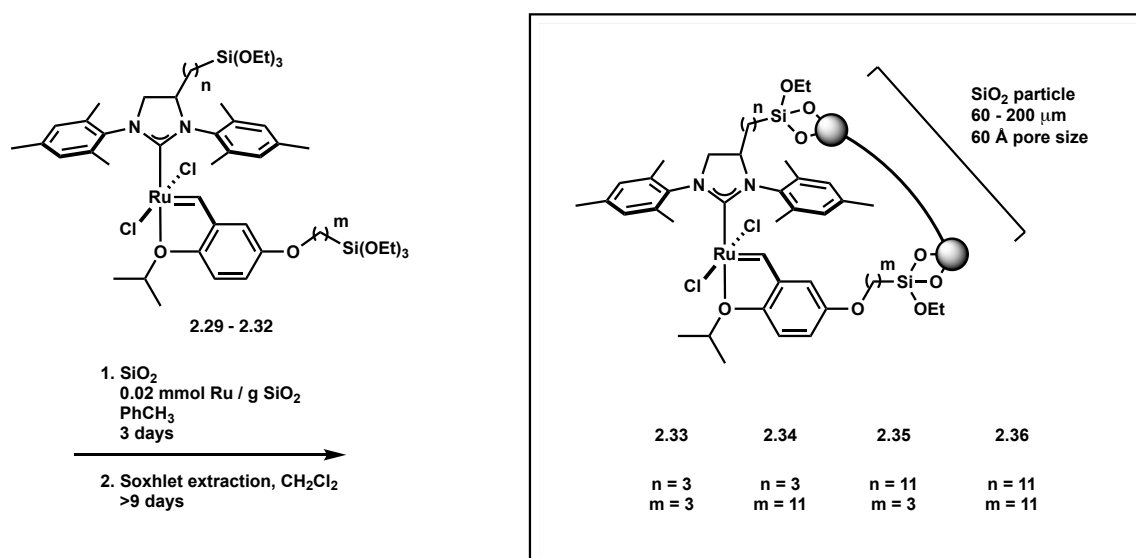


Figure 2.3 | Surface attachment of homogeneous REMP catalysts **2.29** - **2.32** to give supported molecular REMP catalysts **2.33** - **2.26**.

2.3 – Conclusions and Future Outlook

The inherent problems of REMP methodology were discussed, and the poor performance of REMP catalysts was identified as the likely origin of the large

majority of previous negative and inconclusive results from our group. A new REMP catalyst strategy was envisioned, whereby structural elements of the current state-of-the-art ROMP catalysts could be incorporated into a new family of molecular REMP catalysts supported on the surface of silica gel. The synthesis of the new generation of REMP catalysts was reported and shown to be modular for varying tether lengths. This work provided the means to expand REMP methodology for the preparation of large quantities of highly pure cyclic polyolefins.

2.4 – Experimental

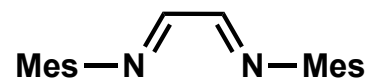
General Information: All reactions were carried out in glassware flame-dried in vacuo (100 mTorr) unless otherwise specified. Reactions were performed using air-free Schlenk technique (100 mTorr vacuum and UHP grade 5.0 argon gas) on the benchtop or in a Vacuum Atmospheres glovebox (N₂-filled, O₂ concentration < 0.25 ppm) unless otherwise specified. All solvents were purchased from Sigma-Aldrich (anhydrous, 99.9%) and further purified by passage through solvent purification columns, sparged with argon, and then stored over 4 Å molecular sieves in Strauss flasks, unless otherwise specified.¹⁵ All 1st generation Grubbs catalyst was received from Materia, Inc. (Pasadena, CA) and used without further purification. All other reagents were purchased from Sigma-Aldrich and used as received unless otherwise stated. All reactions performed in Schlenk tubes at elevated temperature were done so with a blast shield in place. Room temperature was 18-20 °C for all syntheses described herein.

All ^1H NMR spectra were acquired using a Varian Inova 500 MHz or Bruker 400 MHz spectrometer and are reported relative to residual CHCl_3 (δ 7.26 ppm), C_6H_6 (δ 7.16 ppm), or CH_2Cl_2 (δ 5.32 ppm). All ^{13}C NMR spectra were recorded on a Varian Inova 500 MHz spectrometer (125 MHz) or Bruker 400 MHz spectrometer (100 MHz) and are reported relative to CHCl_3 (δ 77.16 ppm), C_6H_6 (δ 128.06), or CH_2Cl_2 (δ 53.84 ppm). Data for ^1H NMR are reported as: chemical shift (δ ppm), multiplicity, coupling constant (Hz), integration value). Multiplicities are reported as: s = singlet, d = doublet, t = triplet, q = quartet, p = pentet, sept = septuplet, m = multiplet, br s = broad singlet. Data for ^{13}C NMR are reported in terms of chemical shifts (δ ppm). Processing of all NMR data was performed with MestReNova version 10.0 from Mestrelabs Research S.L.

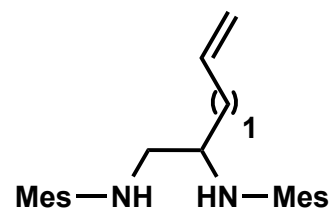
Size-exclusion chromatography (SEC) data was obtained with an HPLC system consisting of two two Agilent PLgel MIXED-B 300 \times 7.5 mm columns with 10 μm beads, and an Agilent 1260 Series pump and autosampler; the columns were connected in series with a Wyatt 18-angle DAWN HELEOS multi-angle laser light scattering detector and Optilab rEX differential refractive index detector. The mobile phase was either pure THF or stabilized THF (50-150 ppm butylated hydroxytoluene (BHT)).

Synthesis of NHC precursors 2.13 – 2.19

The following was developed from previously reported procedures.¹⁰

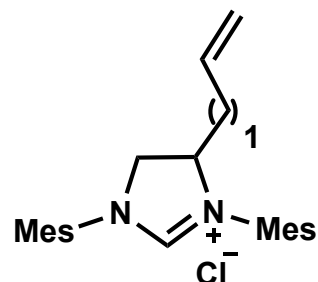
**2.13**

25 mL of 2,4,6-trimethylaniline (24.1 g, 0.178 mmol, 2.25 equiv.) was stirred in 100 mL of isopropyl alcohol and 200 mL deionized water at 0 °C in a 500 mL round bottom flask, in air. A 40% aqueous glyoxal solution (9 mL, 79 mmol, 1.0 equiv.) was added dropwise to the stirring solution and gradually warmed to room temperature. After 12 hours the solution was concentrated via rotovapory distillation. The yellowish-brown precipitate was collected on a coarse frit and washed with water (x1) and hexanes (x3), recrystallized from 1:1 acetone : CH₂Cl₂, and concentrated in vacuo overnight to yield **2.13** as a bright yellow crystalline solid (XX g, XX %). ¹H NMR analysis showed a 90:10 mixture of trans/cis isomers and was used without further purification. *Trans* isomer: ¹H NMR (300 MHz, chloroform-*d*) δ 8.09 (d, *J* = 0.5 Hz, 1H), 6.91 (s, 2H), 2.29 (s, 3H), 2.16 (d, *J* = 0.6 Hz, 7H), 2.01 (d, *J* = 14.5 Hz, 1H). *Cis* isomer: ¹H NMR (300 MHz, chloroform-*d*) δ 8.50 (d, *J* = 8.4 Hz, 1H), 7.47 (d, *J* = 8.4 Hz, 1H), 6.81 (s, 4H), 2.23 (s, 6H), 2.01 (d, *J* = 14.6 Hz, 12H). HRMS (FAB+): found 293.2014, calculated 293.2018.

**2.14**

A 1 L 2-neck flask was charged with a stir bar and flame dried under vacuum. **2.13** (4.58 g, 15.7 mmol, 1.00 equiv.) was added as a solid and the flask was again pumped on and backfilled with argon. The flask was cooled to -78 °C in a dry ice/acetone bath and 0.4 L THF was cannula transferred into the flask to give a yellow slurry. A 1.0 M solution of allylmagnesium bromide in Et₂O (16.2 mL, 16.2 mmol, 1.03 equiv.) was added dropwise over 1-2 minutes. The mixture then changed to amber/reddish-brown upon warming to room temperature. After 90 minutes, 100 mL MeOH was poured into the stirring reaction mixture, followed by solid NaBH₄ (3.56 g, 94.2 mmol, 6.00 equiv.). This mixture was stirred for 3 hours and then slowly quenched with saturated aqueous NH₄Cl until bubbling ceased. The reaction mixture was then extracted with hexanes (x3) and the combined organic layers were washed with water, dried over MgSO₄, filtered, and concentrated via rotovapory distillation to provide a crude yellow-brown viscous oil which was then purified by flash column chromatography (25:1 hexanes : EtOAc) to give **2.14** as a faintly yellow oil (2.28 g, 43% yield)(the fractions which were not pure were discarded so that the next step could proceed more cleanly). ¹H NMR (400 MHz, methylene chloride-*d*₂) δ 6.79 (dd, *J* = 6.6, 0.8 Hz, 4H), 5.80

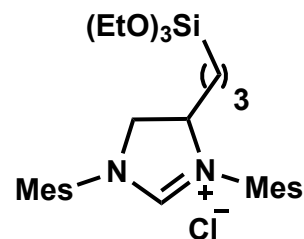
(dddd, $J = 17.1, 10.2, 8.1, 6.1$ Hz, 1H), 5.13 – 5.00 (m, 2H), 3.51 (ddt, $J = 8.2, 6.9, 4.7$ Hz, 1H), 3.17 (dd, $J = 12.0, 4.6$ Hz, 1H), 2.79 (dd, $J = 12.1, 6.9$ Hz, 1H), 2.25 (s, 12H), 2.20 (s, 3H), 2.19 (s, 3H).



2.16

The diamine **2.14** (2.28 g, 6.63 mmol) was transferred to a heavy-walled Schlenk tube equipped with a magnetic stir bar and dissolved in Et₂O. The mixture stirred and was cooled in a 0 °C ice bath. A 2.0 M HCl/Et₂O solution was added dropwise (3.98 mL, 7.95 mmol, 1.20 equiv.) which caused a precipitate to form immediately. All volatile material was removed carefully in vacuo (<100 mTorr) and the solid residue was dissolved in triethyl orthoformate (15 mL, 13.4 g, 90.2 mmol, 13.6 equiv.) which was added via needle and syringe from a sure-seal bottle (neat reaction conditions). The mixture was then stirred at 95 °C overnight. All volatiles were removed in vacuo (100 mTorr) and the sticky brown solid was transferred to a fine fritted filter and then triturated with Et₂O (x3), pentane (x1), and Et₂O (x1). The triturand was then concentrated in vacuo (100 mTorr) to provide **2.16** as a very fine white powder (1.75 g, 69% yield) which could easily be inadvertently sucked into the Schlenk manifold during evacuation. ¹H NMR (400 MHz,

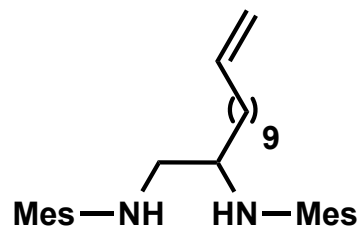
methylene chloride- d_2) δ 10.35 (s, 1H), 7.09 (d, $J = 6.9$ Hz, 4H), 5.72 – 5.60 (m, 1H), 5.30 – 5.17 (m, 2H), 4.92 – 4.79 (m, 1H), 4.50 (t, $J = 11.7$ Hz, 1H), 4.02 (dd, $J = 12.1, 8.4$ Hz, 1H), 2.75 – 2.51 (m, 4H), 2.46 (d, $J = 18.3$ Hz, 12H), 2.37 (d, $J = 2.6$ Hz, 6H). ^{13}C NMR (400 MHz, methylene chloride- d_2) δ 142.55, 142.43, 137.95, 136.86, 132.54, 132.17, 132.11, 131.86, 122.15, 64.75, 38.85, 27.06, 22.75, 22.71, 20.86, 20.17.



2.18

The olefin-terminated NHC salt **2.16** was added to a flame dried Schlenk tube under argon (2.11 g, 5.50 mmol, 1.00 equiv.) with stir bar and 10 mL CH_2Cl_2 was cannula transferred. The mixture was cooled to 0 °C and HSiCl_3 (22.2 mL, 29.8 g, 220 mmol, 40 equiv.) was added via needle and syringe from a sure-seal bottle. A 0.05 M solution of Karstedt's Pt^0 catalyst in xylenes (4.18 mL, 0.209 mmol, 3.8 mol%) was added in three portions over 15 minutes. The reaction was heated to 40 °C and stirred in the dark for 16 hours. The temperature was lowered to 0 °C and external cold trap (-196 °C) was used to concentrate the reaction mixture in vacuo as it was stirring rapidly (100 mTorr) (necessary to remove excess HSiCl_3 , which is highly corrosive and volatile). 10 mL of CH_2Cl_2 was then added to redissolve the crude reaction mixture. A 1:1 EtOH: Et_3N (v/v) solution was added

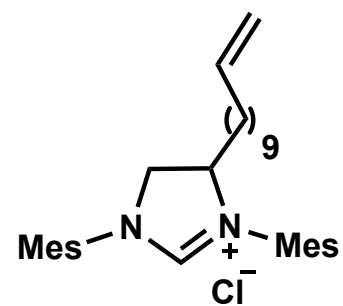
dropwise via needle and syringe (10 mL) at 0 °C which produced a white smoke-like substance that gradually dissolved (presumably $\text{Et}_3\text{N}\cdot\text{HCl}$). The mixture turned brown gradually and was concentrated via rotovapory distillation after 2 hours. Care was taken to not heat above room temperature. Anhydrous PhCH_3 was added to precipitate $\text{Et}_3\text{N}\cdot\text{HCl}$; the solution was then filtered through a F porosity frit and concentrated in vacuo (100 mTorr). Silica gel for flash column chromatography was loaded using 2% $\text{EtOH}/\text{CH}_2\text{Cl}_2$ with 1% additional Et_3N . Two column volumes of 2% $\text{EtOH}/\text{CH}_2\text{Cl}_2$ were then flushed through the silica gel before the crude residue was eluted using 2% \rightarrow 5% \rightarrow 8% $\text{EtOH}/\text{CH}_2\text{Cl}_2$. Purity of fractions was determined primarily using ^1H NMR due to poor resolution by TLC. The clean fractions were concentrated via rotovapory distillation, redissolved in CH_2Cl_2 , and washed with water (x3) to remove residual $\text{Et}_3\text{N}\cdot\text{HCl}$. The organic layer was concentrated via rotovapory distillation and the residue lyophilized from C_6H_6 to furnish the silylated NHC salt **2.18** as a hygroscopic white powder (0.78 g, 26% yield). ^1H NMR (400 MHz, methylene chloride- d_2) δ 10.51 (s, 1H), 7.16 – 6.93 (m, 4H), 4.70 (dq, $J = 11.4, 8.5$ Hz, 1H), 4.54 – 4.42 (m, 1H), 3.95 (dd, $J = 11.8, 9.1$ Hz, 1H), 3.76 (q, $J = 7.0$ Hz, 6H), 2.52 – 2.40 (m, 12H), 2.37 (s, 6H), 1.86 (q, $J = 7.9, 7.4$ Hz, 2H), 1.52 – 1.29 (m, 2H), 1.18 (t, $J = 7.0$ Hz, 9H), 0.69 – 0.58 (m, 2H).

**2.15**

To a 100 mL Schlenk flask was added Mg^0 (0.510 g, 21.0 mmol, 1.01 equiv., freshly cleaned with aqueous 1 M HCl, dried in vacuo), THF (26.7 mL), and 11-bromo-1-undecene (4.61 mL, 4.90 g, 21.0 mmol, 1.01 equiv.). The solution turned metallic gray after stirring overnight and no Mg^0 was evident. This 0.67 M (assumed) 11-undecenyl-1-magnesium bromide solution was used without titration.

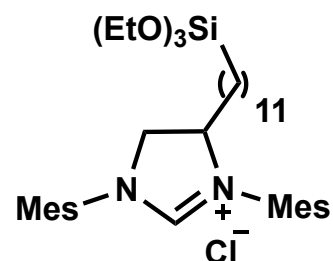
A 1.0 L 2-neck flask was charged with a stir bar and flame dried under vacuum. **2.13** (6.10 g, 20.8 mmol, 1.00 equiv.) was added as a solid and the flask was again pumped on and backfilled with argon. The flask was cooled to $-78\text{ }^\circ\text{C}$ in a dry ice/acetone bath and 0.3 L THF was cannula transferred into the flask. The yellow solid did not appear fully dissolved. All of the 0.67 M 11-undecenyl-1-magnesium bromide solution (31.3 mL, 1.01 equiv.) was added via syringe over 5 minutes. The mixture then changed to amber/reddish brown upon warming to room temperature. After 2 hours, the reaction mixture was diluted with MeOH (100 mL) and solid NaBH_4 (4.7 g, 124 mmol, 6.0 equiv.) was added. After 3 hours the solution was quenched by the dropwise addition of saturated aqueous NH_4Cl until bubbling ceased. The reaction mixture was extracted with hexanes (3x200 mL)

and the combined organic layers were washed with water, dried over MgSO_4 , filtered and concentrated to provide 8.2 g crude yield. Flash column chromatography (SiO_2 , 25:1 hexanes : EtOAc) provided the diamine **2.15** (3.49 g, 37% yield) which was used without further purification. ^1H NMR (400 MHz, chloroform-*d*) δ 6.92 – 6.74 (m, 4H), 5.83 (ddt, $J = 16.9, 10.2, 6.7$ Hz, 1H), 5.13 – 4.81 (m, 2H), 3.45 (q, $J = 6.7, 6.0$ Hz, 1H), 3.21 (dd, $J = 11.8, 4.4$ Hz, 1H), 2.76 (dd, $J = 11.8, 7.1$ Hz, 1H), 2.36 – 2.17 (m, 18H), 2.11 – 1.98 (m, 2H), 1.50 – 1.20 (m, 16H).

**2.17**

The diamine **2.15** (1.69 g, 3.77 mmol, 1.00 equiv.) was transferred to a heavy-walled Schlenk tube and dissolved in Et_2O . The mixture stirred and was cooled in a 0 °C ice bath. A 2.0 M HCl/ Et_2O solution was added dropwise (2.26 mL, 4.52 mmol, 1.20 equiv.) which caused a precipitate to form immediately. All volatile material was removed carefully in vacuo (<100 mTorr) before the solid residue was dissolved in triethyl orthoformate (6.26 mL, 5.58 g, 37.7 mmol, 10.0 equiv.) which was added via needle and syringe from a sure-seal bottle (neat reaction conditions). The mixture stirred at 110 °C overnight. All volatiles were

removed in vacuo (100 mTorr) and the sticky brown solid was transferred to a fine fritted filter and then triturated with Et₂O (x3), pentane (x2), and Et₂O (x3). The triturand was then concentrated in vacuo (100 mTorr) to provide **2.17** as a very fine white powder (0.951 g, 51% isolated yield) which could easily be inadvertently sucked into the Schlenk manifold during evacuation. ¹H NMR (400 MHz, chloroform-*d*) δ 10.47 (s, 1H), 7.04 – 6.90 (m, 4H), 5.79 (ddt, *J* = 16.9, 10.2, 6.7 Hz, 1H), 5.03 – 4.85 (m, 2H), 4.71 (tt, *J* = 9.2, 4.6 Hz, 1H), 3.89 (dd, *J* = 11.7, 8.9 Hz, 1H), 2.50 – 2.24 (m, 18H), 2.04 – 1.98 (m, 2H), 1.76 (dd, *J* = 10.2, 6.2 Hz, 2H), 1.42 – 1.13 (m, 19H), 0.92 – 0.80 (m, 2H). HRMS (FAB+): found 459.3727, calculated 459.3739.

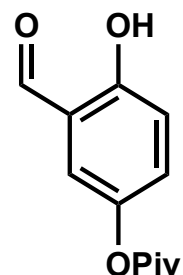
**2.19**

The olefin-terminated NHC salt **2.17** was added to a flame dried Schlenk tube under argon (1.50 g, 3.03 mmol, 1.00 equiv.) with stir bar and 20 mL CH₂Cl₂ was cannula transferred. The mixture was cooled to 0 °C and HSiCl₃ (30 mL, 22 g, 163 mmol, 54 equiv.) was added via needle and syringe from a sure-seal bottle. A 0.05 M solution of Karstedt's Pt⁰ catalyst in xylenes (2.30 mL, 0.115 mmol, 3.8 mol%) was added in three portions over 15 minutes. The reaction was heated to 40 °C and stirred in the dark for 16 hours. The temperature was lowered to 0 °C

and an external cold trap (-196 °C) was used to concentrate the reaction mixture in vacuo as it was stirring rapidly (100 mTorr) (necessary to remove excess HSiCl₃, which is highly corrosive and volatile). 20 mL of CH₂Cl₂ was then added to redissolve the crude reaction mixture. A 1:1 EtOH:Et₃N (v/v) solution was added dropwise via needle and syringe (20 mL) at 0 °C which produced a white smoke-like substance that gradually dissolved (presumably Et₃N·HCl). The mixture turned brown gradually and was concentrated via rotovapory distillation after 3 hours. Care was taken to not heat above room temperature. Anhydrous PhCH₃ was added to precipitate Et₃N·HCl; the solution was then filtered through a F porosity frit and concentrated in vacuo (100 mTorr). Silica gel for flash column chromatography was loaded using 2% EtOH/CH₂Cl₂ with 1% additional Et₃N. Two column volumes of 2% EtOH/CH₂Cl₂ were then flushed through the silica gel before the crude residue was eluted using 2% → 5% EtOH/CH₂Cl₂. Purity of fractions was determined primarily using ¹H NMR due to poor resolution by TLC. The clean fractions were concentrated via rotovapory distillation, redissolved in CH₂Cl₂, and washed with water (x5) to remove residual Et₃N·HCl. The organic layer was concentrated via rotovapory distillation and the residue lyophilized from C₆H₆ to furnish the silylated NHC salt **2.19** as a hygroscopic white powder (0.30 g, 15% isolated yield). ¹H NMR (500 MHz, benzene-*d*₆) δ 10.60 (s, 1H), 7.08 – 6.96 (m, 4H), 4.77 (ddt, *J* = 13.7, 9.3, 4.4 Hz, 1H), 4.60 (t, *J* = 11.4 Hz, 1H), 3.87 (q, *J* = 7.0 Hz, 7H), 2.57 – 2.43 (m, 12H), 2.35 (d, *J* = 4.5 Hz, 6H), 1.54 – 1.22 (m, 27H), 0.85 – 0.52 (m, 2H).

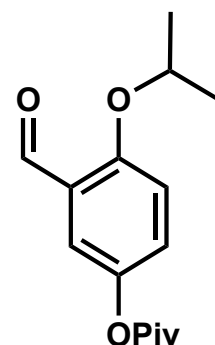
Synthesis of Benzylidene Ligands

The following was developed from previously reported procedures.¹⁰

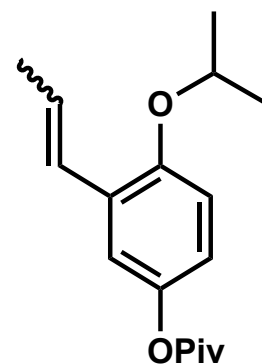


2.21

A 250 mL 3-neck round bottom flask with stir bar was flame-dried and fitted with a dropping funnel. Solid 2,5-dihydroxybenzaldehyde (9.68 g, 70.1 mmol, 1.00 equiv.) was added and dissolved in DMF (0.2 L) and cooled to 0 °C. Triethylamine (10.5 mL, 80.5 mmol, 1.15 equiv.) was added via needle and syringe. Pivaloyl chloride (9.05 mL, 73.6 mmol, 1.05 equiv.) was added to the dropping funnel via needle and syringe and was then added dropwise to the stirring reaction mixture over 1 hour which produced bubbling and a white gas. After 15 hours the reaction mixture was poured into water (200 mL), extracted with EtOAc (200 mL x5), washed with brine, dried over MgSO₄, filtered, concentrated via rotovapory distillation. Flash column chromatography (25:75 hexanes:EtOAc) provided the desired product **2.21** as a colorless oil (11.4 g, 73% yield) (the primary impurity was 2,5-di-pivalated benzaldehyde, a pink oil which eluted first). ¹H NMR (400 MHz, chloroform-*d*) δ 10.28 – 9.79 (m, 1H), 7.24 (dd, *J* = 4.5, 2.9 Hz, 1H), 7.08 – 6.94 (m, 2H), 1.43 (s, 9H).

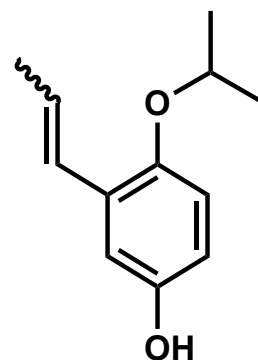
**2.22**

2.21 (5.62 g, 25.28 mmol, 1.00 equiv.) was dissolved in DMF (0.1 L) in a 2-neck round bottom flask. Solid K_2CO_3 (5.24 g, 37.9 mmol, 1.5 equiv.) and solid Cs_2CO_3 (0.70 g, 5.06 mmol, 0.20 equiv.) were added to the stirring solution. 2-iodopropane (6.44 g, 37.9 mmol, 1.5 equiv.) was added via needle and syringe and the mixture stirred at room temperature. Upon complete consumption of starting material by TLC, the reaction mixture was poured into water (0.7 L) and extracted with EtOAc (100 mL x5). The combined organic extracts were washed with 5% aqueous LiCl (x2) and water (x1), dried over MgSO_4 , filtered, concentrated via rotovapory distillation, and further purified using flash column chromatography (10:90 hexanes : EtOAc) to give **2.22** as a colorless oil (5.44 g, 83% yield). ^1H NMR (500 MHz, chloroform-*d*) δ 10.44 (s, 1H), 7.48 (d, $J = 3.0$ Hz, 1H), 7.22 (dd, $J = 9.0, 3.0$ Hz, 1H), 6.99 (d, $J = 8.7$ Hz, 1H), 4.66 (hept, $J = 6.1$ Hz, 1H), 1.41 (d, $J = 6.1$ Hz, 6H), 1.35 (s, 9H). ^{13}C NMR (126 MHz, Chloroform-*d*) δ 189.35, 177.23, 158.14, 144.31, 128.96, 126.13, 120.64, 115.02, 71.76, 39.05, 27.13, 22.00.

**2.23**

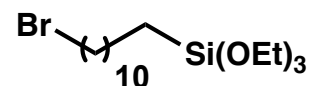
2.22 (1.54 g, 5.83 mmol, 1.00 equiv.) was dissolved in THF (50 mL) and stirred at 0 °C in a 500 mL 2-neck round bottom flask which had been flame dried. A KHMDS/THF solution was prepared in the glovebox (1.28 g, 6.41 mmol, 1.10 equiv.) and transferred to EtPPh₃Br (2.38 g, 6.41 mmol, 1.10 equiv.) which was dissolved in THF (50 mL) and stirred in a 100 mL 2-neck round bottom flask at 0 °C. (Note: LHMDS/THF solution was not suitable for this reaction as it lead to undesired side-products). The ylide solution (vibrant orange) was cannula transferred to the reaction flask which was then allowed to gradually warm to room temperature overnight. The reaction was monitored after 16 hours by TLC (40:60 CH₂Cl₂: hexanes) at which point all starting material was consumed. The reaction mixture was then poured into Et₂O (1 L) to precipitate phosphine oxides and KBr, filtered to remove phosphine oxides and KBr, dried over MgSO₄, filtered, and concentrated via rotovapory distillation. The crude reaction mixture was further purified by flash column chromatography (40:60 CH₂Cl₂ : hexanes) to provide a mixture of *cis/trans* (69:31) olefinated product **2.23** as a clear oil (1.30

g, 80% yield) which was concentrated in vacuo (100 mTorr) and used for further syntheses as the mixture of *cis* and *trans* isomers. ^1H NMR (500 MHz, methylene chloride- d_2) δ 7.17 – 6.50 (m, 4H), 6.28 (dq, $J = 15.9, 6.7$ Hz, 0.29 H (*trans*)), 5.88 (dq, $J = 11.6, 7.1$ Hz, 0.71 H (*cis*)), 4.55 (hept, $J = 6.1$ Hz, 1H), 1.93 (ddd, $J = 33.9, 6.9, 1.8$ Hz, 3H), 1.43 – 1.37 (m, 16H). ^{13}C NMR (500 MHz, methylene chloride- d_2) δ 153.05, 128.39, 126.97, 126.80, 124.93, 122.99, 120.20, 120.15, 118.84, 114.90, 114.48, 71.30, 53.88, 53.66, 53.44, 53.29, 53.23, 53.07, 53.01, 38.85, 26.90, 26.89, 22.34, 21.89, 14.39, 13.82.

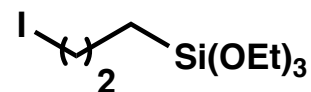
**2.24**

2.23 (1.30 g, 4.71 mmol, 1.00 equiv) was stirred in MeOH (50 mL) at 0 °C in a 250 mL round bottom flask. Solid LiO^tBu (1.885 g, 23.4 mmol, 5 equiv.) was added in one portion and the reaction mixture was allowed to gradually warm to room temperature. After reaction completion by TLC (10:90 hexanes: EtOAc), the reaction mixture was quenched with addition of saturated aqueous NH_4Cl until bubbling ceased. The mixture was added to 500 mL EtOAc and washed with

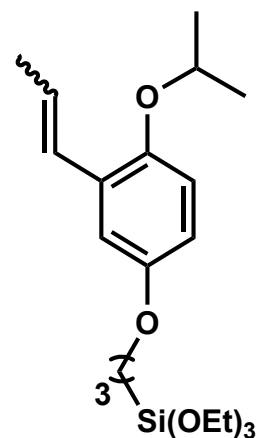
water (3x). The organic layer was dried over MgSO_4 , filtered, concentrated via rotovapory distillation, and further purified by flash column chromatography to provide the desired product as a colorless oil (0.904 g, 95% yield). ^1H NMR (400 MHz, methylene chloride- d_2) δ 6.92 (d, $J = 3.1$ Hz, 1H), 6.86 – 6.76 (m, 2H), 6.73 – 6.62 (m, 2H), 6.56 – 6.46 (m, 1H), 6.22 (dq, $J = 15.9, 6.6$ Hz, 1H), 5.82 (dq, $J = 11.7, 7.1$ Hz, 1H), 4.65 – 4.60 (m, 1H), 4.37 (dtd, $J = 12.1, 6.1, 0.5$ Hz, 1H), 1.91 (dd, $J = 6.7, 1.8$ Hz, 1H), 1.87 (dd, $J = 7.1, 1.9$ Hz, 3H), 1.32 (d, $J = 6.1$ Hz, 3H), 1.30 (d, $J = 6.1$ Hz, 6H). ^{13}C NMR (500 MHz, CD_2Cl_2) δ 149.69, 149.08, 129.26, 126.59, 126.27, 125.45, 125.35, 117.09, 116.71, 114.08, 113.94, 112.27, 72.14, 71.99, 21.94, 18.57, 14.48. HRMS (FAB+): found 192.1168, calculated 192.1150.



A flame dried Schlenk tube was charged with $\text{HSi}(\text{OEt})_3$ (5.5 mL, 0.030 mmol, 1.3 equiv.) and 11-bromo-1-undecene (5.0 mL, 22.8 mmol, 1.0 equiv.). A 0.05 M solution of Karstedt's Pt^0 catalyst (1.125 mL, 0.04 equiv.) was added via needle and syringe and the mixture stirred at 50 °C for 4 hours. 11-bromoundecyl)triethoxysilane was obtained from flash column chromatography (1% to 3% Et_2O : pentane) (visualized TLC with phosphomolybdic acid stain) as a clear oil. ^1H NMR (400 MHz, chloroform- d) δ 3.84 (q, $J = 7.0$ Hz, 6H), 3.43 (t, $J = 6.9$ Hz, 2H), 1.94 – 1.80 (m, 2H), 1.51 – 1.19 (m, 26H), 0.73 – 0.48 (m, 2H). ^{13}C NMR (400 MHz, chloroform- d) δ 58.31, 34.12, 33.21, 32.86, 29.56, 29.50, 29.45, 29.25, 28.79, 28.20, 22.77, 18.33, 10.39.



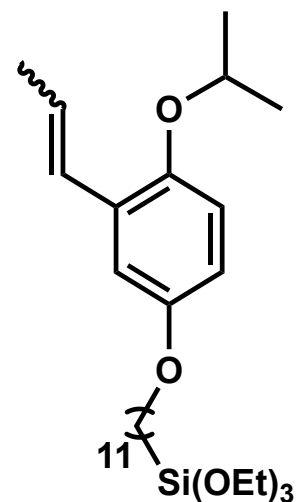
A 100 mL 2-neck round bottom flask was charged with (3-chloro-propyl)triethoxysilane (4.8 g, 0.20 mmol, 1.0 equiv.) and dissolved in dry acetone (30 mL). Recently dried solid NaI (12.0 g, 0.80 mmol, 4.0 equiv.) was added and the suspension stirred for 16 hours. The mixture was poured into pentane (100 mL) to precipitate inorganic salts and concentrated in vacuo (100 mTorr). The yellow oil was then flushed through a silica plug with 10:90 Et₂O: pentane and concentrated in vacuo (100 mTorr) to yield a 75:25 mixture of (3-iodo-propyl)triethoxysilane: (3-chloro-propyl)triethoxysilane which was used without further purification. ¹H NMR (400 MHz, benzene-*d*₆) δ 3.72 (qd, *J* = 7.0, 2.9 Hz, 6H), 3.20 (t, *J* = 6.8 Hz, 0H), 2.83 (t, *J* = 7.0 Hz, 0H), 1.91 – 1.76 (m, 0H), 1.12 (td, *J* = 7.0, 1.6 Hz, 1H), 0.73 – 0.49 (m, 0H).



2.25

Phenol **2.24** (0.120 g, 0.624 mmol, 1.0 equiv.) was stirred in CH₃CN (5 mL) in an oven dried 20 mL vial with septum cap. Solid Cs₂CO₃ (0.305 g, 0.936 mmol,

1.50 equiv.) was flame dried inside a 50 mL 2-neck round bottom flask. The phenol/CH₃CN solution was transferred via needle and syringe to the 2-neck flask and rinsed with an additional 5 mL CH₃CN which was transferred to the 2-neck flask. (3-iodo-propyl) triethoxysilane (0.50 mL, 75% purity) was added via needle and syringe. The reaction mixture stirred at reflux for 16 hours at which point TLC confirmed complete consumption of starting material. The reaction mixture was diluted with 1:1 pentane: Et₂O, the solid precipitate filtered off, and the organic layer concentrated via rotovapory distillation. The crude product was purified via flash column chromatography (3:97 EtOAc: hexanes) to provide **2.25** as a clear colorless oil (0.174 g, 70% yield). ¹H NMR (400 MHz, chloroform-*d*) δ 7.09 – 6.46 (m, 4H), 6.21 (dq, *J* = 15.9, 6.6 Hz, 1H), 6.30 – 5.71 (m, 1H), 5.81 (dq, *J* = 11.6, 7.1 Hz, 1H), 4.36 (dp, *J* = 7.7, 6.0 Hz, 1H), 3.92 (td, *J* = 6.7, 1.5 Hz, 2H), 3.86 (qd, *J* = 7.0, 0.7 Hz, 6H), 1.98 – 1.78 (m, 5H), 1.32 (dd, *J* = 9.0, 6.1 Hz, 6H), 1.25 (td, *J* = 7.0, 0.9 Hz, 9H), 0.86 – 0.70 (m, 2H). ¹³C NMR (400 MHz, CDCl₃) δ 153.46, 152.80, 149.67, 148.75, 129.68, 129.26, 126.65, 126.09, 125.84, 125.68, 117.13, 116.86, 116.53, 113.63, 113.33, 111.99, 77.23, 72.32, 72.27, 70.47, 70.40, 58.43, 58.32, 22.89, 22.27, 18.90, 18.46, 18.32, 14.78, 6.51. HRMS (FAB+),: found 397.1765, calculated 397.1773.

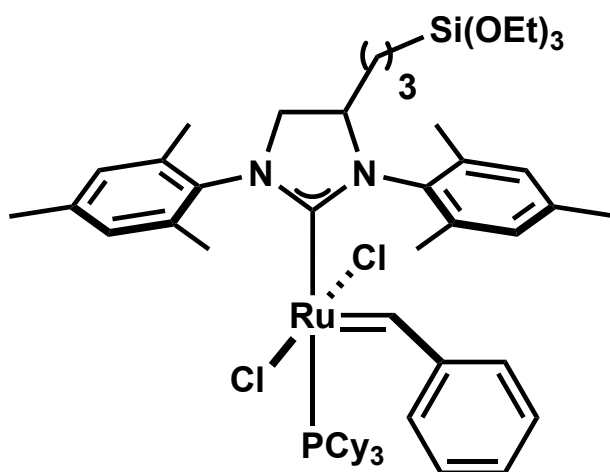
**2.26**

Phenol **2.24** (0.290 g, 1.51 mmol, 1.00 equiv.) was stirred in CH₃CN (15 mL) in an oven dried 20 mL vial with septum cap. Solid Cs₂CO₃ (0.736 g, 2.26 mmol, 1.50 equiv.) was flame dried inside a 100 mL 2-neck round bottom flask. The phenol/CH₃CN solution was transferred via needle and syringe to the 2-neck flask and rinsed with an additional 15 mL CH₃CN which was transferred to the 2-neck flask. (11-bromoundecyl)triethoxysilane (0.800 g, 2.06 mmol, 1.37 equiv.) was added via needle and syringe. The reaction mixture stirred at reflux overnight. The reaction mixture was diluted with 1:1 pentane: Et₂O and the solid precipitate filtered off, and the organic layer concentrated via rotovapory distillation. The crude product was purified via flash column chromatography (2:98 EtOAc: hexanes) to provide **2.26** as a clear, colorless oil (0.492 g, 64% isolated yield). ¹H NMR (400 MHz, chloroform-*d*) δ 7.01 – 6.48 (m, 4H), 5.82 (dq, *J* = 11.6, 7.1 Hz, 1H), 4.36 (dp, *J* = 7.5, 6.0 Hz, 1H), 3.93 (td, *J* = 6.6, 1.0 Hz, 2H), 3.84 (q, *J* = 7.0

Hz, 6H), 1.89 (ddd, $J = 15.3, 6.9, 1.8$ Hz, 3H), 1.78 (pd, $J = 6.6, 2.1$ Hz, 2H), 1.53 – 1.17 (m, 32H), 0.74 – 0.54 (m, 2H). ^{13}C NMR (400 MHz, chloroform- d) δ 129.67, 126.66, 126.10, 125.84, 125.67, 117.12, 116.83, 116.51, 113.58, 113.30, 111.94, 72.31, 68.56, 58.30, 33.23, 29.63, 29.61, 29.56, 29.46, 29.28, 26.10, 22.78, 22.28, 18.91, 18.33, 14.80, 10.39. HRMS (FAB+): found 508.3599, calculated 508.3584.

Homogeneous REMP Catalyst Synthesis

The following was developed from previously reported procedures.¹⁰

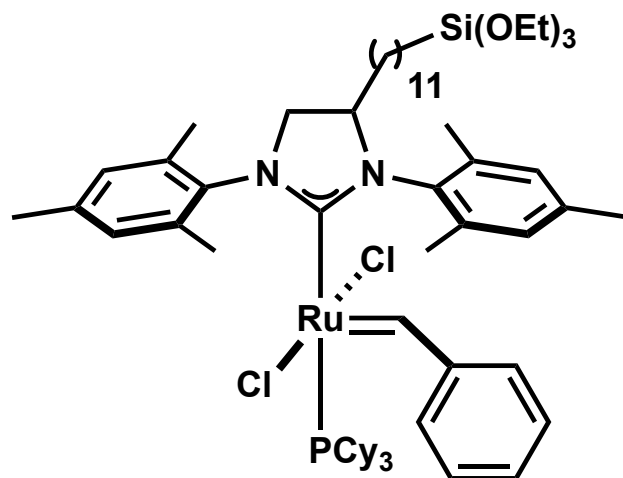


2.27

Outside the glovebox, a vacuum filtration tube half-filled with oven dried celite was fitted to a 25 mL 2-neck round bottom flask containing **2.7** (208 mg, 0.253 mmol, 1.25 equiv.), the first generation Grubbs catalyst. Solid **2.18** (114 mg, 0.202 mmol, 1.00 equiv.) was weighed into a 20 mL vial with stir bar and septum cap inside the glove box and then dissolved in PhCH_3 (2 mL). Solid

KHMDS (42.4 mg, 0.212 mmol, 1.05 equiv.) was dissolved in 2 mL PhCH₃ and transferred to the stirring solution of **2.18**. After 25 minutes, the vial was removed from the glovebox, and the amber solution was transferred via needle and syringe to the top of the celite plug within the vacuum filtration tube. Brief vacuum force was used to draw the solution into the stirring **2.7**. The original vial containing **2.18** was washed with PhCH₃ (5 mL) which was then transferred similarly to the stirring **2.7** via the vacuum filtration tube. After 3 hours, the reaction mixture was transferred directly onto silica gel for column chromatography (without concentration). The silica gel was untreated and the column was run without inert gas. The crude reaction mixture was eluted through the silica column with 10:90 Et₂O: pentane which easily separated the bright purple band (unreacted **2.7**, eluted first), from the pinkish-red band (desired product **2.27**, eluted second). This band was collected and concentrated via rotovapory distillation, redissolved in benzene, transferred to a storage vial, and lyophilized overnight (100 mTorr) to provide **2.27** as a red powder (115 mg, 54% yield). ¹H NMR (400 MHz, benzene-*d*₆) δ 19.69 (s, 1H), 7.03 – 6.88 (m, 5H), 3.69 (dq, *J* = 13.9, 7.0 Hz, 6H), 2.50 (d, *J* = 11.4 Hz, 6H), 2.21 (d, *J* = 15.7 Hz, 6H), 1.83 (d, *J* = 20.5 Hz, 6H), 1.58 (d, *J* = 15.9 Hz, 34H), 1.11 (dt, *J* = 10.6, 7.0 Hz, 32H), 0.43 (dt, *J* = 29.6, 7.9 Hz, 2H). ³¹P NMR (400 MHz, benzene-*d*₆) δ 28.71 (s). ¹³C NMR (400 MHz, C₆D₆) δ 151.66, 151.48, 137.85, 137.59, 137.54, 137.11, 136.88, 135.54, 134.40, 130.26, 129.97, 129.83, 129.41, 128.91, 128.21, 127.80, 127.56, 127.02, 64.63, 58.12, 58.09,

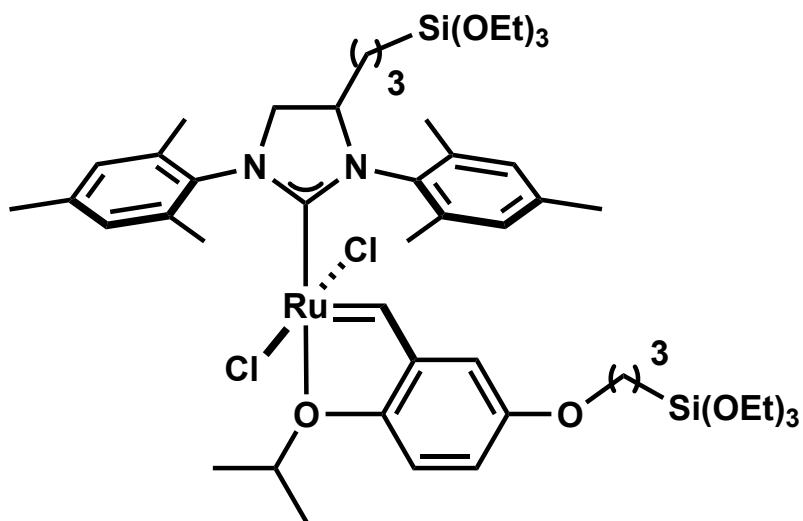
57.08, 36.44, 31.68, 31.51, 29.26, 27.91, 27.81, 26.25, 22.10, 20.89, 20.82, 20.72, 20.65, 20.30, 20.13, 19.99, 19.01, 18.78, 18.23, 18.20, 10.58, 10.48. HRMS (FAB+): found 1052.450, calculated 1052.449.

**2.28**

Outside the glovebox, a vacuum filtration tube with oven dried celite was fitted to a 50 mL 2-neck round bottom flask containing **2.7** (258 mg, 0.313 mmol, 1.25 equiv.), the first generation Grubbs catalyst. Solid **2.19** (172 mg, 0.261 mmol, 1.00 equiv.) was weighed into a 20 mL vial with stir bar and septum cap inside the glove box and then dissolved in 4 mL PhCH₃. Solid KHMDS (57 mg, 0.212 mmol, 1.10 equiv.) was dissolved in 4 mL PhCH₃ and transferred to the stirring solution of **2.19**. After 30 minutes, the vial was removed from the glovebox, and the amber solution was transferred via needle and syringe to the top of the

celite plug within the vacuum filtration tube. Brief vacuum force was used to draw the solution into the stirring **2.7**. The original vial containing **2.19** was washed with PhCH₃ (6 mL) which was then transferred via needle and syringe to **2.7** while stirring via the vacuum filtration tube. After 5 hours, the reaction mixture was transferred directly onto silica gel for column chromatography without concentration, via rotovapory distillation or otherwise. The silica gel was untreated and the column was run without inert gas. The crude reaction mixture was eluted through the silica column with 10:90 Et₂O: pentane which easily separated the bright purple band (unreacted **2.7**, eluted first), from the pinkish-red band (desired product **2.28**, eluted second). A green band developed at the top of the column but could not be eluted with any solvent and was never identified. The pinkish-red band was collected and concentrated via rotovapory distillation, redissolved in benzene, transferred to a storage vial, and lyophilized overnight (100 mTorr) to provide **2.28** as a sticky red solid (204 mg, 85% yield). ¹H NMR (400 MHz, benzene-*d*₆) δ 19.68 (s, 1H), 6.96 (q, *J* = 5.8 Hz, 7H), 3.82 (qd, *J* = 7.0, 1.6 Hz, 11H), 2.49 (d, *J* = 11.6 Hz, 6H), 2.21 (d, *J* = 13.8 Hz, 6H), 1.83 (d, *J* = 18.6 Hz, 7H), 1.71 – 1.47 (m, 34H), 1.18 (td, *J* = 7.0, 1.5 Hz, 17H), 0.82 – 0.74 (m, 4H). ³¹P NMR (400 MHz, benzene-*d*₆) δ 28.76 (s). ¹³C NMR (101 MHz, C₆D₆) δ 151.64, 151.45, 139.11, 137.96, 137.73, 137.54, 137.21, 137.00, 136.68, 135.57, 134.41, 130.28, 130.08, 129.99, 129.86, 129.44, 129.14, 128.95, 64.75, 58.30, 58.27, 58.11, 57.25, 35.74, 35.13, 33.27, 31.95, 31.76, 31.67, 31.51, 31.39, 31.26, 29.78, 29.70,

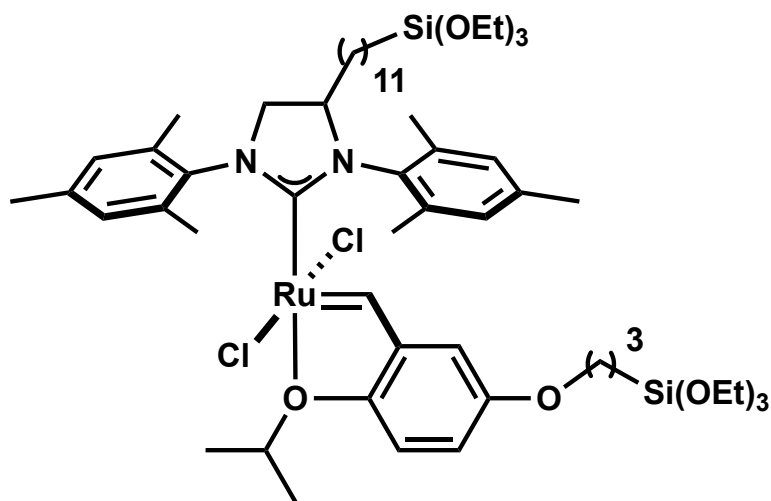
29.67, 29.60, 29.55, 29.53, 29.49, 29.47, 29.45, 29.39, 29.29, 29.28, 27.91, 27.81, 27.73, 27.64, 26.94, 26.82, 26.62, 26.48, 26.45, 26.40, 26.25, 23.16, 22.11, 20.89, 20.82, 20.76, 20.72, 20.65, 20.42, 20.33, 20.31, 19.05, 18.80, 18.31, 10.86. HRMS (FAB+): found 1164.575, calculated 1164.574.



2.29

Solid **2.27** (58.9 mg, .0551 mmol, 1.00 equiv.) was weighed into a 20 mL vial inside the glove box and then dissolved in PhCH₃ (5 mL). **2.25** (65.6 mg, 0.165 mmol, 3.00 equiv.) was dissolved in PhCH₃ (2 mL) and this solution was transferred to the dark red stirring solution of **2.27**. The reaction mixture turned brown over the course of 60 minutes, at which point CuCl (10 mg) was added directly to the solution as a powdery white solid. This suspension stirred in the glovebox for 4 hours and gradually became a forest green color during this period. This solution was transferred directly to a 10:90 Et₂O: pentane silica gel column and a few column volumes of 10:90 Et₂O: pentane were flushed through to elute an

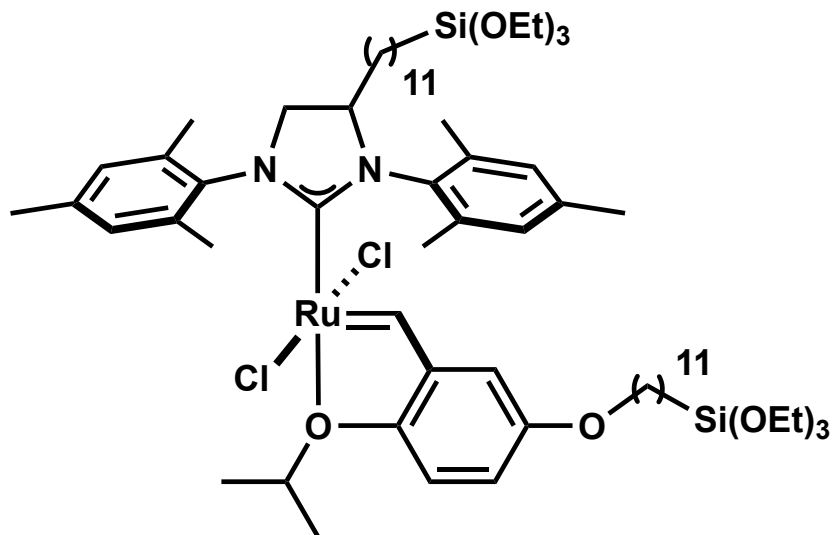
undesired broad yellow band. 30:70 Et₂O: pentane was then used to elute the green band which was collected, concentrated via rotovapory distillation, redissolved in Et₂O, transferred to a storage vial, concentrated in vacuo (100 mTorr) to provide **2.29** as a dark green sticky solid (48 mg, 82%). ¹H NMR (400 MHz, benzene-*d*₆) δ 16.55 (s, 1H), 6.92 (dd, *J* = 8.9, 2.9 Hz, 1H), 6.73 (d, *J* = 3.0 Hz, 1H), 6.34 – 6.14 (m, 1H), 4.44 (hept, *J* = 6.1 Hz, 1H), 4.32 – 4.18 (m, 1H), 3.77 (dq, *J* = 30.4, 7.0 Hz, 11H), 3.62 (t, *J* = 10.2 Hz, 1H), 3.48 (t, *J* = 10.2 Hz, 1H), 2.25 (d, *J* = 14.0 Hz, 5H), 2.09 – 1.97 (m, 2H), 1.86 – 1.57 (m, 2H), 1.37 – 1.25 (m, 6H), 1.25 – 1.11 (m, 16H), 0.98 – 0.81 (m, 2H), 0.51 (t, *J* = 7.9 Hz, 2H).



2.31

Solid **2.28** (56 mg, 0.048 mmol, 1.0 equiv.) was dissolved in PhCH₃ (4 mL) in a 20 mL vial inside the glovebox. **2.25** (57 mg, 0.144 mmol, 3.0 equiv.) was dissolved in PhCH₃ (4 mL) and transferred to the stirring solution of **2.28**. The solution turned brown over the course of 1 hour, at which point CuCl (20 mg) was

added as a solid white powder. The reaction mixture turned green after 4 hours, and after an additional hour, it was added directly to a 10:90 Et₂O: pentane silica gel column and a yellow band eluted first. The green band of desired product **2.31** was eluted using 25:75 Et₂O: pentane, collected, concentrated via rotovapory distillation, redissolved in Et₂O, and transferred to a 20 mL storage vial, concentrated in vacuo to give **2.31** as a dark green sticky solid (34.9 mg, 62% yield). ¹H NMR (400 MHz, benzene-*d*₆) δ 16.32 (s, 1H), 6.70 (dd, *J* = 8.9, 3.0 Hz, 1H), 6.51 (d, *J* = 3.0 Hz, 1H), 6.09 – 5.84 (m, 1H), 4.22 (hept, *J* = 6.1 Hz, 1H), 4.02 (tt, *J* = 11.5, 7.3 Hz, 1H), 3.61 (q, *J* = 7.1 Hz, 1H), 3.44 (dd, *J* = 11.6, 8.7 Hz, 1H), 3.22 (t, *J* = 10.2 Hz, 1H), 2.03 (d, *J* = 13.1 Hz, 6H), 1.88 – 1.71 (m, 2H), 1.50 – 1.38 (m, 3H), 1.19 – 1.06 (m, 8H), 0.97 (td, *J* = 7.0, 3.6 Hz, 17H), 0.84 – 0.72 (m, 2H), 0.70 – 0.61 (m, 2H), 0.61 – 0.54 (m, 2H). ¹³C NMR (400 MHz, C₆D₆) δ 154.53, 146.39, 145.85, 140.26, 138.24, 138.20, 129.99, 129.54, 129.25, 128.32, 127.80, 127.57, 114.51, 112.94, 107.58, 74.41, 70.43, 58.24, 58.13, 34.03, 33.30, 30.56, 30.11, 29.74, 29.72, 29.65, 29.57, 29.49, 29.43, 26.98, 26.15, 25.82, 23.19, 21.08, 20.75, 20.68, 18.31, 18.29, 10.89, 6.91.

**2.32**

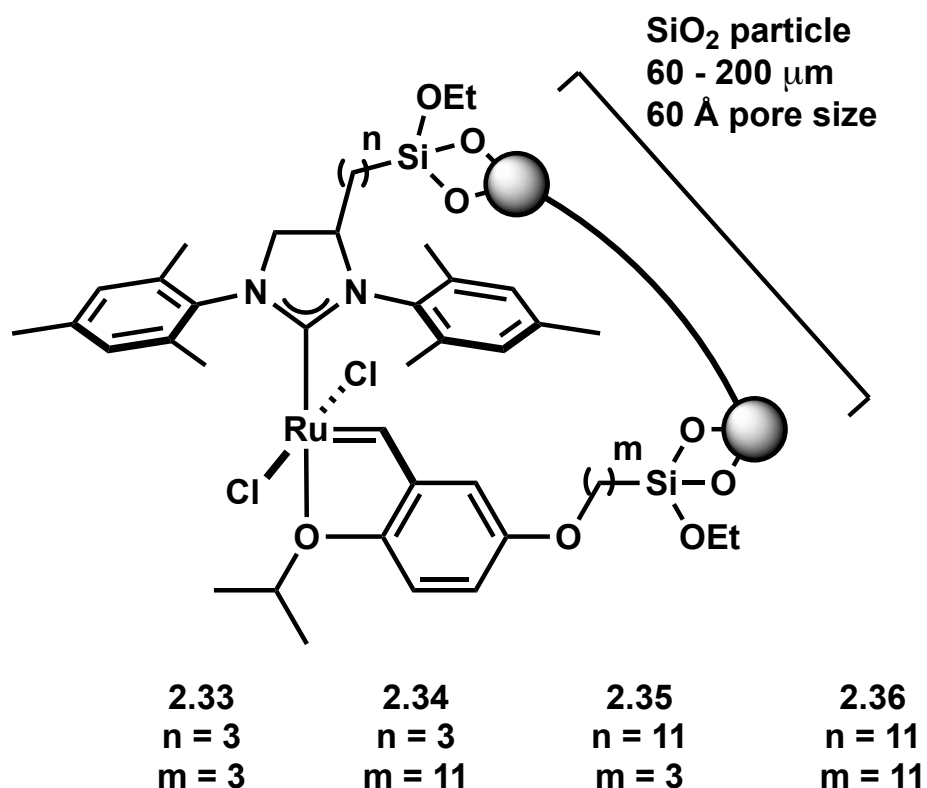
Solid **2.28** (56 mg, 0.048 mmol, 1.0 equiv.) was dissolved in PhCH₃ (4 mL) in a 20 mL vial inside the glovebox. **2.26** (73.3 mg, 0.144 mmol, 3.0 equiv) was dissolved in PhCH₃ (4 mL) and transferred to the stirring solution of **2.28**. The solution turned brownish green over the course of 1 hour, at which point CuCl (20 mg) was added as a solid white powder. The reaction mixture turned green after 4 hours, and after an additional hour it was added directly to a 10:90 Et₂O: pentane silica gel column and a yellow band eluted first. The green band of desired product **2.32** was eluted using 30:70 Et₂O: pentane, collected, concentrated via rotovapory distillation, redissolved in Et₂O, and transferred to a 20 mL storage vial, and concentrated in vacuo to give **2.32** as a dark green sticky solid (34.9 mg, 62% yield).

¹H NMR (400 MHz, benzene-*d*₆) δ 16.35 (s, 1H), 6.72 (dd, *J* = 8.9, 3.0 Hz, 1H), 6.52 (d, *J* = 2.9 Hz, 1H), 6.22 – 5.64 (m, 1H), 4.24 (p, *J* = 6.2 Hz, 1H), 4.09 – 3.92 (m,

1H), 3.61 (qd, $J = 7.0, 3.6$ Hz, 11H), 3.54 – 3.40 (m, 2H), 3.22 (t, $J = 10.1$ Hz, 1H), 2.04 (d, $J = 12.9$ Hz, 6H), 1.53 – 1.37 (m, 4H), 1.26 – 1.17 (m, 4H), 1.16 – 1.05 (m, 19H), 0.97 (td, $J = 7.0, 3.3$ Hz, 17H), 0.84 – 0.72 (m, 2H), 0.63 – 0.53 (m, 4H).

Supported Molecular REMP Catalysts 2.33 – 2.36

The following was developed from previously reported procedures.¹⁰



General Procedure for 2.33 – 2.36: The corresponding molecular REMP catalyst (2.29-2.32) (0.100 mmol) was weighed into a 40 mL scintillation vial inside the glovebox and dissolved in PhCH₃ (10 mL). SiO₂ (5.00 g) was added as a powder along with stir bar and enough PhCH₃ to create a SiO₂/PhCH₃ slurry. The

suspension was then stirred in the glovebox for 3.5 days. The vial was then removed from the glove box, and the supernatant of the slurry was decanted. The slurry was concentrated in vacuo until it was a free-flowing green powder (100 mTorr, >1 day). At this point, the green powder was transferred to a cellulose extraction thimble and placed in a flame-dried Soxhlet extraction apparatus, under positive argon flow. The green powder was then continuously extracted with CH_2Cl_2 for 10 days. The extraction thimble was removed from the Soxhlet extraction apparatus, placed in a jar within a vacuum chamber and concentrated in vacuo (100 mTorr, 2 days). See Appendix for solid state ^1H NMR spectrum of

2.34.

2.5 – References

- (1) Bielawski, C. W.; Grubbs, R. H. *Science* **2002**, 297 (5589), 2041–2044.
- (2) Trnka, T. M.; Grubbs, R. H. *Acc. Chem. Res.* **2001**.
- (3) Bielawski, C. W.; Benitez, D.; Grubbs, R. H. *J. Am. Chem. Soc.* **2003**, 125 (28), 8424–8425.
- (4) Boydston, A. J.; Xia, Y.; Kornfield, J. A.; Gorodetskaya, I. A.; Grubbs, R. H. *J. Am. Chem. Soc.* **2008**, 130 (38), 12775–12782.
- (5) Xia, Y.; Boydston, A. J.; Yao, Y.; Kornfield, J. A.; Gorodetskaya, I. A.; Spiess, H. W.; Grubbs, R. H. *J. Am. Chem. Soc.* **2009**, 131 (7), 2670–2677.
- (6) Xia, Y.; Boydston, A. J.; Yao, Y.; Kornfield, J. A.; Gorodetskaya, I. A.; Spiess, H. W.; Grubbs, R. H. *J. Am. Chem. Soc.* **2009**, 131 (7), 2670–2677.
- (7) Xia, Y.; Boydston, A. J.; Grubbs, R. H. **2011**, 50 (26), 5882–5885.
- (8) Boydston, A. J.; Holcombe, T. W.; Unruh, D. A.; Fréchet, J. M. J.; Grubbs, R. H. *J. Am. Chem. Soc.* **2009**, 131 (15), 5388–5389.
- (9) Bielawski, C. W.; Benitez, D.; Grubbs, R. H. *J. Am. Chem. Soc.* **2003**, 125 (28), 8424–8425.
- (10) Allen, D.; Giardello, M. August 30, 2016, pp 1–57.
- (11) Allen, D. P.; Van Wingerden, M. M.; Grubbs, R. H. *Org. Lett.* **2009**, 11 (6), 1261–1264.
- (12) Pastva, J.; Čejka, J.; Žilková, N.; Mestek, O.; Rangus, M.; Balcar, H. *“Journal of Molecular Catalysis. A, Chemical”* **2013**, 378, 184–192.
- (13) Monge-Marcet, A.; Pleixats, R.; Cattoën, X.; Wong Chi Man, M. *Tetrahedron* **2013**, 69 (1), 341–348.
- (14) Monge-Marcet, A.; Pleixats, R.; Cattoën, X.; Wong Chi Man, M. *“Journal of Molecular Catalysis. A, Chemical”* **2012**, 357, 59–66.
- (15) Pangborn, A. B.; Giardello, M. A.; Grubbs, R. H.; Rosen, R. K.; Timmers, F. J. *Organometallics* **1996**, 15, 1518–1520.

Chapter 3

Initial Investigations with Supported Molecular REMP Catalysts

3.0 – Abstract

Successful development of a supported molecular REMP catalyst system was achieved, thereby creating the opportunity to explore its polymerization profiles and topological fidelity for the REMP of cycloolefin monomers. The polymerization profiles of CP, COE, and COD were compared and CP was chosen for subsequent experiments due to its superior processability. Optimization experiments for CP REMP were conducted such that multi-gram quantities of cyclic polycyclopentene could be achieved. Topological fidelity of CP REMP reactions were found to depend on a variety of reaction conditions: monomer purity, choice of solvent, and oxygen contamination. The purity of cyclic polycyclopentene was determined using interaction chromatography.

Chapter 3 Acknowledgments

Bob Grubbs, Scott Virgil

Anthony Ndiripo and Harald Pasch (University of Stellenbosch, South Africa)

3.1 – Introduction

The use of a simple cycloalkene hydrocarbon monomer has been an important aspect of the REMP project since its inception. Unbranched, main-chain polymers lacking heteroatoms were thought to be the best starting point for investigation of the physical properties of melt-state cyclic polymers. Such investigations are more straightforward for simple polymer compositions.^{1,2} Additionally, the physical properties of polyethylene (PE) have been thoroughly studied in the literature and would be useful for comparison to the PE derived from our hydrogenated REMP polymers.¹

The most attractive monomers for initial investigations were cyclopentene (CP), cyclooctene (COE), and cyclooctadiene (COD) due to commercial availability and precedent for their participation in ROMP and REMP reactions. ROMP reactions with CP, COE, and COD were envisioned as a predictor for the polymerization profiles of the more challenging and time-consuming REMP syntheses. These polymers would also constitute a library of linear polymers of varying MW and \bar{D} and would provide the linear component in physical blends of ROMP- and REMP-derived polymers of varying composition which could be used in the development of a protocol to quantify the cyclic:linear purity and to establish an analytical detection limit for the same.

A variety of metathesis catalysts were available for exploring the polymerization profiles of low ring strain monomers: the supported molecular REMP catalyst **3.0** and the ROMP catalysts **3.1 – 3.6** (Fig 3.1).

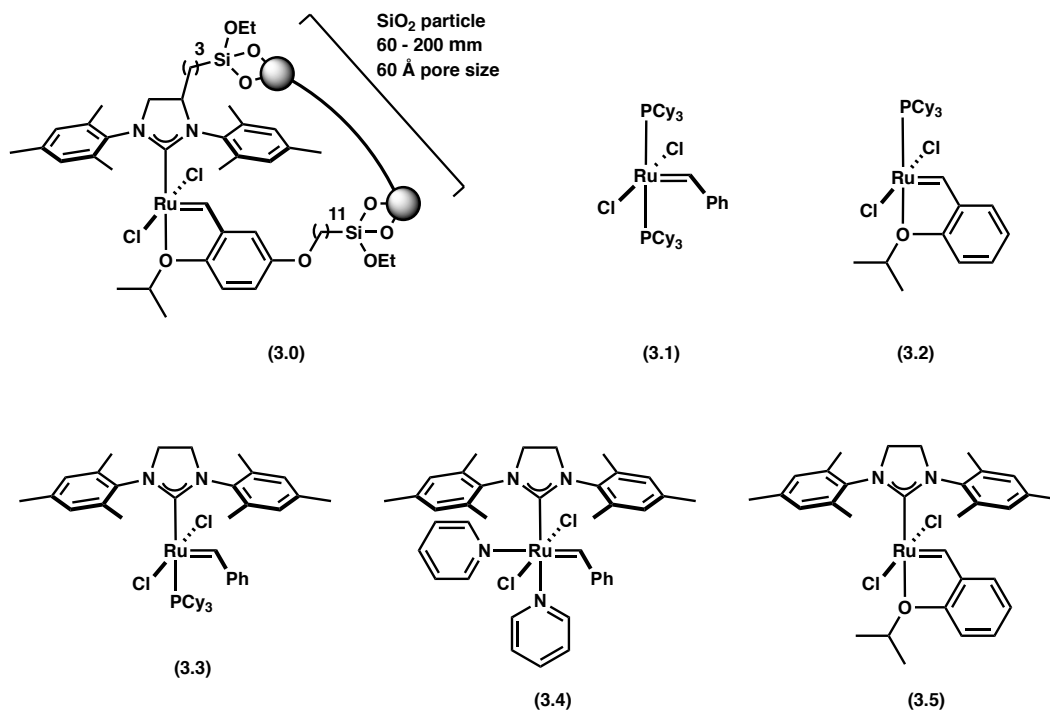


Figure 3.1 | The REMP (3.0) and ROMP (3.1 – 3.5) catalysts considered for experiment design.

The importance of linear impurity in REMP reactions was reported in our group before the outset of the work described in this chapter.² Although a quantitative description of the effects of linear olefin impurity does not exist for REMP, the mechanism by which it was thought to be deleterious was well understood. Every molecule of linear impurity which reacts during REMP (Fig 3.2, red) produces one linear chain. Exclusion of linear olefin impurity and anything which could cause catalyst decomposition was a necessary consideration throughout the design and implementation of the REMP methodology described in this chapter.

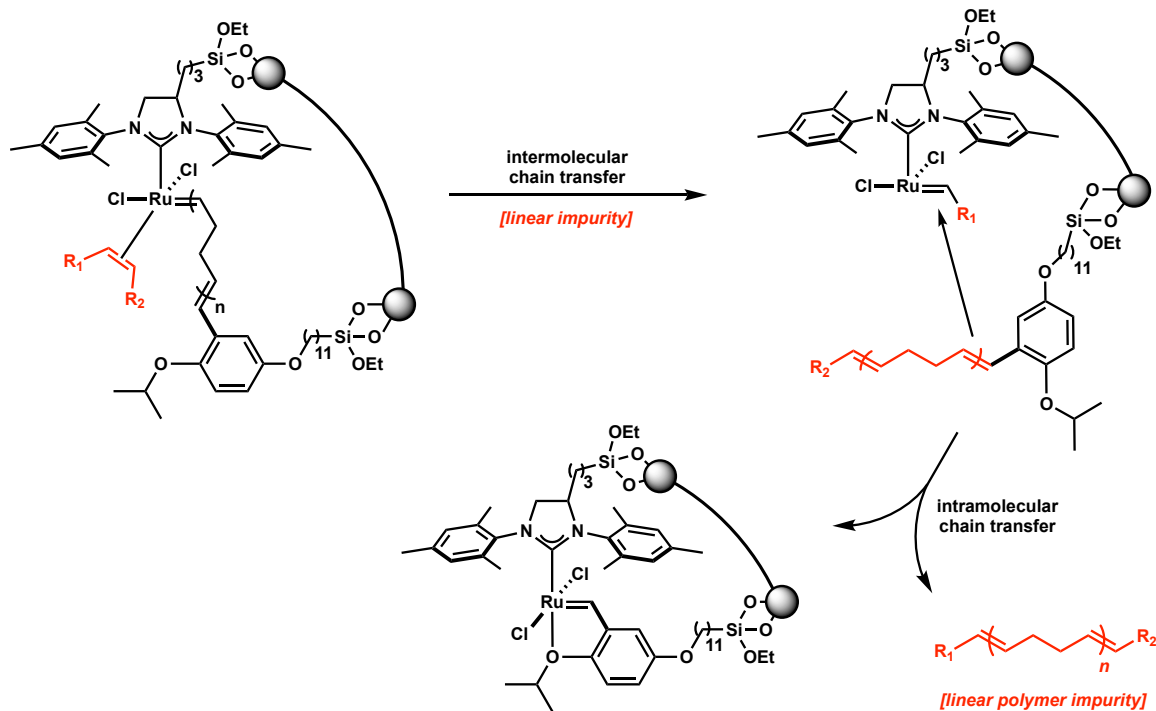


Figure 3.2 | The effect of linear impurity in REMP reactions catalyzed by **3.0**.

3.2 – Results and Discussion

Once a sufficient quantity of catalyst **3.0** was available, an investigation of its polymerization profile and topological selectivity became our primary focus. The supported REMP catalyst **3.0** was used for all cyclic polymers described in this chapter. COE and COD were chosen as the first monomers for exploration of the new catalyst system due to the higher ring strain they possess relative to CP. This ring-strain would provide the enthalpic driving force of polymerization such that higher MW and narrower \bar{D} could be achieved.³ The relative frequency of chain transfer events (secondary metathesis) to monomer propagation (productive metathesis) increases as monomer ring strain decreases. Similarly, at

[monomer]/[polymer] steady-state, low ring strain decreases the frequency of the desired intramolecular chain transfer event which releases a polymer chain, and increases the frequency of undesired monomeric and oligomeric depolymerization events which decrease yield and M_n .

The study of ROMP and REMP profiles of COE and COD was conducted using six individual ruthenium-based metathesis catalysts (Fig 3.1). The development of experimental ROMP procedures and conditions was desired to both serve as a model for REMP reactions with **3.0** (investigation of **3.0** as a polymerization catalyst was unprecedented) and to produce the library of linear polymers for comparison to their cyclic counterparts. To accomplish this, homogeneous catalysts **3.1** – **3.5** were used to provide control of the molecular weight distributions of linear PCOE and PBD due to their distinct initiation and propagation rates (k_i and k_p , respectively). The ratio k_i/k_p is well known to dictate the polymerization characteristics of olefin metathesis catalysts.⁴⁻⁸

Initially, COE and COD were successfully polymerized with catalysts **3.1**–**3.5** to high yields (>80%), but were consistently either nearly insoluble or completely insoluble in common organic solvents. This was initially attributed to secondary metathesis reactions leading to abundant chain transfer and thus high M_w and broad \mathcal{D} . Their extremely low solubility in common solvents precluded the acquisition of reliable data. Although the importance of removing impurity from monomer prior to polymerization was known, the extent to which this was

absolutely critical was not initially appreciated. In lieu of problems with COE and COD, ROMP and REMP experiments with CP were then undertaken.

Although initial experiments were somewhat successful, the low M_n and broad dispersity of both linear and cyclic PCP were unacceptably poor. Optimization experiments were begun to improve these properties, but concomitant decomposition of PCP—evident from gradual discoloration and decreasing solubility in common solvents—suggested greater rigor preparing monomer stocks prior to polymerization was necessary.

The lack of instrumentation necessary to determine CP purity necessitated a different approach to assessing purity. An appropriate GC column to separate CP (bp = 44 °C) was not available. The addition of linear olefin chain transfer agents (CTAs) has been well established to decrease MW by chain-scission via secondary metathesis reactions during ROMP and REMP.⁹⁻¹¹ Therefore, the polymerization of high purity cyclic monomers should give higher M_n polymers. This phenomenon was exploited in a chemical test to indirectly determine the relative purity of 7 successive distillate fractions of CP. Aliquots of each fraction were polymerized in triplicate under identical conditions (Fig 3.3) and the M_n and yields of the resulting PCP measured (Fig 3.4) to determine relative purity. The fractions with the highest M_n were considered to be the most pure. This indirect means to measure relative purity had not been explicitly reported, but it was validated by results to be discussed later in this chapter.

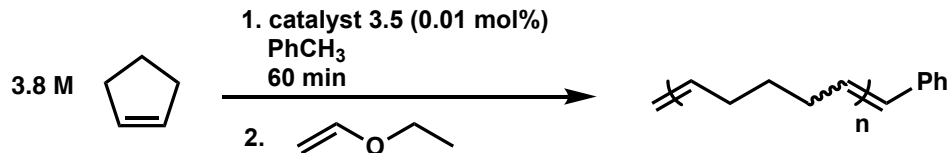


Figure 3.3 | Scheme for the ROMP of 7 successive CP distillate fractions

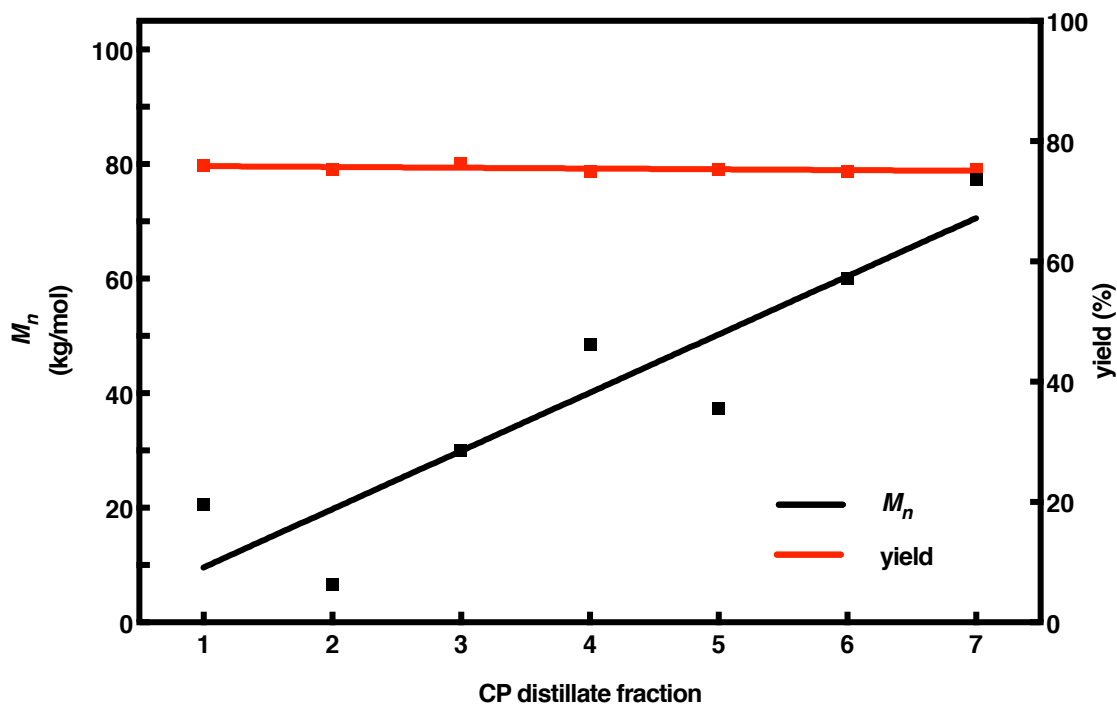


Figure 3.4 | ROMP of 7 successive CP distillate fractions.

The data in Fig 3.4 strongly suggests the presence of CTAs in early CP distillate fractions. The gradual increase in M_n (black line) with the concomitant unchanging yield (red) indicated that the impurity was not inducing catalyst decomposition, which would coincide with reduced yield. Given that ROMP of CP was highly dependent on the purity of the monomer, the rigorous purification of all monomers for both ROMP and REMP was essential.

With the purified CP, we were able to access linear PCP with M_n significantly higher than previously reported examples (Table 3.1).¹²⁻¹⁵

Table 3.1 | The highest MW linear PCPs reported in the literature.

ref.	catalyst loading (ppm)	catalyst	M_n (kg/mol)	\mathcal{D}	time (hr)	yield
Feast et al. (1995)	1700	Mo[NAr][CHC(CH ₃) ₂ Ph][OCBu ^t] ₂	95	1.53	5	-
Register et al. (2000)	100	W(CHBu ^t)(NAr)(OBu ^t) ₂	73	1.08	1	-
Register et al. (2008)	330	Ru(CHPh)(PCy) ₃ (Cl) ₂	106	1.63	6	-
Register et al. (2017)	400	Mo[NAr][CHC(CH ₃) ₂ Ph][OCBu ^t] ₂	290	1.32	6	<35%

Catalyst **3.5** had previously been chosen for the ROMP of CP because it was the closest analog to supported REMP catalyst **3.0** available. After finding that our CP ROMPs were somewhat controlled when using the pure monomer stock, we investigated the ROMP of CP using **3.1** because it is known to restrict back-biting relative to other ROMP catalysts, despite its low activity. We were able to exceed the highest reported MW of PCP by a factor of 5 (Table 3.2, entry **3.16**).

Table 3.2 | ROMP using the most pure CP monomer stock.

entry	catalyst	catalyst loading (ppm)	M_n (kg/mol)	\bar{D}	yield (%)	$[M]_0$ (mol/L)
3.6	3.4	100	116	1.54	52	5.7
3.7	3.4	20	203	1.53	81	5.7
3.8	3.4	10	219	1.51	82	5.7
3.9	3.4	5	205	1.60	82	5.7
3.10	3.4	1	192	1.57	22	5.7
3.11	3.4	0.5	215	1.51	12	11.4
3.12	3.4	5	292	1.48	64	11.4
3.13	3.4	5	258	1.53	87	11.4
3.14	3.4	1	185	1.58	6	11.4
3.15	3.4	5	286	1.46	88	11.4
3.16	3.1	5	1,400	1.42	17	11.4

The ultra-high MW PCP was ultimately unrelated to our goal of producing cyclic polymers via REMP, but we also would not have stumbled across these findings without the extreme rigor in monomer purification for REMP. The ultra-high MW PCP became the subject of ongoing research which will be described later in this dissertation.

A collaboration with the research group of Professor Nikos Hadjichristidis at King Abdullah University of Science and Technology (KAUST) encouraged us to produce the multi-gram quantity of cyclic PCP which would be necessary for his group to perform characterization of its bulk properties. We envisioned a scale-up of CP REMP using catalyst **3.0** would be feasible, and we also sought to determine the feasibility of catalyst **3.0** recycling to produce multiple batches of PCP—this capability was incorporated into our initial catalyst design (Chapter 2), but we had not yet attempted it.

Our large-scale CP REMP succeeded in producing 4 batches of PCP and indicated that low catalyst loading and increased $[CP]_0$ gave higher yields, but control over MW was not achieved (Table 3, **3.17 – 3.20**). During these experiments, PCP was isolated by filtration of the supernatant of the polymerization medium. Solid-supported catalyst **3.0** accumulated on the bottom of the reaction flask and a vertical viscosity gradient was clearly apparent. Filtration was challenging, but nevertheless, we produced quantities sufficient for bulk property analysis.

Table 3.3 | Large-scale catalyst recycling REMP of CP (**3.17 – 3.20**) and REMP viscosity optimization experiments (**3.21 – 3.25**).

entry	solvent	$[CP]_0:[3.0]_0$	M_w (kg/mol)	yield (%)	$[CP]_0$ (mol/L)
3.17	PhCH ₃	48,000	58	70	4.6
3.18	PhCH ₃	24,000	64	31	2.3
3.19	PhCH ₃	24,000	62	30	2.3
3.20	PhCH ₃	10,000	57	56	2.3
3.21	CH ₂ Cl ₂	15,000	44	40	3.3
3.22	4%tBuOH/PhCH ₃	10,000	55	72	3.3
3.23	4%tBuOH/PhCH ₃	10,000	58	71	3.3
3.24	1%tBuOH/PhCH ₃	10,000	55	72	3.3
3.25	PhCH ₃	10,000	50	43	3.3

We assumed a tractable polymerization medium would yield more PCP with narrower dispersity and better material properties, so we attempted to decrease the viscosity of the polymerization medium by changing solvent conditions. PhCH₃ was originally chosen due its low toxicity and reactivity, but CH₂Cl₂ solvated PCP better than any other common solvent. A small-scale REMP

of CP using CH_2Cl_2 was performed (polymer **3.21**) and the filtration was significantly faster (1 minute compared to 45 minutes) because the PCP was well-solvated. Although solvation of the polymerization medium was considerably better with CH_2Cl_2 , catalyst **3.0** particles aggregated and were not evenly dispersed, just as with PhCH_3 .

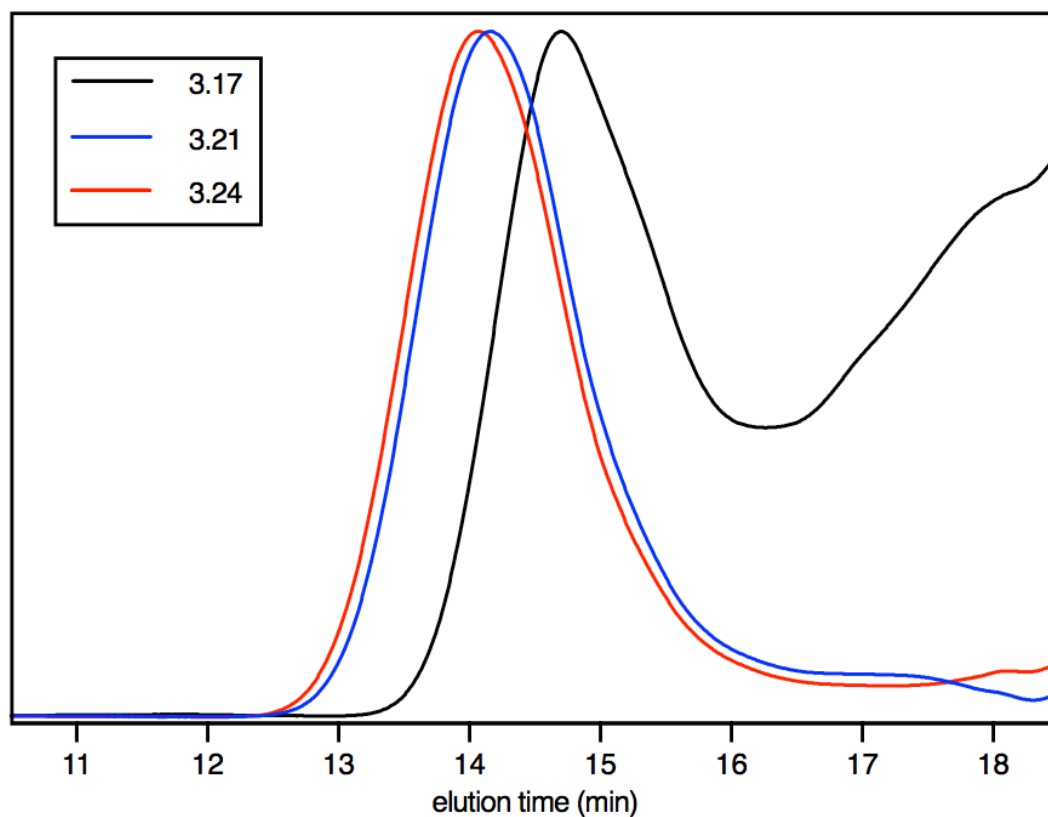


Figure 3.5 | Elution profiles of PCP polymerized in different solvent conditions.

A co-solvent system of $t\text{BuOH}/\text{PhCH}_3$ was explored as a means to disrupt the electrostatic forces responsible for catalyst particle aggregation. The PhCH_3 would be adequate to solvate the polymer, and a small amount of $t\text{BuOH}$ would form solvent shells around the catalyst particles through hydrogen bonding with

the SiOH—terminated surface. Visually, the ^tBuOH additive had a substantial effect on the polymerization: an evenly dispersed suspension of catalyst particles was immediately apparent and the filtration to isolate the polymer was facile (Table 3.3, polymers **3.22** – **3.24**). Polymers **3.22** – **3.24** were well solvated and gave higher yields than the control, **3.25**. The SEC traces for polymers **3.17** (PhCH₃ solvent), polymer **3.21** (CH₂Cl₂ solvent), and polymer **3.24** (^tBuOH/PhCH₃ cosolvent)(Fig 3.5) clearly indicated that good solvents provide narrow D and higher MW. With this important information in hand, our attention then turned to analysis of PCP topological purity.

All of the PCP samples listed in Table 3.3 were analyzed using an HT-HPLC system operating in interaction chromatography (IC) mode, which separates polymers by composition, as opposed to size-exclusion chromatography (SEC), which separates polymers by hydrodynamic volume.¹⁶⁻¹⁸ Other than the type of separation column used, the key distinction of IC vs. SEC is the use of a solvent gradient. Each cyclic chain has a distinct column condition at which it separates from its linear counterpart of the same MW. By gradually varying the composition of the IC eluent, each cyclic chain can be separated from its linear counterpart. This requires a judicious choice of IC column, solvent system, and temperature. For the work described herein, the solvent gradient changed with the relative ratio of 1-decanol to 1,2,4-trichlorobenzene (Fig 3.6).

The IC chromatograms for **3.17** – **3.25** (Fig 3.7) show that topology depends on both monomer purity and choice of solvent. The linear region in

polymers **3.17** – **3.20** was likely due to impurity in the monomer. They were prepared with the second-most pure CP distillate fraction (Fig 3.3, Fraction 6). The purest fraction only consisted of approximately 10 mL, so it could not be used for large-scale REMP experiments.

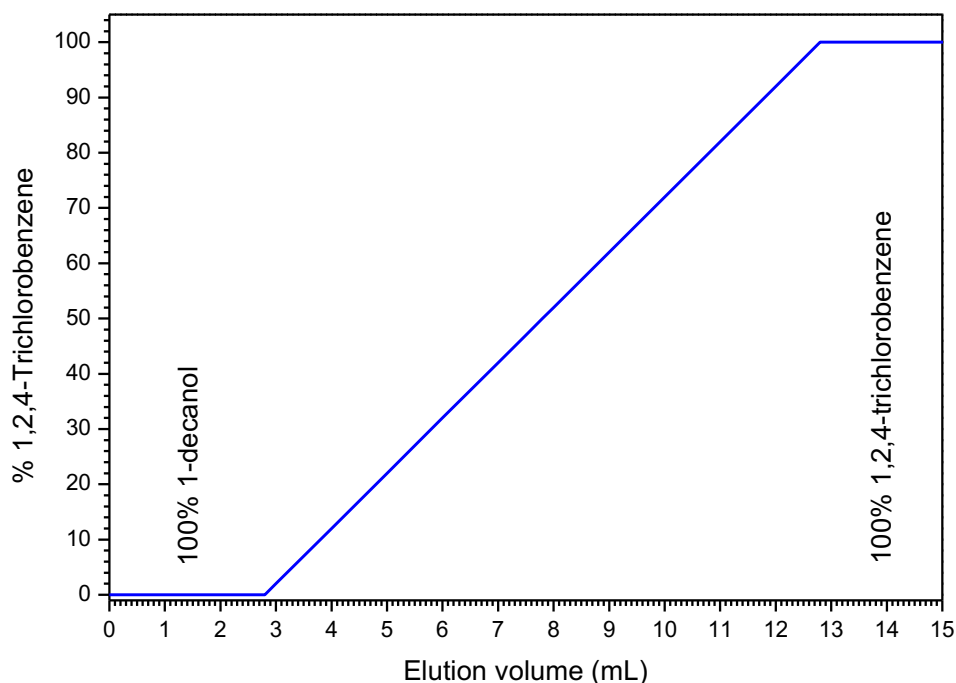


Figure 3.6 | The solvent gradient used in IC for PCP analysis.

The choice of CH_2Cl_2 for **3.21** strongly affected the cyclic purity by IC (Fig 3.5). This may have been due to linear C5 contaminants which were present in the CH_2Cl_2 . To prevent carbene formation, CH_2Cl_2 is often stabilized with 150 ppm amylenes (mixture of pentene isomers), which was the case for solvent used in REMP polymer **3.21**. Alternatively, CH_2Cl_2 may have facilitated deleterious catalyst detachment from the SiO_2 particle surface which would produce linear chains. Similarly, the ${}^t\text{BuOH}/\text{PhCH}_3$ co-solvent system seemed promising, but the

linear region for **3.22** – **3.24** suggests it leads to considerable linear impurity. A definite explanation for this could not be made, but catalyst detachment caused by ^tBuOH may have been the root cause. However, polymer **3.25** appears purely cyclic by IC (Fig 3.7), and polymer **3.24**, produced with only 1% ^tBuOH appears nearly as pure. The instrumentation and techniques available at the time precluded direct measurement of cyclic purity by IC, but we learned about the paramount importance of solvent and monomer purity during REMP nonetheless. Although monomer purity was already known to be important, the extent to which it was important was admittedly not fully appreciated at the outset of this work.

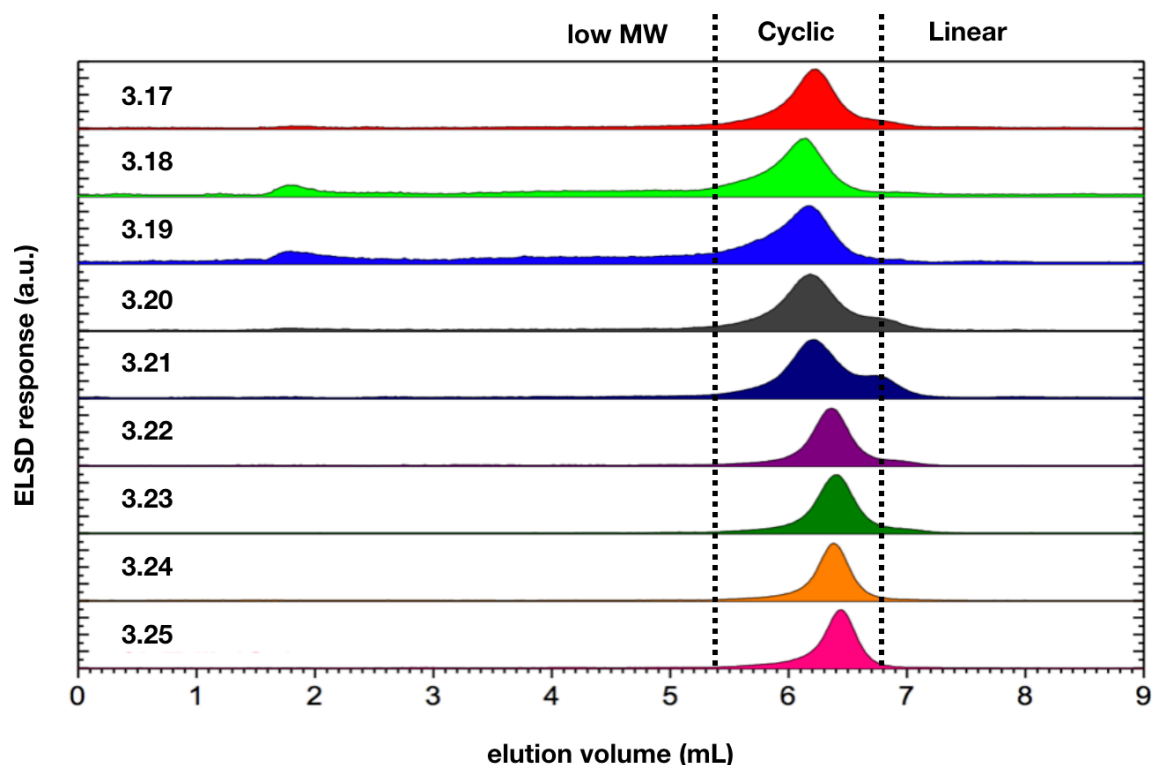


Figure 3.7 | IC of PCPs **3.17** – **3.25** with low MW, cyclic, and linear elution components demarcated by dotted lines.

A 2D IC-SEC elution method was used to ascertain the molecular homogeneity of polymers **3.17** and **3.20** (Fig 3.8). Elution conditions using this technique ideally separate polymers exclusively by either IC or SEC principles. In that case, polymers with topological homogeneity but a distribution of MWs would elute simultaneously in IC (Fig 3.8, y-axis), and be separated only by SEC (Fig 3.8, x-axis). Similarly, polymers with different topologies but identical and monodisperse MWs would elute simultaneously in SEC (Fig 3.8, x-axis), and be separated only by IC (Fig 3.8, y-axis). This ideal case cannot be achieved with modern instrumentation and techniques, but comparisons of the molecular homogeneity can be made based on the topography of the 2D IC-SEC chromatograms. Polymer **3.17** has a more broad and gradually changing evaporative light-scattering detector (ELSD) response than for polymer **3.20** which indicates it is less topologically pure. This can be explained by making an analogy to topographical maps: if **3.17** and **3.20** were mountains, **3.20** would be much steeper than **3.17**; the steeper the "mountain," the more topologically pure it is. We believe **3.17** is less pure topologically than **3.20** because it was produced from REMP catalyst which had been recycled 3 times prior and so levels of adventitious O₂ were likely higher. O₂ would have caused catalyst decomposition which we have long suspected leads to linear polymer impurity.¹⁶

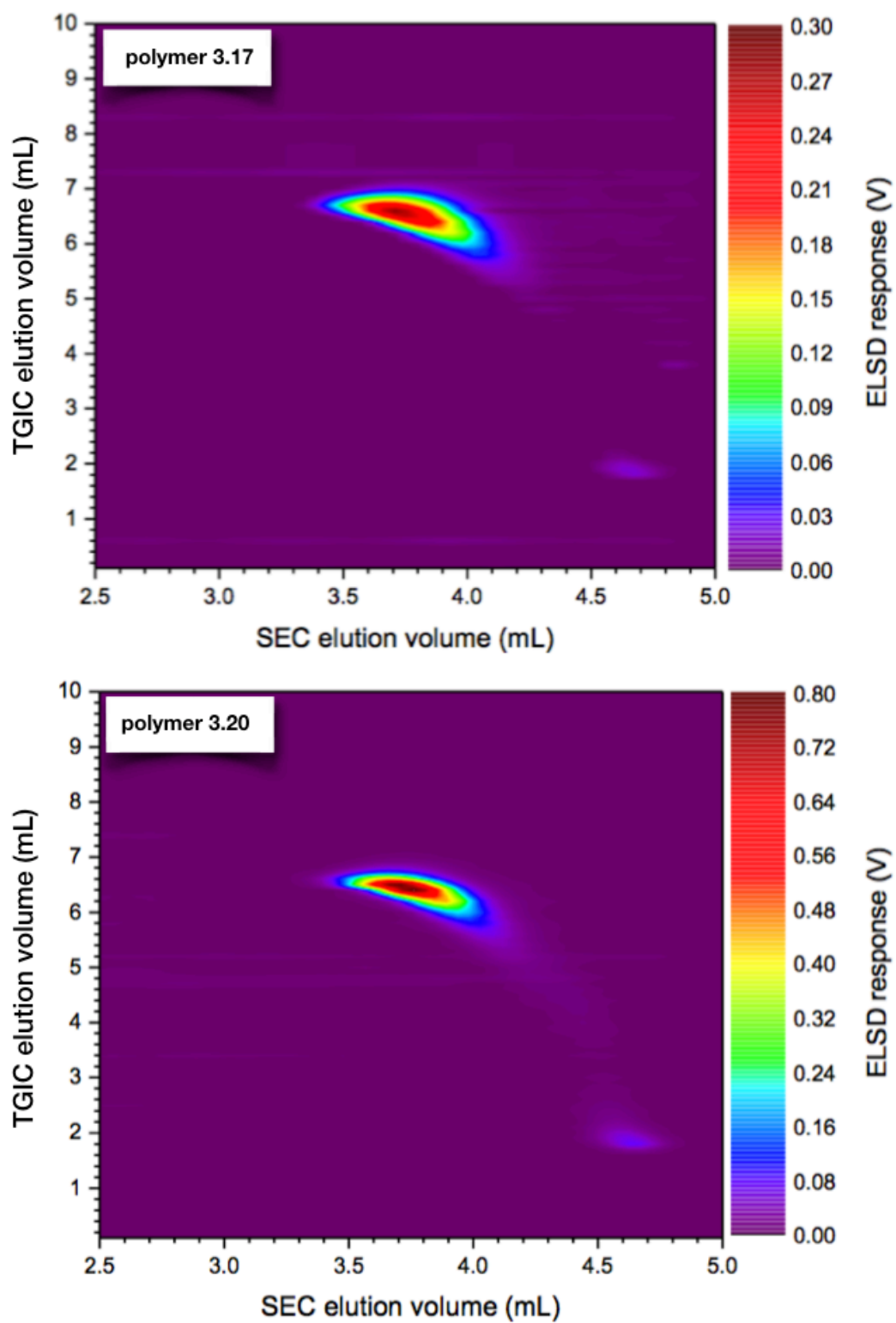


Figure 3.8 | 2D IC-SEC for polymers **3.17** and **3.20**.

3.4 – Conclusion and Future Work

The capabilities of supported molecular REMP catalyst **3.0** were explored. REMP reactions with simple cycloolefin monomers COE, COD, and CP were conducted, which led us to pursue CP as the best REMP monomer due to its superior processability. The purity of CP was found to be critical for ensuring purely cyclic polymer product. Evidence for linear pentene isomers as contaminants in certain CP monomer stocks was found. The topological purity of PCP was confirmed using IC and 2D IC-SEC.

Experimental conditions were successfully determined as the basis for future REMP work. The knowledge and expertise necessary to explore the polymerization profiles and reactivities of other cycloolefin monomers was achieved.

3.4 – Experimental

General Information

All reactions were carried out in glassware flame-dried in vacuo (100 mTorr) unless otherwise specified. Reactions were performed using air-free Schlenk technique (100 mTorr vacuum and UHP grade 5.0 argon gas) on the benchtop or in a Vacuum Atmospheres glovebox (N_2 -filled, O_2 concentration < 0.25 ppm) unless otherwise specified. All solvents were purchased from Sigma-Aldrich (anhydrous, 99.9%) and further purified by passage through solvent purification columns, sparged with argon, and then stored over 4 Å molecular sieves in Strauss flasks, unless otherwise specified.¹⁷ All homogeneous Grubbs catalyst

(**3.1 – 3.6**, Fig 3.1) were received as a generous gift by Materia, Inc. (Pasadena, CA) and used without further purification. All other reagents were purchased from Sigma-Aldrich and used as received unless otherwise stated. Room temperature was 18-20 °C for all syntheses described herein.

All ^1H NMR spectra were acquired using a Varian Inova 500 MHz or Bruker 400 MHz spectrometer and are reported relative to residual CHCl_3 (δ 7.26 ppm), C_6H_6 (δ 7.16 ppm), or CH_2Cl_2 (δ 5.32 ppm). All ^{13}C NMR spectra were recorded on a Varian Inova 500 MHz spectrometer (125 MHz) or Bruker 400 MHz spectrometer (100 MHz) and are reported relative to CHCl_3 (δ 77.16 ppm). Data for ^{13}C NMR are reported in terms of chemical shifts (δ ppm). Processing of all NMR data was performed with MestReNova version 10.0 from Mestrelabs Research S.L.

Size-exclusion chromatography (SEC) data was obtained with an HPLC system consisting of two two Agilent PLgel MIXED-B 300 \times 7.5 mm columns with 10 μm beads, and an Agilent 1260 Series pump and autosampler; the columns were connected in series with a Wyatt 18-angle DAWN HELEOS multi-angle laser light scattering detector and Optilab rEX differential refractive index detector. The mobile phase was either pure THF or stabilized THF (50-150 ppm butylated hydroxytoluene (BHT)).

Orbital agitation of REMP reactions was performed using an IKA KS 260 basic flat orbital shaker with a swivel motion (no z-axis motion). Orbital agitation rate varied between 200 and 400 rot/min.

Fractional distillation of cyclopentene

The following procedure was adapted from a procedure reported in patent literature.¹⁸ Fractional distillation of cyclopentene was conducted using a 24-inch Pro-Pak[®] column which was the best performing fractionating column available. Prior to the collection of distillate fractions, the crude cyclopentene was refluxed for 48 hours over 20 weight percent H-form Amberlyst[®] 15 resin which was reported to effect the acid-catalyzed oligomerization of olefinic impurity. Following this procedure, 7 CP distillate fractions were collected over 48 hours with the distillation pot held at a temperature such that CP distilled slowly, dropwise. Instrumentation to directly measure purity was not available, so an indirect method for purity determination was devised and conducted. The seven distillate fractions collected were stored in Schlenk flasks and degassed by ultra-high purity (UHP) argon sparging prior to use (UHP argon had not previously been used). Each CP distillate fraction was then subjected to identical ROMP conditions in triplicate. The molecular weights and yields were used to measure the relative purity of CP batches (Figure 3.4) because an absolute purity determination was not possible due to instrumental limitations.

Interaction chromatography

IC experiments were performed using a solvent gradient interaction chromatograph (SGIC) constructed by Polymer Char (Valencia, Spain). For solvent gradient elution in HPLC, a high- pressure binary gradient pump (Agilent, Waldbronn, Germany) was utilized. The evaporative light scattering detector

(ELSD, model PL-ELS 1000, Polymer Laboratories, Church Stretton, England) was used with the following parameters: gas flow rate of 1.5 SLM, 160 °C nebuliser temperature and an evaporative temperature of 270 °C. A Hypercarb column (Hypercarb®, Thermo Scientific, Dreieich, Germany) with 100 × 4.6 mm internal diameter packed with porous graphite particles which have a particle diameter of 5 µm (making a surface area of 120 m²g⁻¹) and pore size of 250 Å was used for all HT-HPLC experiments. The column was placed in an oven and the temperature maintained at 160 °C. The flow rate of the mobile phase during analysis was 0.5 mLmin⁻¹. To achieve separation, a linear gradient was applied from 100 % 1-decanol to 100 % TCB within 10 min after sample injection. These conditions were held for 20 minutes before re-establishing 1-decanol to 100 %. For all HT-HPLC analyses a concentration of 1 – 1.2 mgmL⁻¹ was used (approximately 4 mg in 4 mL of 1-decanol) with 20 µL of each sample being injected.

2D-IC-SEC

HT-HPLC and HT-SEC were coupled with the aid of an electronically controlled eight-port valve system (VICI Valco instruments, Houston, Texas) equipped with two 100 µL sample loops. Injection into the first dimension (HT-HPLC) was carried out using a 110 µL sample loop and the flow rate was 0.05 mLmin⁻¹. A linear gradient was applied from 100% 1-decanol to 100% TCB within 20 mL (200 mins). A flow rate of 2.75 mLmin⁻¹ was used in the second

dimension (HT-SEC) and TCB was used as the mobile phase. In the second dimension, a PL Rapide H (Polymer Laboratories, Church Stretton, U.K.) 100 × 10 mm internal diameter column with a 6 μm particle diameter was used at 160 °C. The column was kept in an oven at this temperature during the analysis. The evaporative light scattering detector (ELSD, model PL-ELS 1000, Polymer Laboratories, Church Stretton, England) was used with the following parameters: gas flow rate of 1.5 SLM, 160 °C nebuliser temperature and an evaporative temperature of 270 °C.

Large-scale PCP REMP

A 1.0 L 2-neck round bottom flask was flamed-dried, and charged with 1.20 g catalyst **3.0** (0.024 mmol) in the glovebox. The flask was removed from the glovebox and charged with 104 mL anhydrous PhCH₃, followed by 21.1 mL CP (batch 5, figure 3.4). Orbital agitation at 150 rot/min. A separate air-free fritted filtration funnel with round-bottom collection flask was set up nearby, and after 45 minutes, the REMP reaction medium was allowed to settle and the supernatant was cannula transferred (two 18 gauge cannulae) into the filtration apparatus. Following filtration, additional PhCH₃ was added to wash the reaction flask, and the supernatant was again transferred into the filtration funnel. This process was repeated 4 times (Table 3.4.1). Each cycle was concentrated in vacuo (100 mTorr) for isolation.

Table 3.4.1 | Large-scale CP REMP reaction parameters.

cycle	volume CP (mL)	volume PhCH ₃ (mL)	[CP] ₀ (mol/L)	reaction time (min)	[CP] ₀ :[cat 3.0] ₀
1	21.1	104	2.3 M	45	10000
2	24.0	130	2.3 M	30	11000
3	50	250	2.3 M	25	24000
4	100	250	4.6 M	50	48000

3.5 References

- (1) Bielawski, C. W.; Grubbs, R. H. *Science* **2002**, 297 (5589), 2041–2044.
- (2) Bielawski, C. W.; Benitez, D.; Grubbs, R. H. *J. Am. Chem. Soc.* **2003**, 125 (28), 8424–8425.
- (3) Hejl, A.; Scherman, O. A.; Grubbs, R. H. *Macromolecules* **2005**, 38 (17), 7214–7218.
- (4) Grubbs, R. H. *Tetrahedron* **2004**, 60 (34), 7117–7140.
- (5) Schwab, P.; France, M. B.; Ziller, J. W.; Grubbs, R. H. *Angew. Chem. Int. Ed.* **1995**, 34 (18), 2039–2041.
- (6) Scholl, M.; Ding, S.; Lee, C. W.; Grubbs, R. H. *Org. Lett.* **1999**, 1 (6), 953–956.
- (7) Choi, T.-L.; Grubbs, R. H. *Angew. Chem. Int. Ed. Engl.* **2003**, 42 (15), 1743–1746.
- (8) Trnka, T. M.; Grubbs, R. H. *Acc. Chem. Res.* **2001**.
- (9) Ji, S.; Hoye, T. R.; Macosko, C.; 2004. *Macromolecules* **2004**, 37 (15), 5485–5489.
- (10) Morita, T.; Maughon, B. R.; Bielawski, C. W.; Grubbs, R. H. *Macromolecules* **2000**, 33 (17), 6621–6623.
- (11) Hillmyer, M. A.; Grubbs, R. H. *Macromolecules* **1995**, 28 (25), 8662–8667.
- (12) Dounis, P.; Feast, W. J.; Kenwright, A. M. *Polymer* **1995**, 36 (14), 2787–2796.
- (13) Trzaska, S. T.; Lee, L.; Register, R. A. *Macromolecules* **2000**, 33 (25), 9215–9221.
- (14) Myers, S. B.; Register, R. A. *Polymer* **2008**, 49 (4), 877–882.
- (15) Mulhearn, W. D.; Register, R. A. *ACS Macro Lett.* **2017**, 6 (2), 112–116.
- (16) Xia, Y. *California Institute of Technology* **2010**, 1–208.
- (17) Pangborn, A. B.; Giardello, M. A.; Grubbs, R. H.; Rosen, R. K.; Timmers, F. J. *Organometallics* **1996**, 15, 1518–1520.
- (18) Johnson, M. M.; Tabler, D. C. US Patent Office 1971.

Chapter 4

Large-Scale Cyclic Polybutadiene Synthesis

4.0 – Abstract

The importance of polybutadiene (PBd) as a commercial material and a model system in fundamental research is discussed. A process for producing cyclic PBd via REMP and on scale was desired. Small-scale optimization experiments for the REMP of COD to PBd using a supported molecular REMP catalyst were pursued. A large-scale REMP reactor and recycling process were devised. The REMP recycling process succeeded twice in producing multi gram quantities of PBd, which vastly exceeded previous capabilities. The purity of cyclic PBd was established using IC. Unusual *cis*-selectivity in COD REMP reactions was observed.

Chapter 4 Acknowledgments

Bob Grubbs, Alice Chang, Dick Pederson and Adam Johns (Materia, Inc.)

Anthony Ndiripo and Prof. Harald Pasch (U. of Stellenbosch, S. Africa)

4.1 – Introduction

Polybutadiene

Polybutadiene (PBd) represents a substantial portion of all polymers produced worldwide, with over 3 trillion kg produced in 2015 alone. Approximately 70% of PBd produced globally goes into the manufacture of automobile tires, with the remaining share composing a wide variety of plastics and rubbers. PBd synthetic strategies provide microstructure control to achieve the desired 1,4-*cis*-insertion, 1,4-*trans*-insertion, and 1,2-insertion composition for modulating material properties. High-*cis* PBd generally comes from organolithium-mediated anionic polymerization, while high-*trans* generally comes from Ziegler-Natta α -olefin polymerization catalysts (Fig 4.1). Commercial PBd always contains some of the branched 1,2-insertion component, which is used to enhance toughness of PBd through cross-linking. Copolymerization of butadiene with styrene provides styrene-butadiene rubber (SBR), which is the most common material in automobile tires.¹

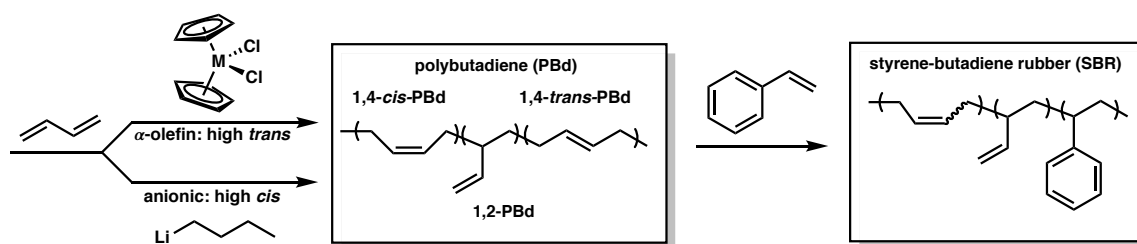


Figure 4.1 | Industrial production of PBd and SBR via either metallocene catalysts (M = Zr, Ti, Hf) or organolithium species to furnish high *trans* or high *cis* PBd, respectively.

Cyclic PBd and PS have been used as model systems for studying cyclic polymer melt-state viscoelastic properties, namely their rheological behavior.²⁻⁶ The cycles used in these studies required a ring-closure strategy, followed by topological purification with preparative interaction chromatography (IC). Trace linear impurity has long been known to drastically alter cyclic polymer rheological responses, with 0.07% linear PS detectable by stress relaxation measurements.⁷

The first, and still only, report of cyclic polybutadiene from olefin metathesis came from our group in 2003.⁸ Numerous reports of linear PBd from ROMP, including telechelic PBd^{9,10} and PBd copolymers,^{11,12} emerged from our group, and others, beginning in the 1990's (Fig 4.2). The power of olefin metathesis to prepare PBd-derived materials with diverse architectures and properties has been well demonstrated. Conversely, the numerous problems with the previous REMP strategy for cyclic PBd in our group precluded our efforts to generate the quantity and quality of material necessary to properly elaborate our synthetic methodology and to study bulk properties.⁹

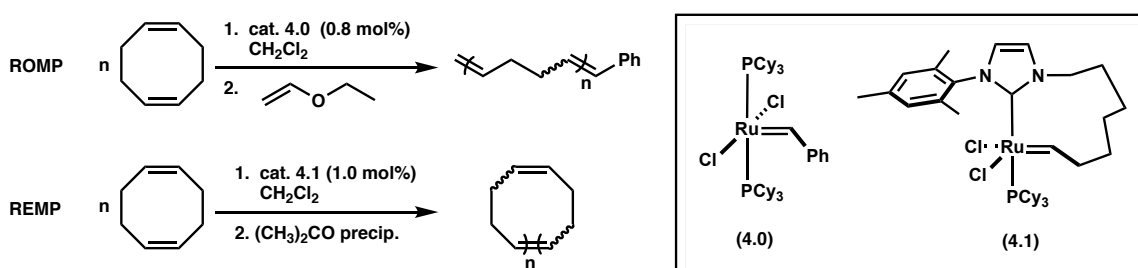


Figure 4.2 | The ROMP¹⁰ (top) and REMP⁸ (bottom) of COD by catalysts **4.0** and **4.1** (top), respectively.

With the success of the supported molecular REMP catalyst **4.2** described in the previous two chapters, we sought to expand our methodology such that multi-gram quantities of cyclic polymers could be reliably produced. A third party expressed interest in acquiring 50 g of cyclic PBd for bulk property analysis and we felt confident in our ability to fulfill their request. This chapter will discuss the design and implementation of large scale REMP methodology for the synthesis of cyclic PBd, complemented by thorough characterization of physical properties, including topological purity.

4.2 – Results and Discussion

Olefin metathesis can produce PBd from a variety of monomers, including cyclobutene, cyclooctadiene, and cyclododecatriene (CDT). That is, any cyclic oligomer of cyclobutene will produce PBd (COD is a dimer, CDT is a trimer, etc.), although they will have drastically different polymerization profiles due to the range of ring strain and steric profiles they encompass. We considered these monomers as we designed the methodology necessary to produce 50 g of cyclic PBd and 50 g of linear PBd, which were both requested by a third party (Fig 4.3, top). Our exploration of the reactivity of REMP catalyst **4.2** described in the previous chapter was again chosen for cyclic PBd, our new target; ROMP catalysts **4.3** and **4.4** were chosen for the linear PBd we also targeted (Fig 4.3, bottom). Catalyst **4.3** was the state-of-the-art ROMP catalyst and catalyst **4.4** was the closest available analog to **4.2**.

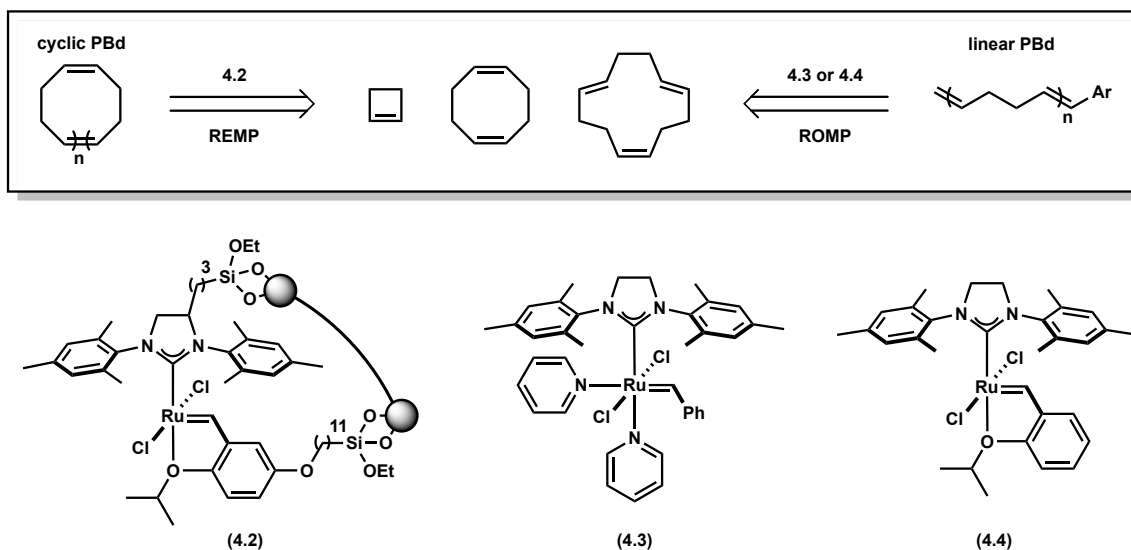


Figure 4.3 | Cycloolefin monomers which produce cyclic (top, left) and linear (top, right) PBd via olefin metathesis catalysts **4.2** – **4.4** (bottom).

Small-Scale REMP and ROMP

The high concentration necessary for COD polymerization leads to a dramatic viscosity increase of the reaction medium as the polymerization proceeds. The filtration process required to isolate cyclic PBd from catalyst **4.2** demanded that we closely monitor the viscosity of the polymerization medium so that filtration would not become untenable. This viscosity increase was indistinguishable between cyclic and linear PBd, so although different catalysts were used, the polymerization profiles of linear PBd ROMP were instructive in the design of cyclic PBd REMP experiments.

Previous efforts to produce cyclic PBd from COD with supported molecular REMP catalyst **4.2** (described in Chapter 3) led us to consider other monomers. We eventually realized the source of our initial COD REMP problems likely arose from trace 4-vinyl-cyclohexene present in our monomer stock. We had not found

evidence of this chain transfer agent present in these experiments, but we did observe signs of radical crosslinking, which 4-vinyl-cyclohexene mediates, particularly when incorporated into the PBd backbone. Although the COD used had been purified by distillation, the extent to which its purity impacted material properties, including cyclic purity, were not originally appreciated. As such, all monomers used in this chapter were extensively purified (see experimental section).

We chose COD over cyclododecatriene and cyclobutene because of the former's poor reactivity and the latter's operational difficulty, since it is a gas at room temperature. Once ultra-pure COD was prepared, small-scale ROMP and REMP optimization experiments were used to establish the reaction parameters and experimental procedures which would be used in large-scale PBd synthesis (Fig 4.4).

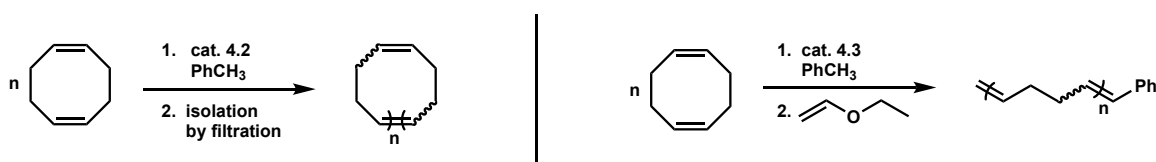


Figure 4.4 | Small-scale REMP (left) and ROMP (right) experiments.

Olefin metathesis catalysts for ROMP are well known to provide excellent MW control and narrow D for polynorbornene and other high ring-strain monomers. Through rigorous experiment design, they can also provide similarly desirable material properties with low and intermediate ring-strain monomers

such as COE, COD and CP.^{13,14} The ratio of $[\text{monomer}]_0:[\text{catalyst}]_0$ determines the degree of polymerization (n), and thus MW, during ROMP, particularly with high ring-strain monomers. Naturally, we explored this method to control the MW of PBd during ROMP and REMP of COD (Figs 4.5 and 4.6).

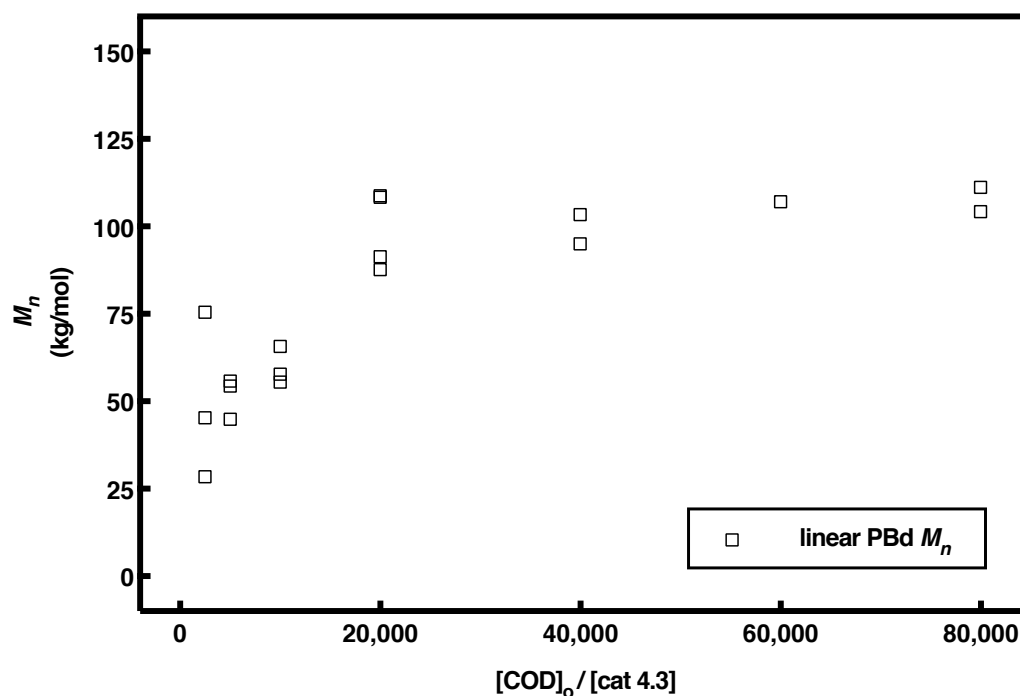


Figure 4.5 | M_n vs. catalyst loading for ROMP of COD to linear PBd.

The relationship M_n vs. $[\text{monomer}]_0:[\text{catalyst}]$ is linear for ROMP of norbornene-based monomers whereby each catalyst produces one chain. The ring-strain of the monomer, and steric bulk along the backbone, prevent depolymerization completely, and thus secondary metathesis events which broaden \mathcal{D} and reduce M_n cannot occur.

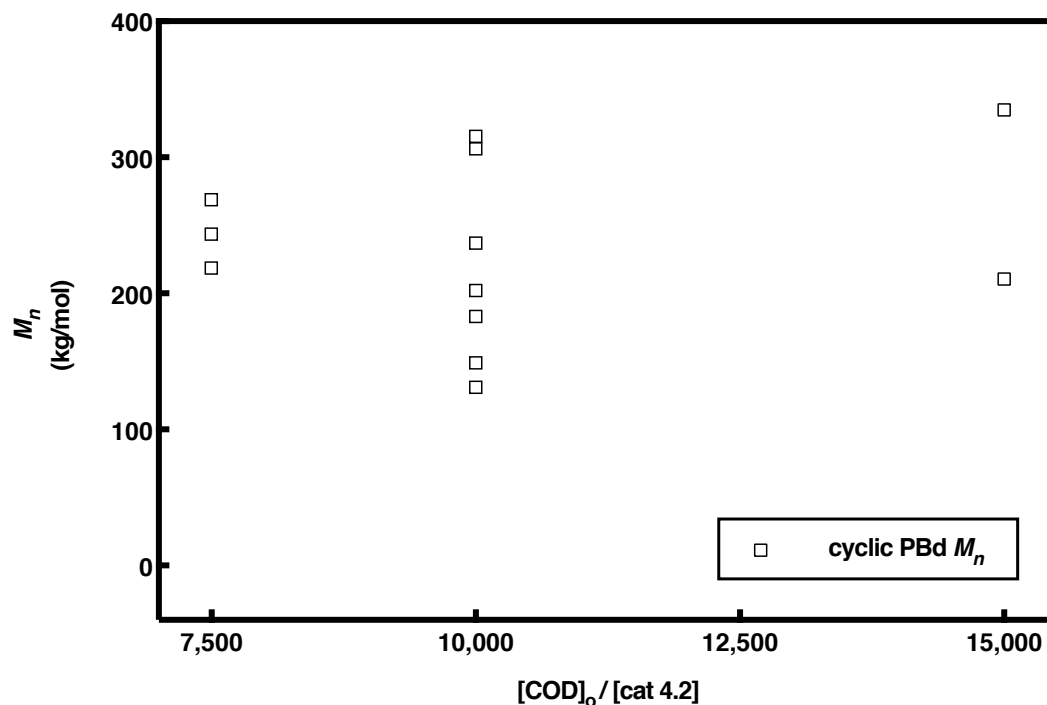


Figure 4.6 | M_n vs. catalyst loading for REMP of COD to cyclic PBd.

A non-linear relationship for ROMP of COD by catalyst **4.3** was observed (Fig 4.5), although the $[\text{monomer}]_0:[\text{catalyst}]_0$ could still be exploited to target a specific M_n , based on purely empirical findings; i.e., M_n was somewhat predictable once an array of variables were explored (non-linear regression $R^2 = 0.7335$, not shown). Conversely, no predictive model was obtained for analogous REMP experiments (Fig 4.6). A linear regression of this data provided the best fit, albeit an extremely poor one, with $R^2 = 0.03$ (not shown). Clearly, reproducibility of COD REMP with catalyst **4.2** proved challenging. The heterogeneous nature of REMP using **4.2** was certainly the fundamental reason for the lack of reproducibility, a theme which will be evident throughout this chapter.

The ROMP of norbornene-based monomers provides quantitative yields with near-perfect reproducibility. We found the ROMP of COD to provide high yields (> 90%), with good reproducibility (Fig 4.7). Conversely, the yield for COD REMP to cyclic PBd with **4.2** was erratic and irreproducible (Fig 4.8), although a generally negative trend between yield and catalyst loading was somewhat evident. Despite sincere efforts, conditions and procedures to enhance reproducibility could not be established. Due to time constraints, we elected to proceed with large-scale REMP experiments without further optimization.

Large-Scale REMP and ROMP

We needed to design a new experimental process to produce 50 g of cyclic PBd because common polymerization procedures were unsuitable: conventional glassware could not accommodate the recycling of catalyst **4.2**, a reactor with a flat surface was required due to the heterogeneity of REMP catalyst **4.2**, and a fritted filtration disc integrated into the reactor would be required to separate cyclic PBd from the catalyst. We incorporated these design principles into the schematic of a custom reactor which was fabricated by Rick Gerhart (Caltech Glassblowing Facilities) (Fig 4.9, left) such that our catalyst recycling process (Fig 4.9, right) could produce the requisite quantity of cyclic PBd (50 g). This scale would constitute a 50-fold increase from our group's previous capabilities up to that point.

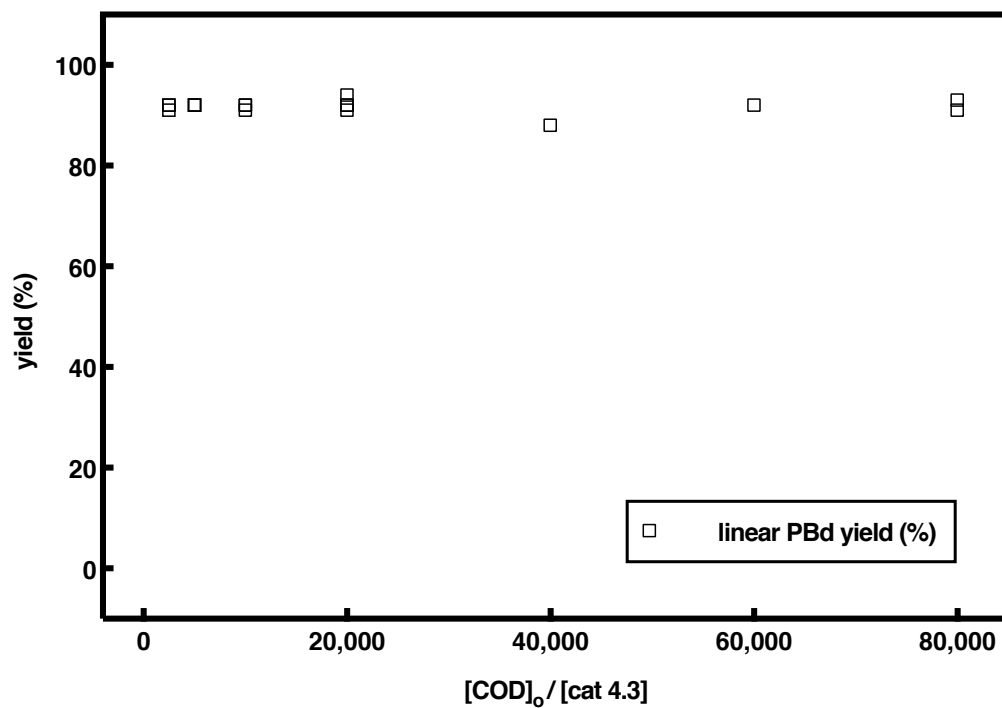


Figure 4.7 | Yield vs. catalyst loading for ROMP of COD to linear PBd.

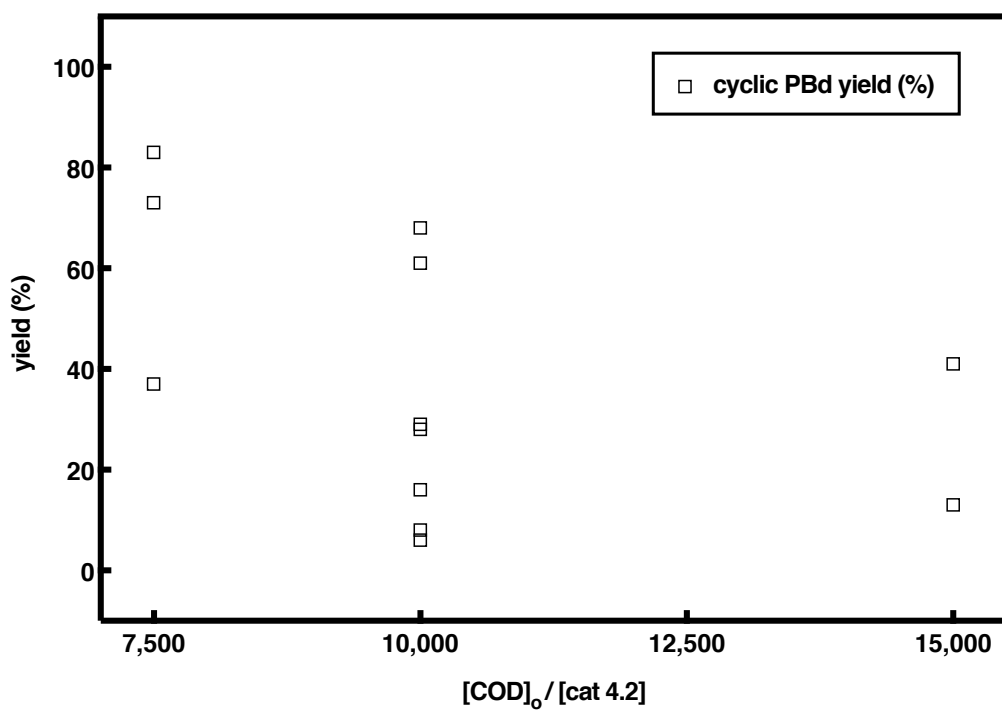


Figure 4.8 | Yield vs. catalyst loading for REMP of COD to cyclic PBd.

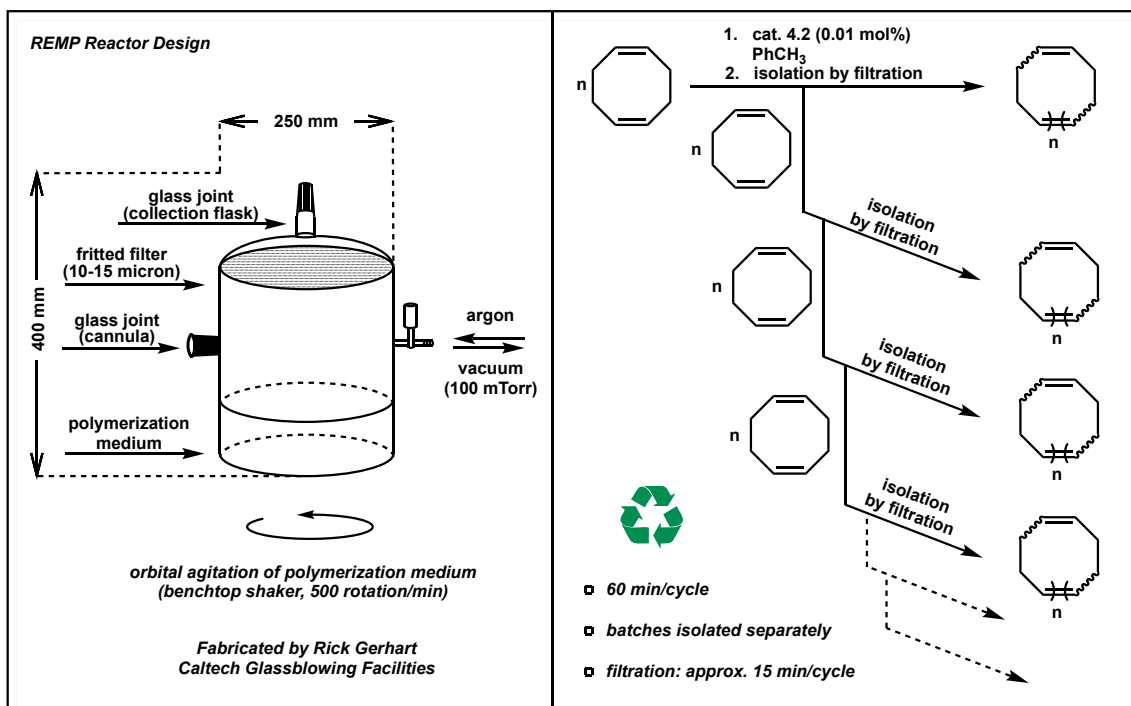


Figure 4.9 | REMP reactor design (left) to accommodate a catalyst recycling process (right).

The first large scale REMP reaction succeeded in producing multi-gram quantities of PBd for each cycle, with 6 total cycles performed. The M_n of each cycle remained reasonably constant throughout the entire recycling process, shown by the range of 210 – 245 kDa for each cycle (Fig 4.10, top). The decrease in yield throughout the process (Fig 4.10, bottom) likely arose from a gradual decline in activity of catalyst **4.2**. Although yields were not excellent for the later cycles, this experiment was certainly a success overall: the 6 cycles cumulatively produced 50.5 g PBd.

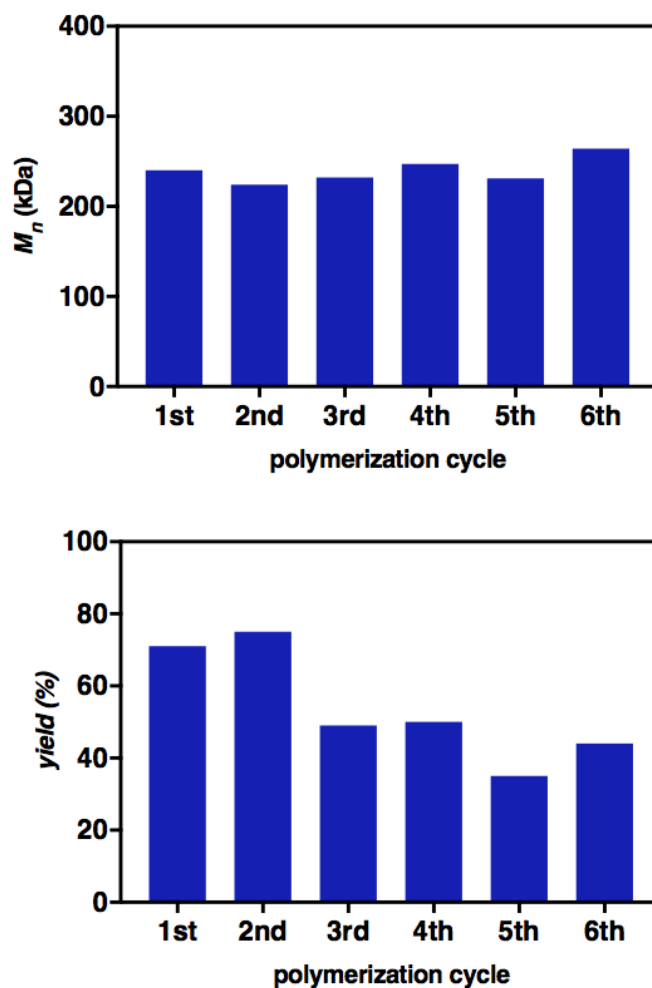


Figure 4.10 | The M_n (top) and yield (bottom) for each of the batches produced in the large-scale REMP recycling experiment.

GPC indicated that each cycle exhibited very similar elution profiles, and each cycle contained substantial low MW material (elution time 15 – 18 min, Fig 4.11), which led to $D > 2$. Although not an explicit requirement from the third party that requested the material, we elected to precipitate the cycles in order to lower the D so that the material would be easier to study. We precipitated our PBd into MeOH 3 total times, which greatly improved D , although approximately 20% of our material was lost in the process (Fig 4.12). We then performed another

recycling experiment, but with only 4 cycles, in order to produce sufficient material. The results from this second large scale recycling experiment corroborated the trends we saw previously: M_n remained mostly unchanged, and yields gradually decreased (Fig 4.13). Additionally, the elution profiles by SEC appeared reasonably consistent for each cycle. After precipitation of these 4 cycles, we obtained the requisite 50 g of cyclic PBd for the third party, as well as sufficient material for IC analysis.

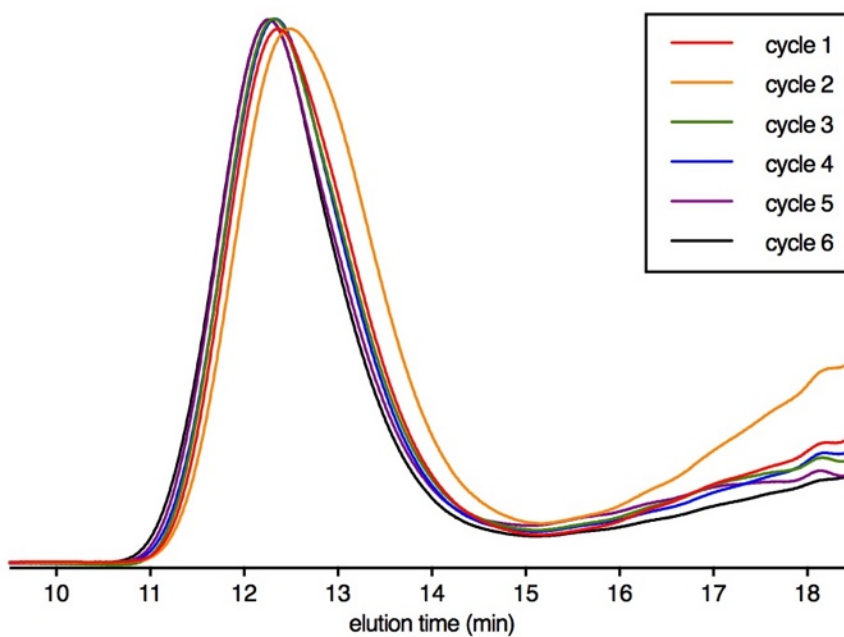


Figure 4.11 | The elution profiles of each PBd cycle.

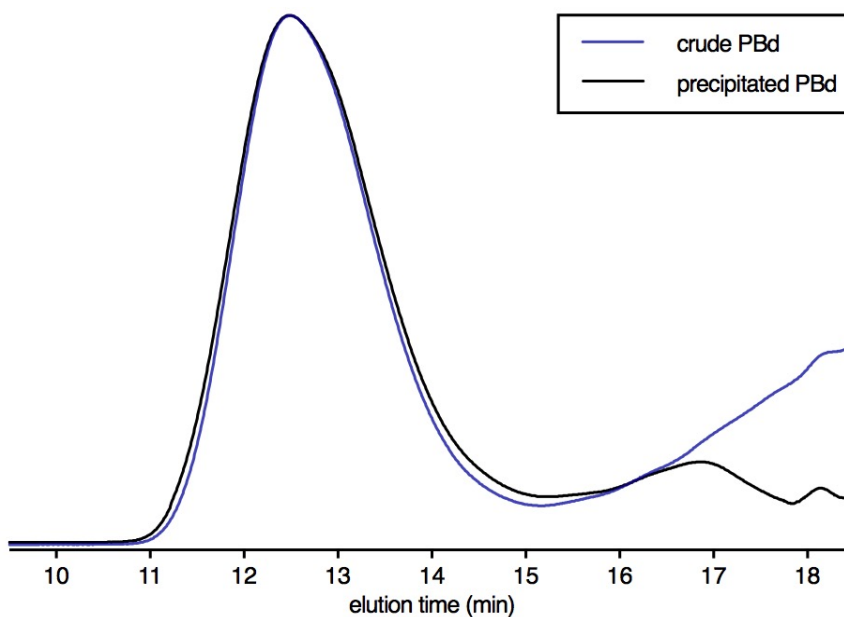


Figure 4.12 | The GPC elution profiles for the crude PBd produced from cycle 2 (blue line), and the same sample after it was precipitated (black line).

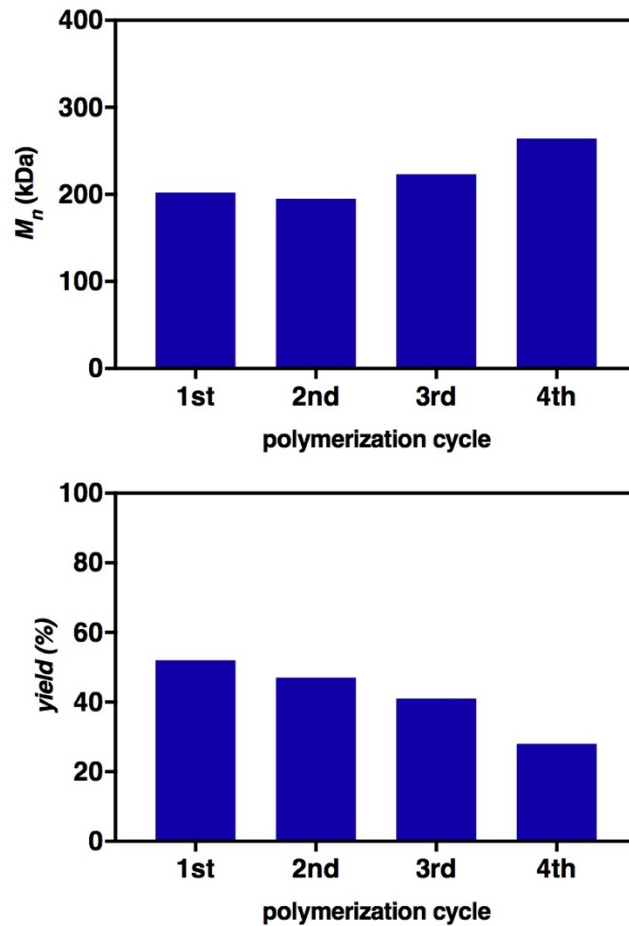


Figure 4.13 | The M_n (top) and yield (bottom) for each of the batches produced in the second large-scale REMP recycling experiment.

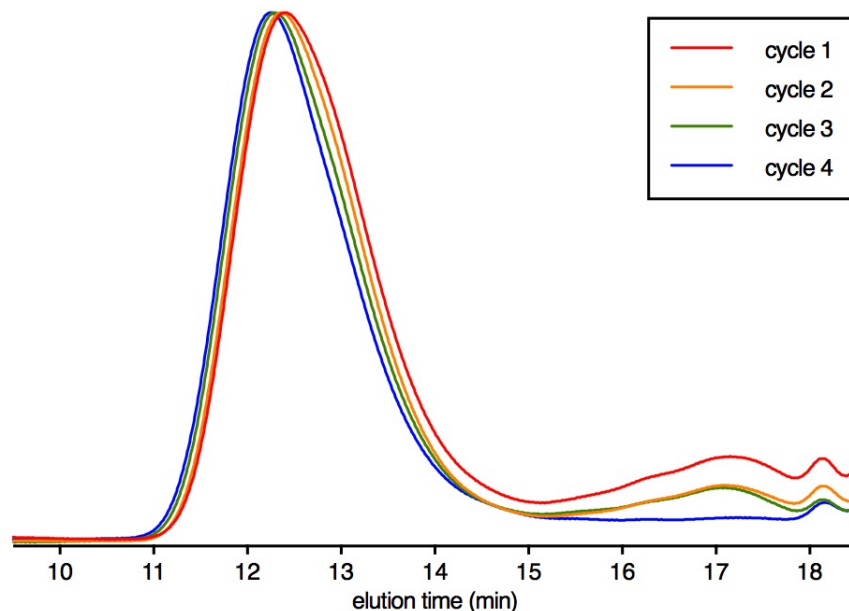


Figure 4.14 | The elution profiles of each PBd cycle in the second recycling experiment.

The IC profiles for cyclic PBd, produced via the large-scale REMP process described above, and linear PBd, produced with catalyst **4.1**, were distinct (Fig 4.15). A bimodal distribution of topologies is clearly seen for ROMP-derived PBd, but a monomodal distribution is observed for REMP-derived PBd. During the ROMP of COD, back-biting inevitably results in cyclic chains within the largely linear population of chains, which explains the bimodal distribution seen for ROMP-derived PBd. That is, our linear PBd also contains a measurable quantity of cyclic chains. This demonstrated both the high purity of our cyclic PBd, and the merit of IC in ascertaining the topological homogeneity of macromolecules.

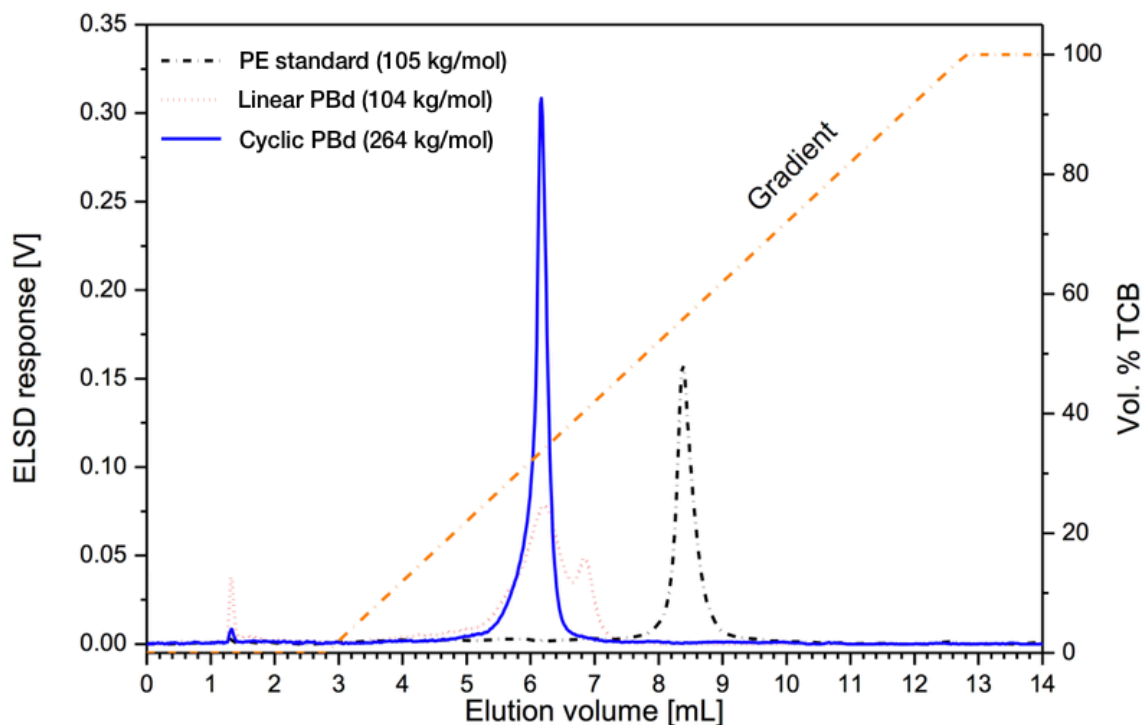


Figure 4.15 | Interaction chromatography elution profiles for cyclic (blue) and linear (dotted red) PBd, as well as a PE standard (dotted black). The solvent gradient of 1-decanol/1,2,4-trichlorobenzene (TCB) is also shown vs elution volume (dotted orange).

At the conclusion of this project, we realized that our cyclic PBd was high-*cis*, as much as 80% by ^{13}C NMR, whereas all PBd we produced via ROMP was 20% *cis*, the thermodynamic ratio. Furthermore, we observed a concentration dependence for the *cis/trans* ratio, which we had not found with ROMP using similar conditions (Fig 4.16). We then began an investigation into the *cis/trans* selectivity afforded during REMP by cat **4.2**, which will be described in detail in Chapter 5 of this dissertation.

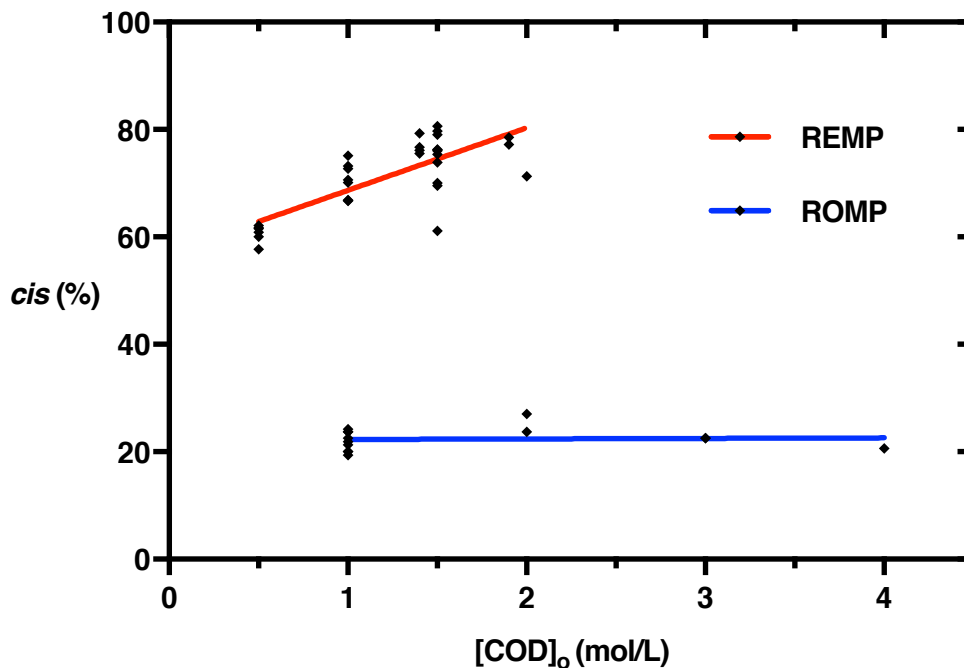


Figure 4.16 | The concentration dependence of the cis content of COD-derived PBd from REMP with catalyst **4.2** and ROMP with catalysts **4.0-4.1**.

4.3 – Conclusions and Future Outlook

The importance of PBd and the potential uses of cyclic PBd were discussed. We developed a strategy to solve a long-term goal of the cyclic polymer project in our group: produce multi-gram quantities of highly pure cyclic polymer. This was accomplished through a series of small-scale optimization experiments and the design and implementation of a novel large-scale REMP catalyst recycling process. We additionally demonstrated the purity of our cyclic PBd using IC.

4.4 – Experimental

GPC

The molar mass and molar mass dispersity of the polyethylene samples were determined on a PL- GPC 220 High Temperature Chromatograph (Polymer Laboratories, Church Stretton, UK) equipped with a differential refractive index (RI) detector. The polyethylene samples (4 mg) were dissolved in 2 mL of TCB for 1 hr together with 0.025 % BHT which acted as a stabiliser to prevent sample decomposition/degradation. TCB with 0.0125 % BHT was used as the mobile phase at a flow rate of 1 mLmin^{-1} . Three $300 \times 7.5 \text{ mm}^2$ PLgel Olexis columns (Polymer Laboratories, Church Stretton, UK) were used together with a $50 \times 7.5 \text{ mm}^2$ PLgel Olexis guard column and 200 μL of each sample was injected. All experiments in HT-SEC were carried out at $150 \text{ }^\circ\text{C}$. The instrument was calibrated using narrowly distributed polystyrene standards (Polymer Laboratories, Church Stretton, UK).

Interaction chromatography (HT-HPLC)

Chromatographic experiments were performed using a solvent gradient interaction chromatograph (SGIC) constructed by Polymer Char (Valencia, Spain). For solvent gradient elution in HPLC, a high- pressure binary gradient pump (Agilent, Waldbronn, Germany) was utilised. The evaporative light scattering detector (ELSD, model PL-ELS 1000, Polymer Laboratories, Church Stretton,

England) was used with the following parameters: gas flow rate of 1.5 SLM, 160 °C nebuliser temperature and an evaporative temperature of 270 °C. A Hypercarb column (Hypercarb®, Thermo Scientific, Dreieich, Germany) with 100 × 4.6 mm internal diameter packed with porous graphite particles which have a particle diameter of 5 µm (making a surface area of 120 m²g⁻¹) and pore size of 250 Å was used for all HT-HPLC experiments. The column was placed in an oven and the temperature maintained at 160 °C. The flow rate of the mobile phase during analysis was 0.5 mLmin⁻¹. To achieve separation, a linear gradient was applied from 100 % 1-decanol to 100 % TCB within 10 min after sample injection. These conditions were held for 20 minutes before re-establishing 1-decanol to 100 %. For all HT- HPLC analyses a concentration of 1 – 1.2 mgmL⁻¹ was used (approximately 4 mg in 4 mL of 1-decanol) with 20 µL of each sample being injected.

4.5 – References

- (1) Brandt, H. D.; Nentwig, W.; Rooney, N.; LaFlair, R. T.; Wolf, U. U.; Duffy, J.; Puskas, J. E.; Kaszas, G.; Drewitt, M.; Glander, S. *Ullmann's Encyclopedia of Industrial Chemistry*, 1, 2nd ed.; Wiley-VCH: Weinheim, Germany, 2000; Vol. 39, pp 30–32.
- (2) Roovers, J. *Macromolecules* **1988**, 21 (5), 1517–1521.
- (3) Lee, H. C.; Lee, H.; Lee, W.; Chang, T.; Roovers, J. *Macromolecules* **2000**, 33 (22), 8119–8121.
- (4) Cho, D.; Park, S.; Kwon, K.; Chang, T.; Roovers, J. *Macromolecules* **2001**, 34 (21), 7570–7572.
- (5) McKenna, G. B.; Hostetter, B. J.; Hadjichristidis, N.; Fetters, L. J.; Plazek, D. J. *Macromolecules* **1989**, 22 (4), 1834–1852.
- (6) Doi, Y.; Matsubara, K.; Ohta, Y.; Nakano, T.; Kawaguchi, D.; Takahashi, Y.; Takano, A.; Matsushita, Y. *Macromolecules* **2015**, 48 (9), 3140–3147.
- (7) Kapnistos, M.; Lang, M.; Vlassopoulos, D.; Pyckhout-Hintzen, W.; Richter, D.; Cho, D.; Chang, T.; Rubinstein, M. *Nat Mater* **2008**, 7 (12), 997–1002.
- (8) Bielawski, C. W.; Benitez, D.; Grubbs, R. H. *J. Am. Chem. Soc.* **2003**, 125 (28), 8424–8425.
- (9) Xia, Y. *California Institute of Technology* **2010**, 1–208.
- (10) Fraser, C.; Hillmyer, M. A.; Gutierrez, E.; Grubbs, R. H. *Macromolecules* **1995**, 28 (21), 7256–7261.
- (11) Trnka, T. M.; Grubbs, R. H. *Acc. Chem. Res.* **2001**.
- (12) Grubbs, R. H. *Tetrahedron* **2004**, 60 (34), 7117–7140.
- (13) Neary, W. J.; Kennemur, J. G. *Macromolecules*.
- (14) Walker, R.; Conrad, R. M.; Grubbs, R. H. *Macromolecules* **2009**, 42 (3), 599–605.

Chapter 5

Selectivity in Cyclic Polybutadiene Synthesis

5.0 – Abstract

The *cis*-selectivity in REMP reactions using a family of supported molecular REMP catalysts is explored. A model for *cis*-selectivity is proposed and evaluated. The synthesis of cyclic and linear PBd analogs through the intentional addition of linear olefin chain transfer agent (CTA) is explored, and their topologies are evaluated using IC. The tether lengths attaching supported molecular REMP catalysts to the surface of SiO₂ were thought to provide selectivity in REMP reactions, but initial evidence was inconclusive. A relationship between *cis* content and catalyst loading is established.

Chapter 5 Acknowledgments

Bob Grubbs, Quan Gan, Alice Chang, Willie Wolf, Dave VanderVelde, Scott Virgil
Anthony Ndiripo and Harald Pasch (U. of Stellenbosch, S. Africa)

5.1 – Introduction

Cyclic Polybutadiene

The ratio of *cis* and *trans* olefins in the PBd backbone greatly affects its physical properties, notably transition temperatures and modulus.¹ Industrially, the *cis/trans* ratio is well-controlled through reaction conditions, but mostly through catalyst design. Traditional alpha-olefin polymerization catalysts produce high-*trans* PBd and anionic polymerization strategies produce high-*cis* PBd (Fig 5.1)

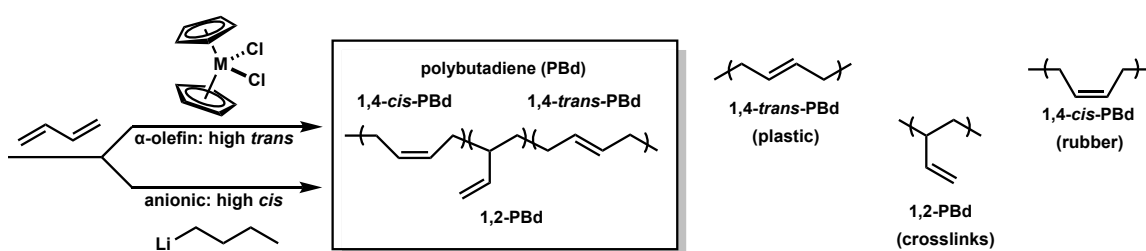


Figure 5.1 | Modulating PBd physical properties through control of *cis/trans*.

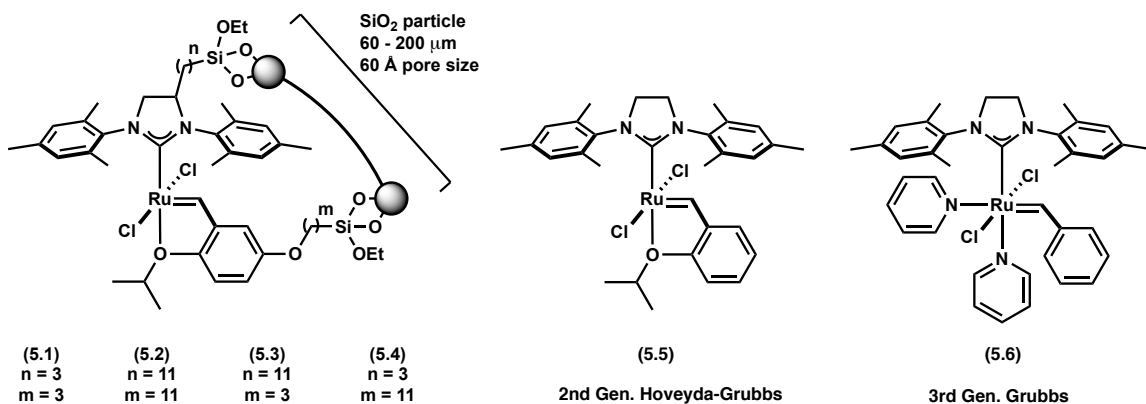


Figure 5.2 | Metathesis catalysts used in the work described herein.

The previous chapter discussed the successful synthesis of multi-gram quantities of cyclic PBd—using supported molecular REMP catalysts **5.1 – 5.4** (Fig 5.2)—and its unexpected high *cis* content, relative to ROMP-derived linear PBd from catalysts **5.5 – 5.6** (Fig 5.3). This chapter will explore the origins of this selectivity, and also various methods to control the MW and D of cyclic PBd.

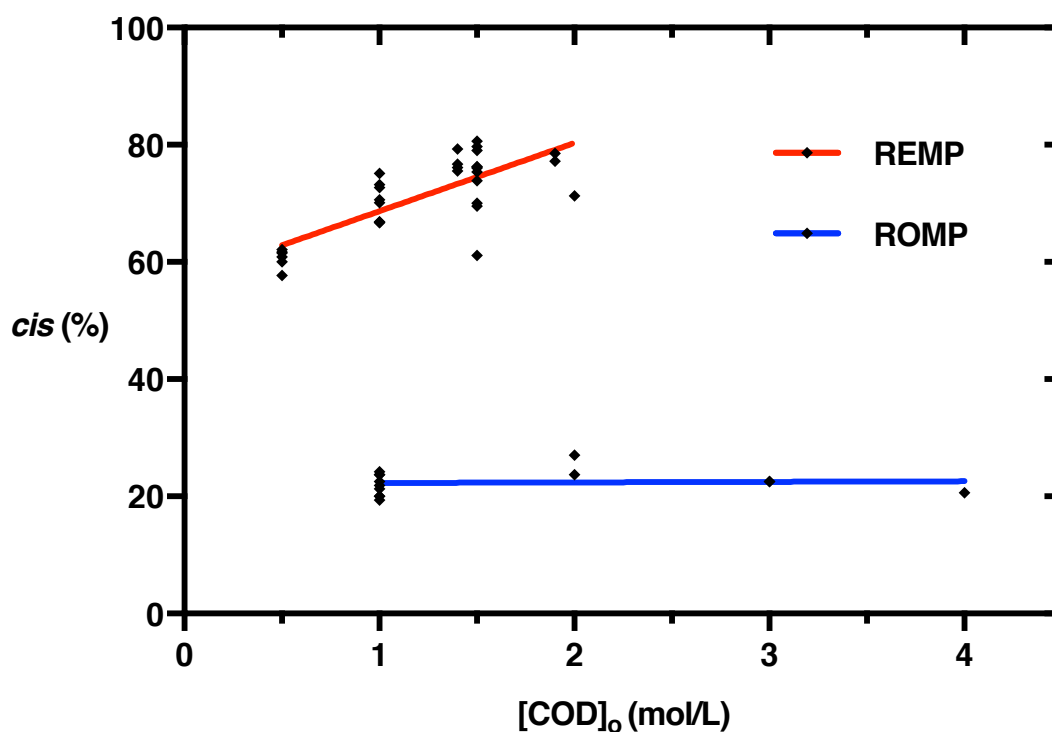


Figure 5.3 | The concentration dependence of *cis* content for REMP of COD compared to the concentration independence of *trans* content for ROMP of COD.

In addition to the *cis* content, the COD REMP reactions discussed in the previous chapter invariably produced PBd with $M_n = 190 - 260$ kDa. Controlling the microstructure and MW of polymers is a fundamental and recurring challenge

in polymer synthesis, so efforts were also undertaken to control M_n of PBd, which will also be discussed in this chapter.

5.2 – Results and Discussion

Initial Investigations of Selectivity in REMP

We developed a model for *cis* selectivity around the relative frequency of secondary metathesis events during REMP: intramolecular chain transfer and intermolecular chain transfer. The former releases a PBd chain from the catalyst and the latter combines to PBd chains into a higher MW species which is still attached to the supported molecular REMP catalyst (Fig 5.3). As shown, this model describes a fundamental *cis*-selectivity of the supported catalyst. We suspected that the SiO₂ surface induced ligand conformations such that a *cis* orientation in the ruthenacyclobutane intermediate was preferred—this is the same general principle which governs the *cis*-selective homogeneous metathesis catalysts developed by our group, and others. Again, this rests upon the assumption that intramolecular chain transfer of cyclic PBd into an actively growing chain occurs much less frequently than the intermolecular chain transfer which releases a cyclic PBd chain into the bulk mixture. In order for the *cis* content to become comparable to the 20% *cis* seen in ROMP, the red olefins (Fig 5.4) would have to coordinate to the catalyst in order to be isomerized to *trans*. The above ideas framed our strategy for finding answers to the general questions of selectivity during REMP with catalysts **5.1 – 5.4**.

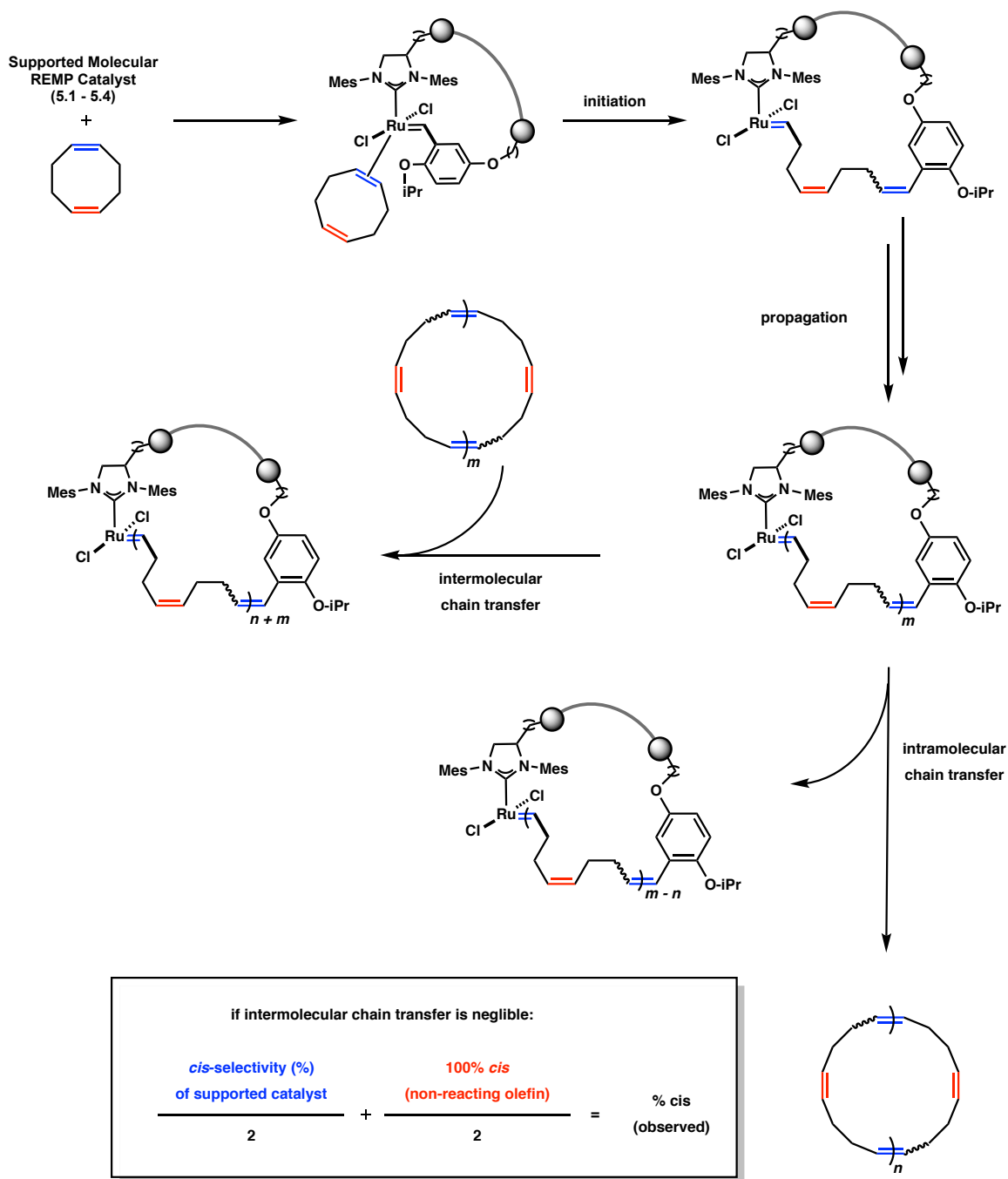


Figure 5.4 | Original model for *cis*-selectivity in REMP of COD.

Along with its *cis* selectivity, the REMP of COD produced PBd with $M_n = 190 - 260$ kDa. Generally speaking, ROMP catalysts and methods provide

excellent control of M_n , so we sought to investigate the preference for this M_n range when catalysts **5.1 – 5.4** were used to REMP COD. In addition to pure curiosity, the overall goal of the project necessitated control *cis/trans* and M_n : to verify the purity of our cyclic polymers via physical property determination, in part using analogous linear polymers as controls.

One general strategy to control microstructure and M_n of PBd was the use of other monomers, namely *cis,trans,trans-* and *trans,trans,trans-* cyclododecatriene (EEZ-CDT and EEE-CDT, respectively). The ring strain and steric profile of CDT isomers varies sufficiently to provide PBd's with significantly different microstructures and M_n 's. The three monomers COD, EEZ-CDT, and EEE-CDT all provide PBd via metathesis polymerization, and there exist 3 strategies for controlling PBd properties and topology using these monomers (Fig 5.5). We focused on EEZ-CDT for most experiments because EEE-CDT was not reactive in REMP reactions (Figure 5.6), presumably from a combination of its lower ring-strain and the steric environment surround a reacting *trans* olefin versus a reacting *cis* olefin. Both EEZ-CDT and EEE-CDT were reactive with homogeneous ROMP catalysts **5.5 – 5.6**, however.

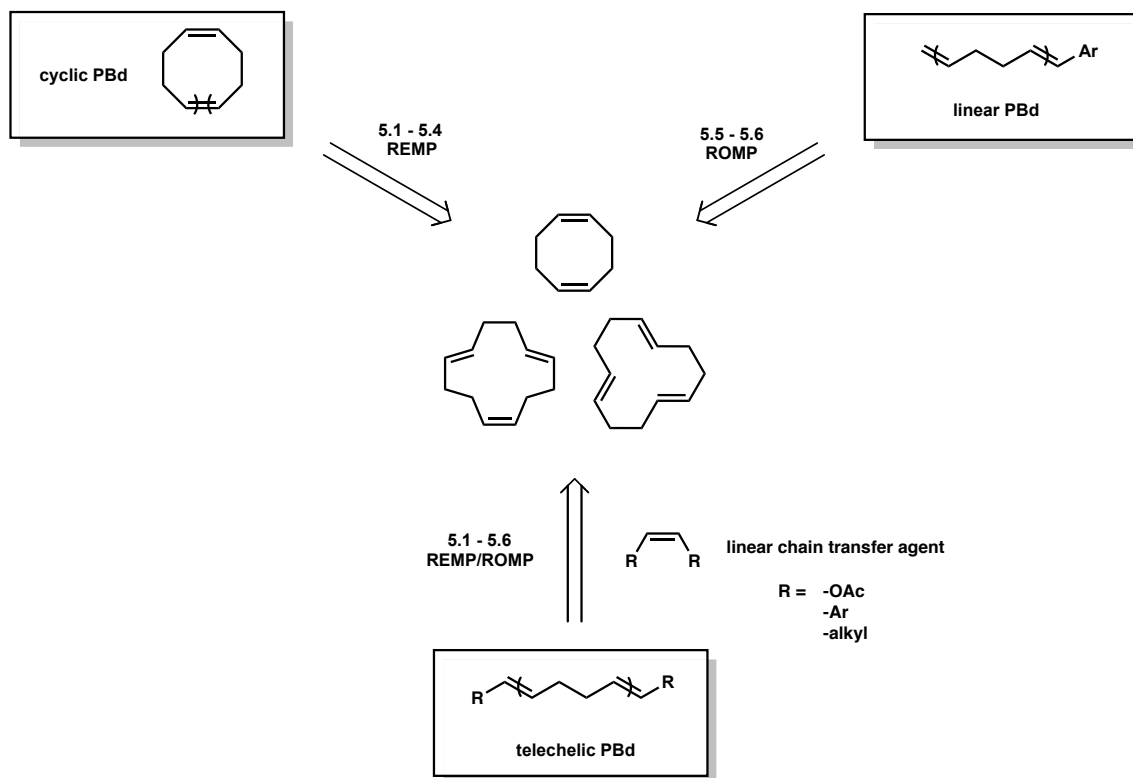


Figure 5.5 | Strategies for preparing cyclic PBd (upper left), linear PBd (upper right), and telechelic PBd, which is also of course linear (bottom).

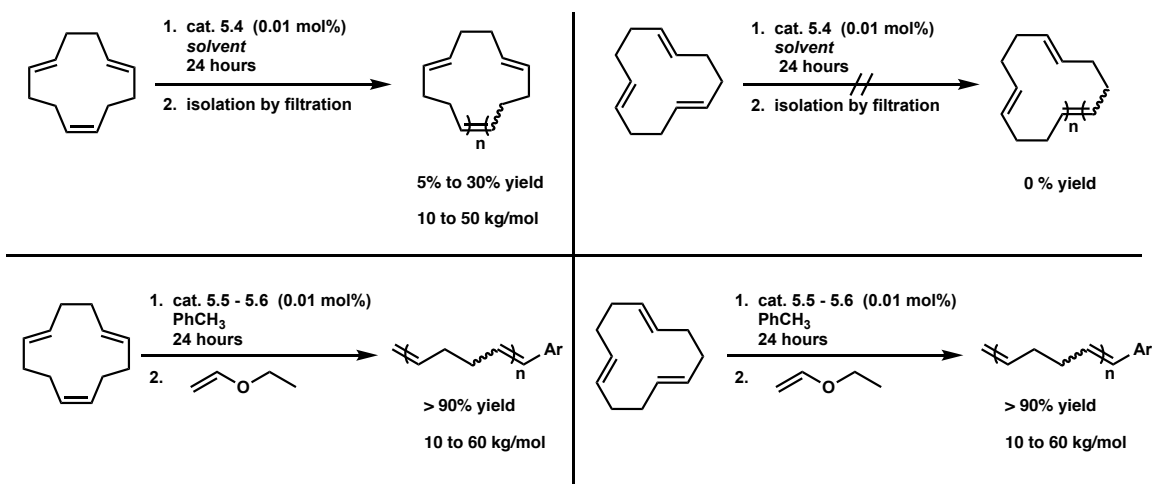


Figure 5.6 | REMP (top) and ROMP (bottom) of both CDT isomers.

The finding discussed in Chapter 3 where 1% ^tBuOH/PhCH₃ co-solvent system improved the REMP of CP was evaluated again. We also needed to produce multi-gram quantities of cyclic PBd for analysis by rheology and IC, and they had to be lower M_n than the samples described in Chapter 4 in order to simplify analysis and data interpretation. We produced four batches of PBd with REMP catalyst **5.4** using different conditions and delivered them to collaborators for further analysis (Table 5.1). Polymer **5.02** was produced with recycled cat. **5.4** from polymer **5.01**, and Polymer **5.04** was produced with recycled cat. **5.4** from polymer **5.03**. As with the PCP produced in Chapter 3, the ^tBuOH led to higher yields, higher M_n , and lower \mathcal{D} . The GPC elution profiles were markedly different for **5.01 – 5.02** versus **5.03 – 5.04** (Figure 5.7).

Table 5.1 | REMP of EEZ-CDT to cyclic PBd using catalyst **5.4** under varying solvent conditions. ^aDetermined by ¹³C NMR.

entry	solvent	cis ^a (%)	M_n (kg/mol)	\mathcal{D} (M_w/M_n)	yield (%)
5.01	PhCH ₃	30	1.8	1.9	17
5.02	1% H ₂ O / PhCH ₃	34	1.7	1.8	13
5.03	1% ^t BuOH / PhCH ₃	13	5.1	2.0	71
5.04	1% ^t BuOH / PhCH ₃	13	3.8	2.1	37

These samples were the first of our PBd samples analyzed through IC, and the elution conditions necessary to separate these samples required considerable effort to develop. The first solvent gradient attempted, Gradient 1 (Fig 5.7), was

sufficient to indicate considerable topological heterogeneity in **5.03** – **5.04**, although **5.01** – **5.02** appeared completely topologically homogeneous (Fig 5.8). In order to enhance the topological separation, more sophisticated gradients were explored (Fig 5.9) using **5.04** as the analyte. Polymer 5.04 was chosen because it appeared to be the least topologically pure, so would be a good benchmark for the efficiency of the desired separation conditions. The data presented in Figures 5.9 – 5.16 illuminate two critical successes of this work: we achieved highly pure cyclic PBd and demonstrated the power of IC in topological characterization of macromolecules. Figures 5.11 and 5.12 show the importance of choosing an appropriate solvent system for efficient separation, which is unfortunately not universal for all topologically distinct macromolecules.

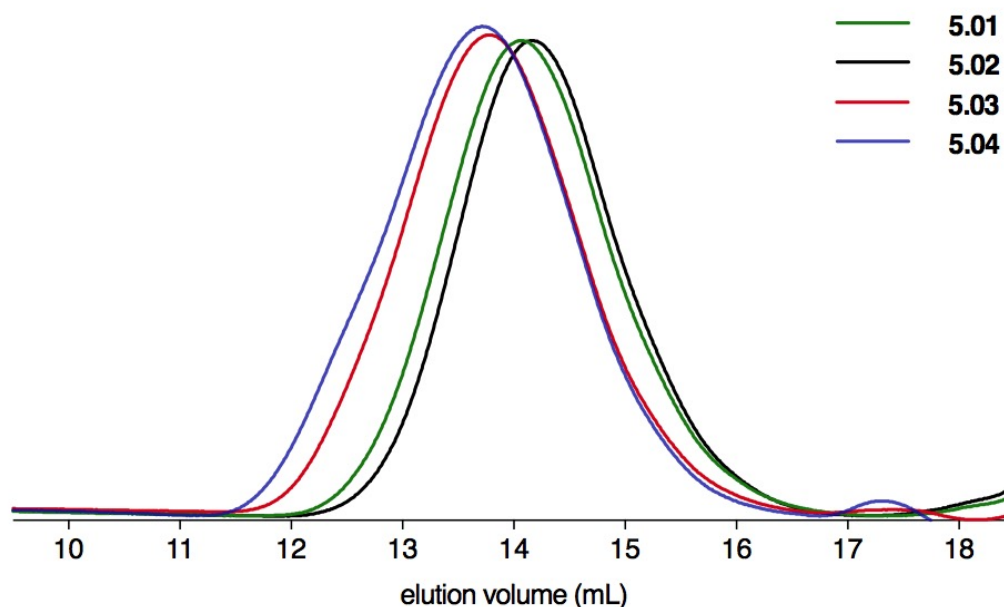


Figure 5.7 | GPC elution profiles for PBd's **5.01** - **5.04**.

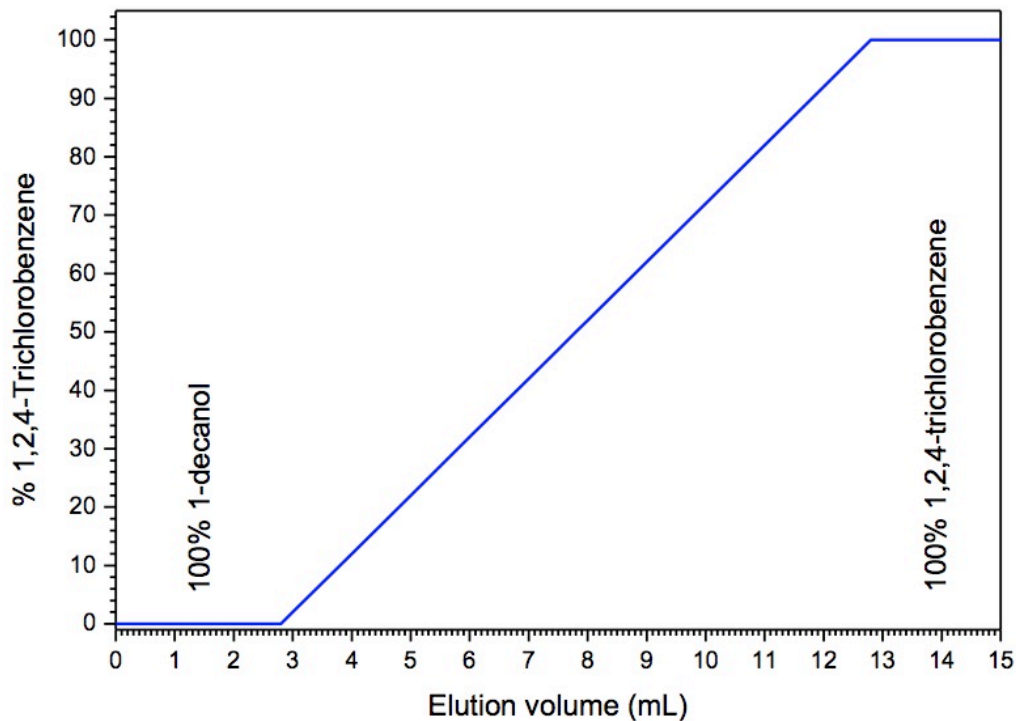


Figure 5.8 | Gradient 1 (blue line) used in IC separation of PBd's 5.01 – 5.04.

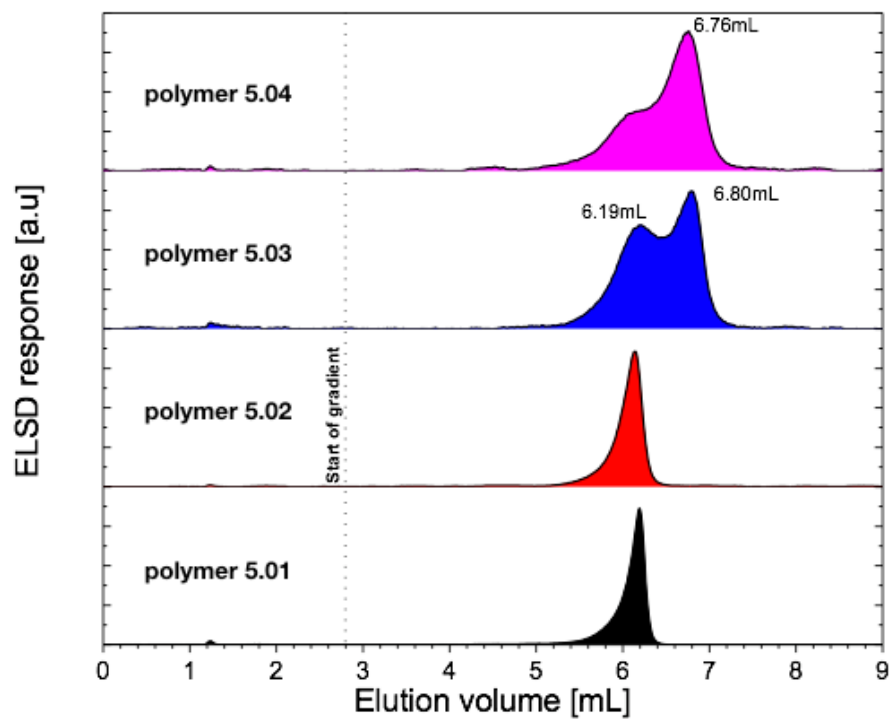


Figure 5.9 | The IC elution profiles for 5.01 – 5.04. Quantified by normalized evaporative light-scattering detector instrument response.

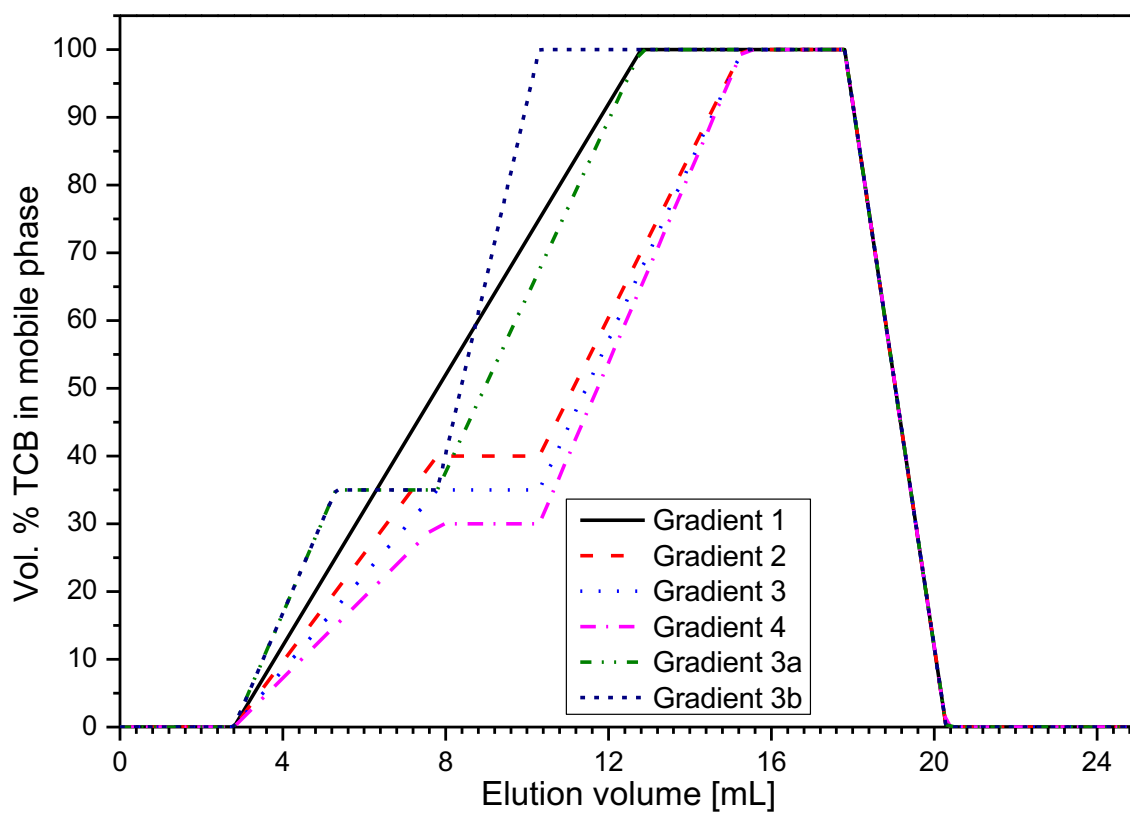


Figure 5.10 | IC elution gradients explored for PBd separations. Eluent consisted of 1-decanol / 1,2,4-trichlorobenzene.

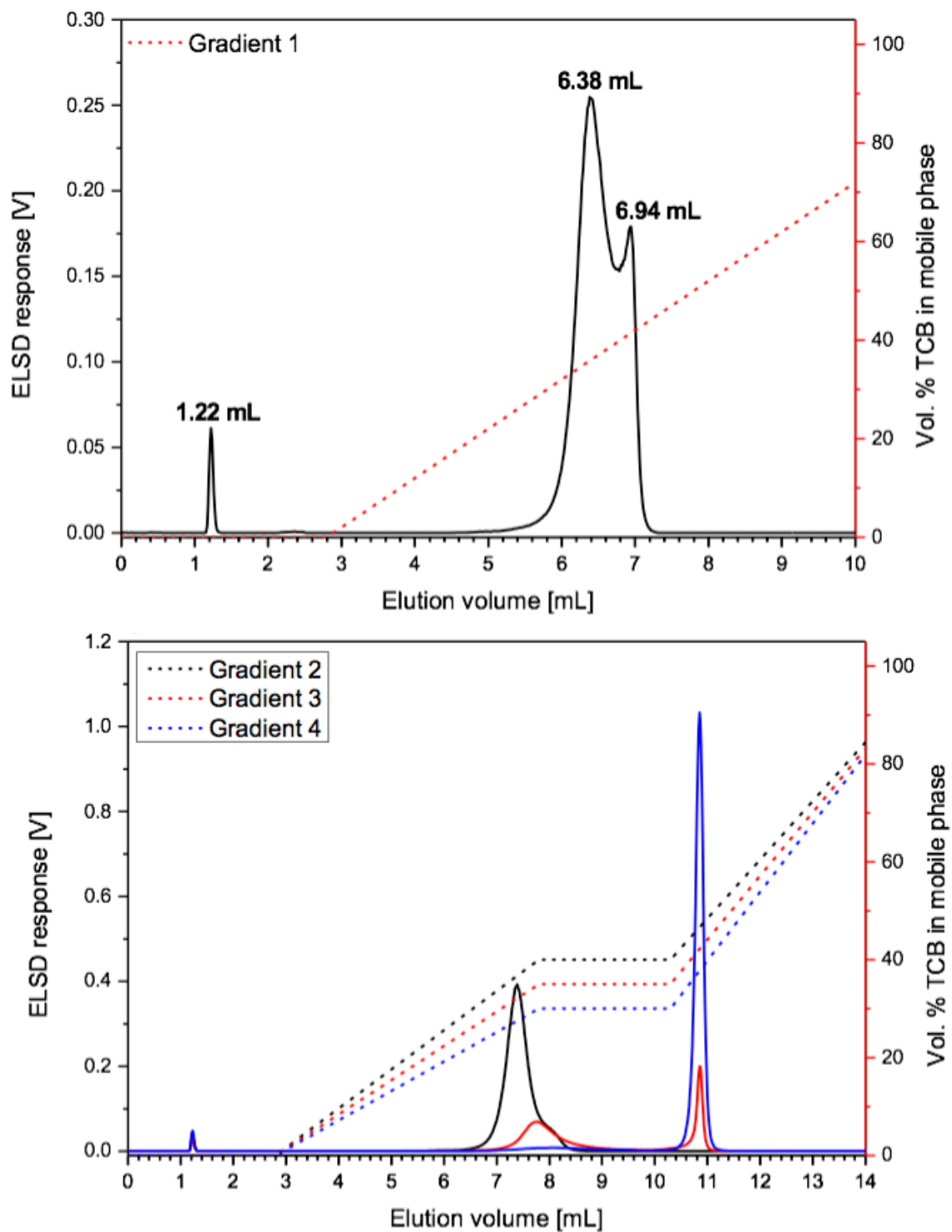


Figure 5.11 | Elution gradient 1 (top) and comparison of elution gradients 1 – 3 (bottom), all with polymer **5.04**.

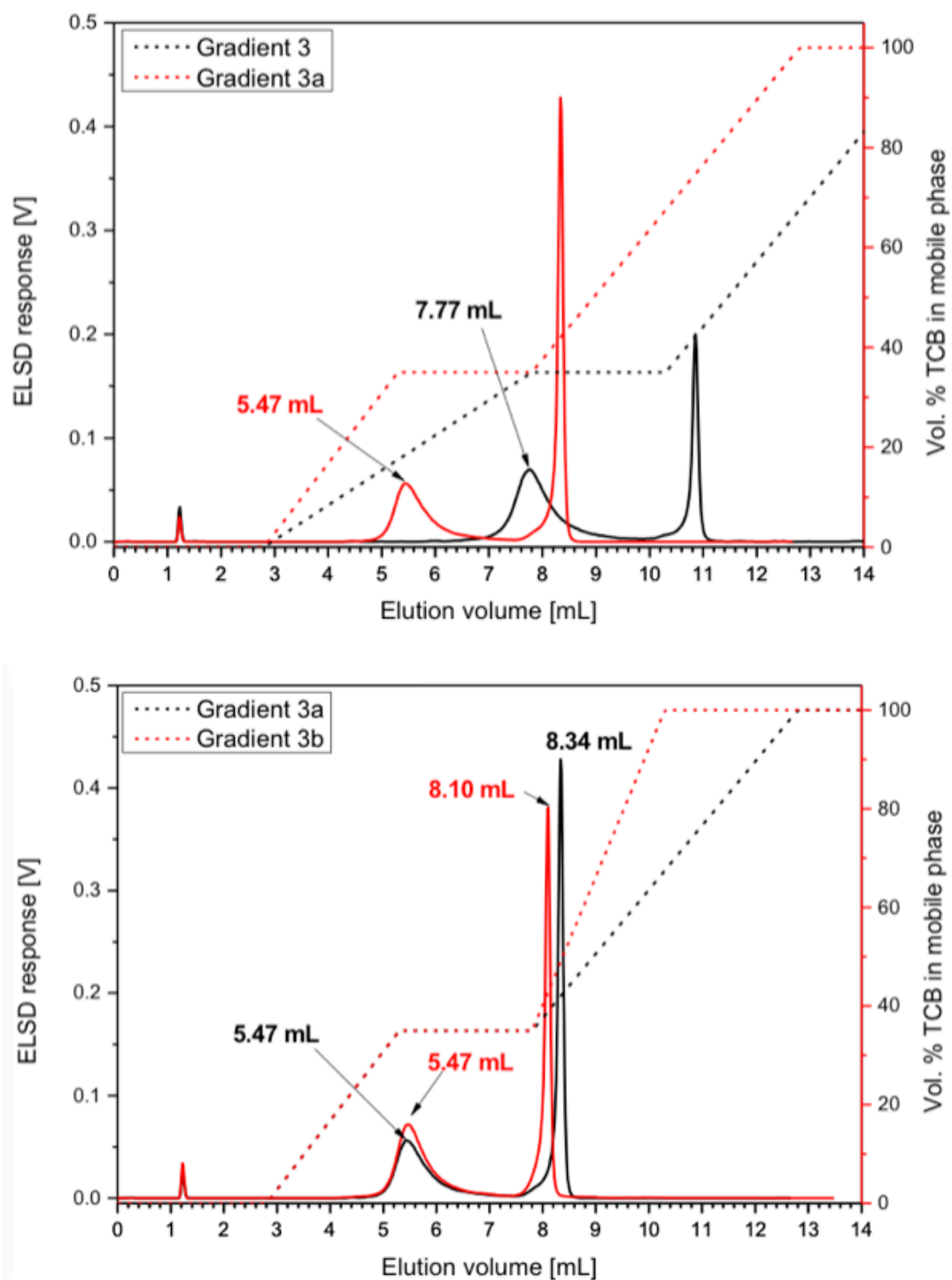


Figure 5.12 | Elution gradients 3 and 3a (top) and elution gradients 3a and 3b (bottom), all with polymer **5.04**.

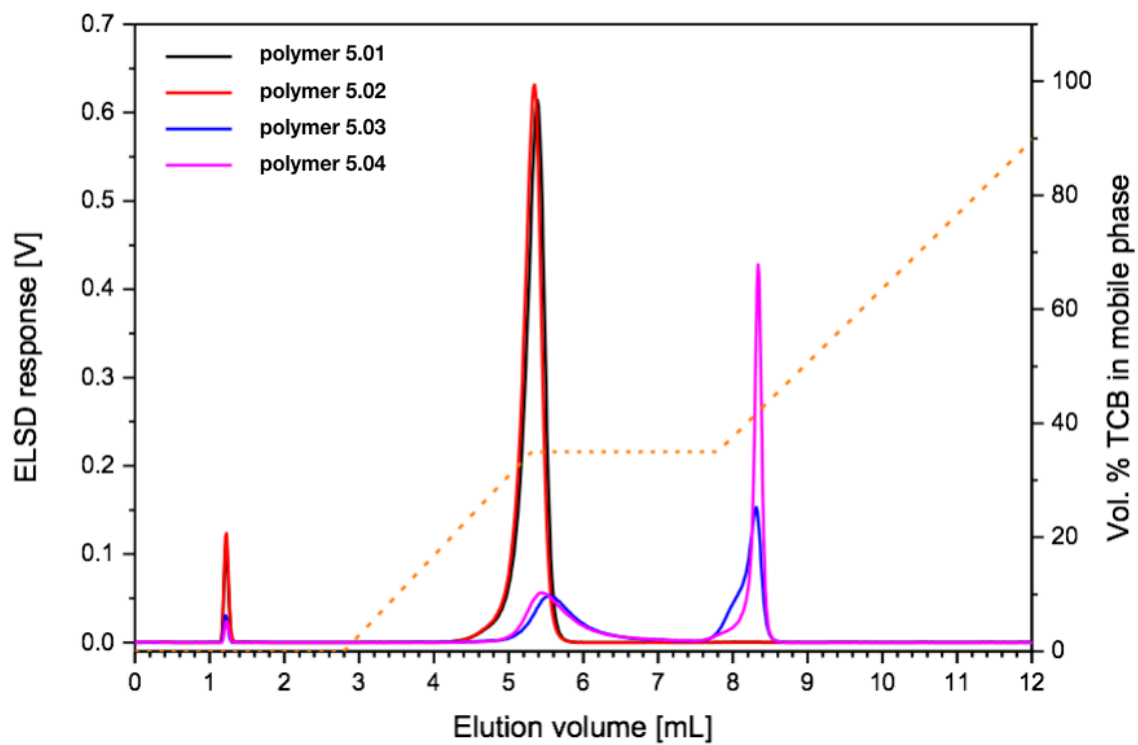


Figure 5.13 | Gradient 3a IC separation of PBd's 5.01 – 5.04. Unretained material at 1.2 mL was small molecule impurity (present in all samples).

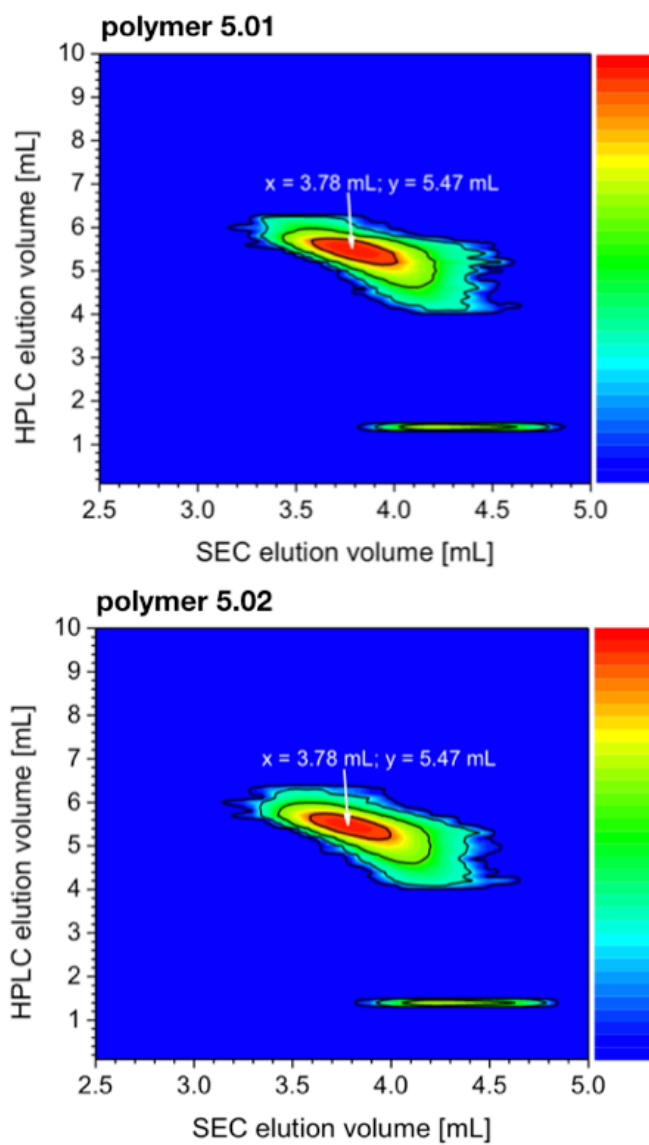


Figure 5.14 | 2D IC-SEC plots for polymers **5.01** – **5.02** with logarithmic color bar scale.

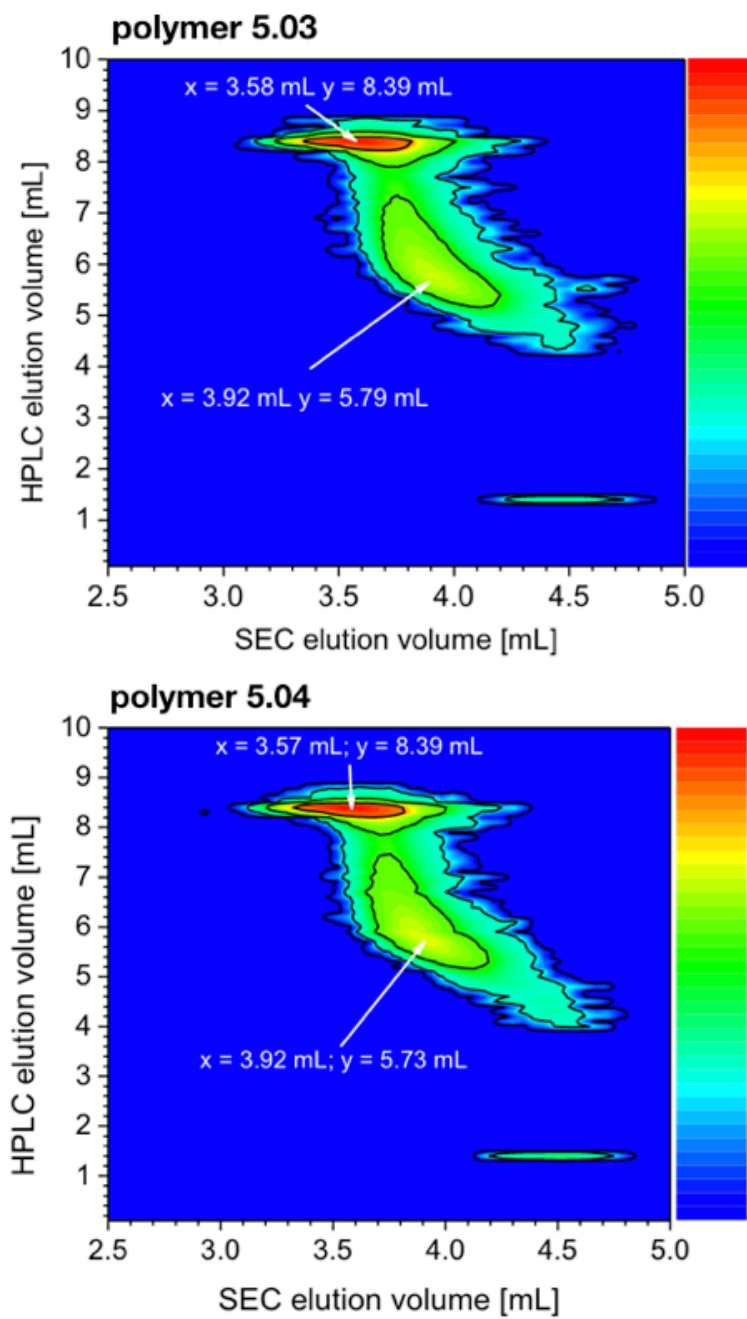


Figure 5.15 | 2D IC-SEC plots for polymers **5.03** – **5.04** with logarithmic color bar scale.

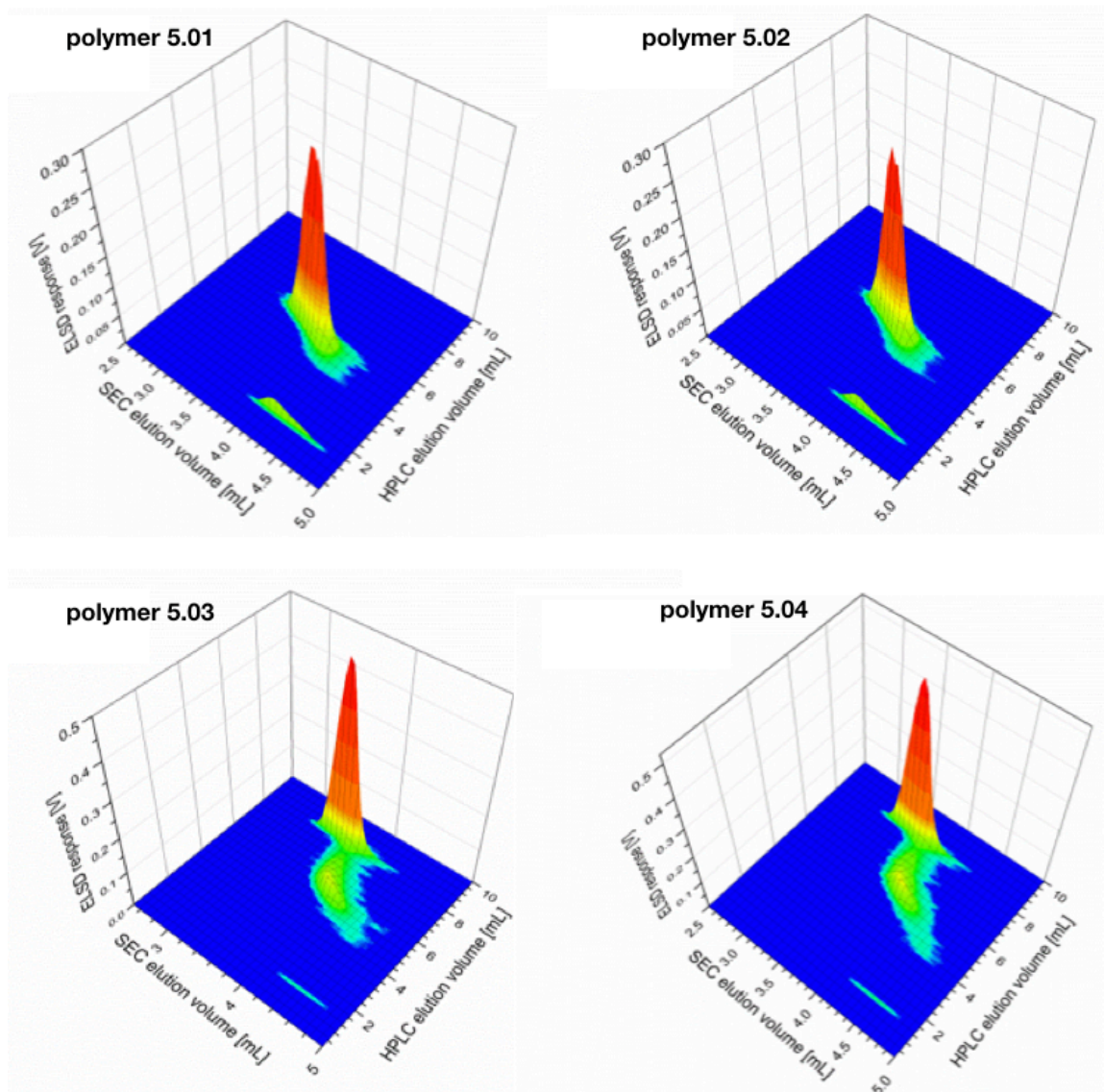


Figure 5.16 | 3-D plot of the IC data shown in Fig 5.14 and 5.15.

Despite the topological impurity of PBd synthesized with the tBuOH/PhCH₃ co-solvent system, the polymerization was otherwise better: higher MWs achieved and lower D. Visually, the tBuOH caused the SiO₂ catalyst particles to disperse more evenly in the polymerization medium. We believe this likely occurs due to H-bonding of tBuOH with the -OH terminated SiO₂ surface which forms solvent shells and prevents particle aggregation. We attempted to optimize REMP of EEZ-CDT using various solvents and conditions, including the use of the more electronegative aromatic solvents chlorobenzene, dichlorobenzene, m-xylene and fluorobenzene; benzene, without a dipole, was also investigated (Table 5.2). Quite unfortunately, we were unable to reproduce the positive results of the tBuOH co-solvent using any other conditions. The GPC elution profiles show that polymers **5.9** – **5.13** were lower MW and higher D than polymer **5.03** (Fig 5.17).

Table 5.2 | Small-scale REMP optimization experiments (all with 0.01 mol % catalyst **5.4**).

entry	[CDT] ₀ (mol/L)	solvent	yield (%)	cis ^a (%)	<i>M_n</i> (kg/mol)	<i>D</i> (<i>M_w</i> / <i>M_n</i>)	reaction time (hour)
5.1	1.0	PhCH ₃	7	30	1.8	2.4	24
5.2	1.5	PhCH ₃	13	36	1.7	1.9	24
5.3	2.0	PhCH ₃	15	36	5.1	3.9	24
5.4	3.0	PhCH ₃	23	34	3.8	6.2	24
5.5	5.4	PhCH ₃	20	30	26.3	1.8	66
5.6	5.4	PhCH ₃	10	33	14.0	1.8	66
5.7	5.4	PhCH ₃	6	35	11.5	2.0	66
5.8	5.4	PhCH ₃	11	34	13.5	1.8	66
5.9	3.0	PhH	11	33	16.6	1.7	24
5.10	3.0	C ₆ H ₅ Cl	6	36	16.6	1.8	24
5.11	3.0	C ₆ H ₄ Cl ₂	4	36	11.8	1.7	24
5.12	3.0	<i>m</i> -Ph(CH ₃) ₂	10	34	20.5	1.9	24
5.13	3.0	C ₆ H ₅ F	12	35	21.8	1.9	24

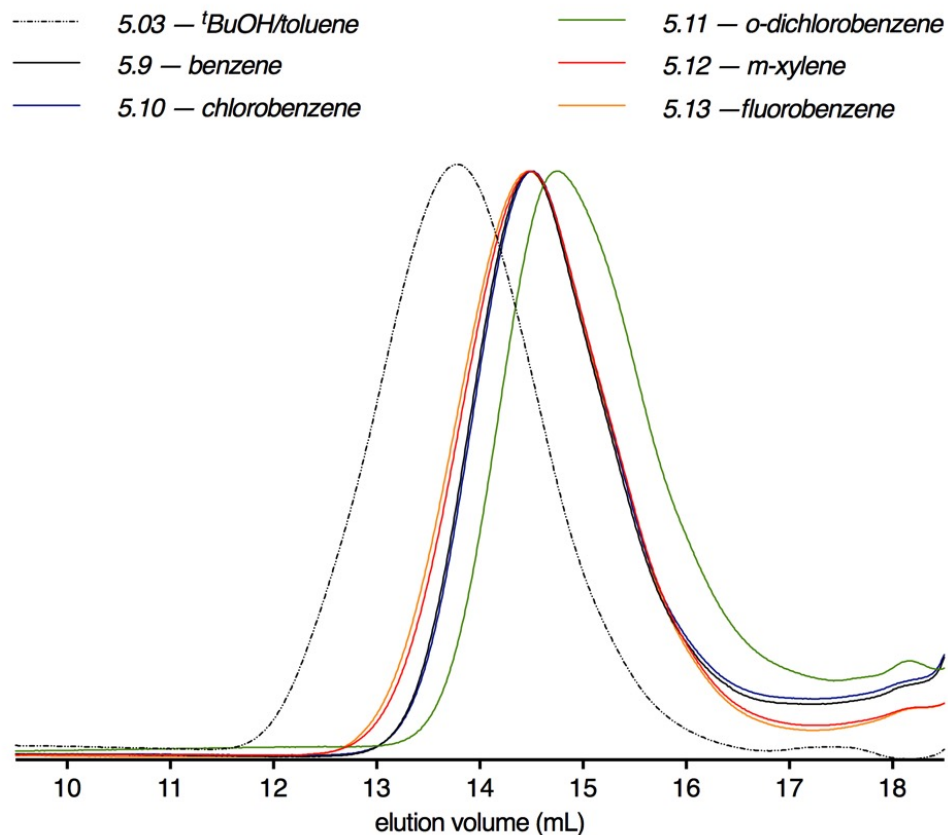


Figure 5.17 | GPC elution profiles (dRI traces) for EEZ-CDT-derived PBd prepared with REMP catalyst **5.04**.

Cyclic and Linear PBd Analogs

We were largely unsuccessful in gaining control of material properties of PBd produce with REMP of EEZ-CDT using catalyst **5.4**. We then shifted our focus to the synthesis of linear PBd analogs using the supported molecular REMP catalysts, instead of homogeneous ROMP catalysts **5.5** – **5.6**. The obvious route to linear polymers is to ROMP COD or CDT using a homogeneous ROMP catalyst, but we decided to take advantage of the chain cleavage caused by incorporation

of linear chain transfer agent (CTA) during REMP (Fig 5.18). This process is, of course, detrimental when synthesizing cyclic polymers, but we felt this strategy would be the best control for making perfect cyclic/linear analogs since they could be *cis/trans* and MW matched if polymerized with the same catalyst.

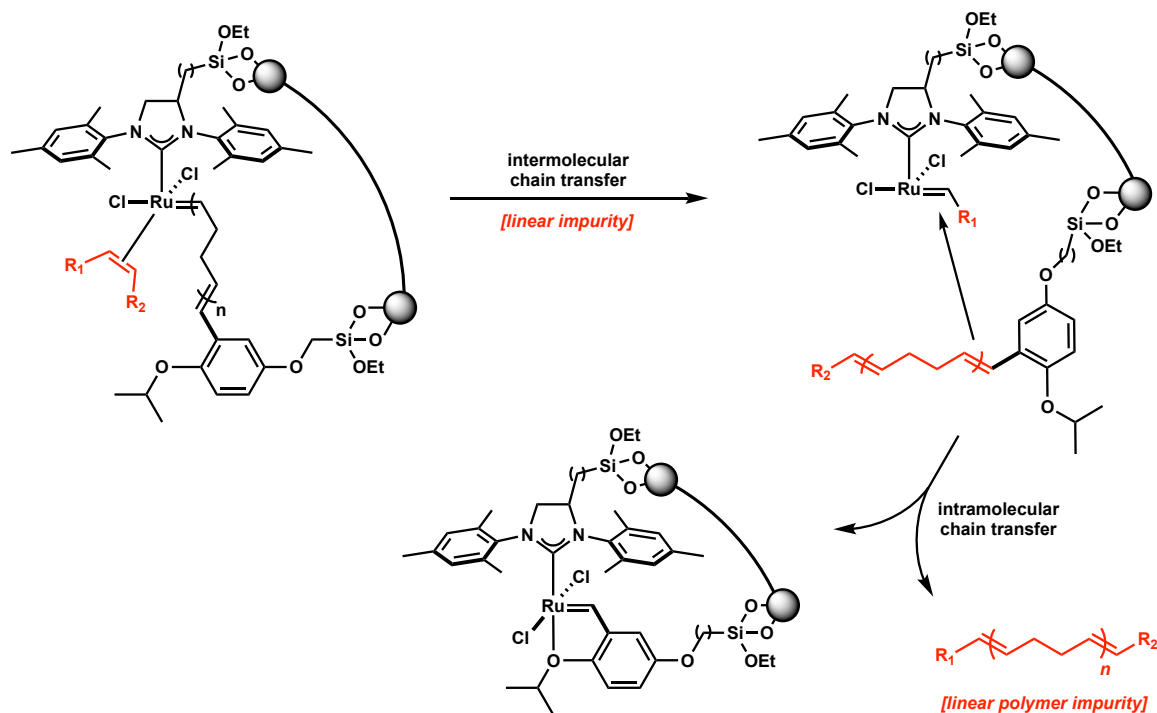


Figure 5.18 | The process during REMP where linear CTA (red) causes chain cleavage and a linear polymer (red, bottom right).

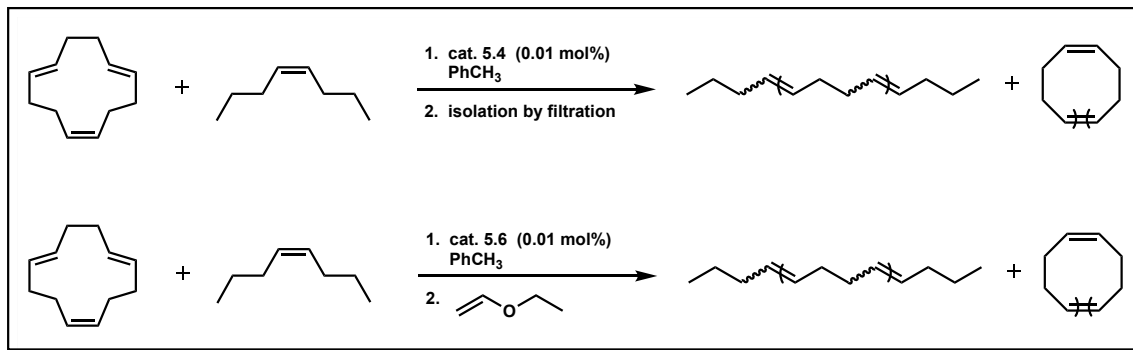


Figure 5.19 | Synthesis of cyclic and linear PBd analogs using *cis*-4-octene.

We synthesized cyclic and linear PBd using **5.4** and **5.6** with varying amounts of the CTA *cis*-4-octene (Figure 5.19). By monitoring M_n vs. $[cis\text{-}4\text{-octene}]_0$, we were able to get a sense for the relative ratio cyclic:linear in the PBd produced. Because the M_n of a cyclic chain does not change when one *cis*-4-octene molecule inserts into the backbone, there was a threshold $[cis\text{-}4\text{-octene}]_0$ where a M_n change would be observed. Our initial experiments were according to the scheme in Fig 5.19, bottom, using homogeneous cat. **5.6** (Fig 5.20). We were able to gain control of M_n through variable reaction time and equivalents of added CTA.

The addition of CTA to REMP reactions then proceeded according to the scheme in Fig 5.20, top. According to our initial assumptions about the system, we hoped to see a gradual decrease in M_n as more equivalents of CTA were added (Fig 5.21, top, polymers **5.14** – **5.19**). This experiment was mostly successful, as the control without CTA eluted first, and the PBd with the most added CTA eluted last. However, the intermediate entries eluted somewhat unpredictably. We elected to repeat this experiment using the exact same conditions (Fig 5.21, bottom, polymers **5.20** – **5.25**). Fortunately we were able to see a predictable trend in GPC elution profiles depending on added CTA. These samples were being analyzed by IC and rheology at the time this dissertation was submitted.

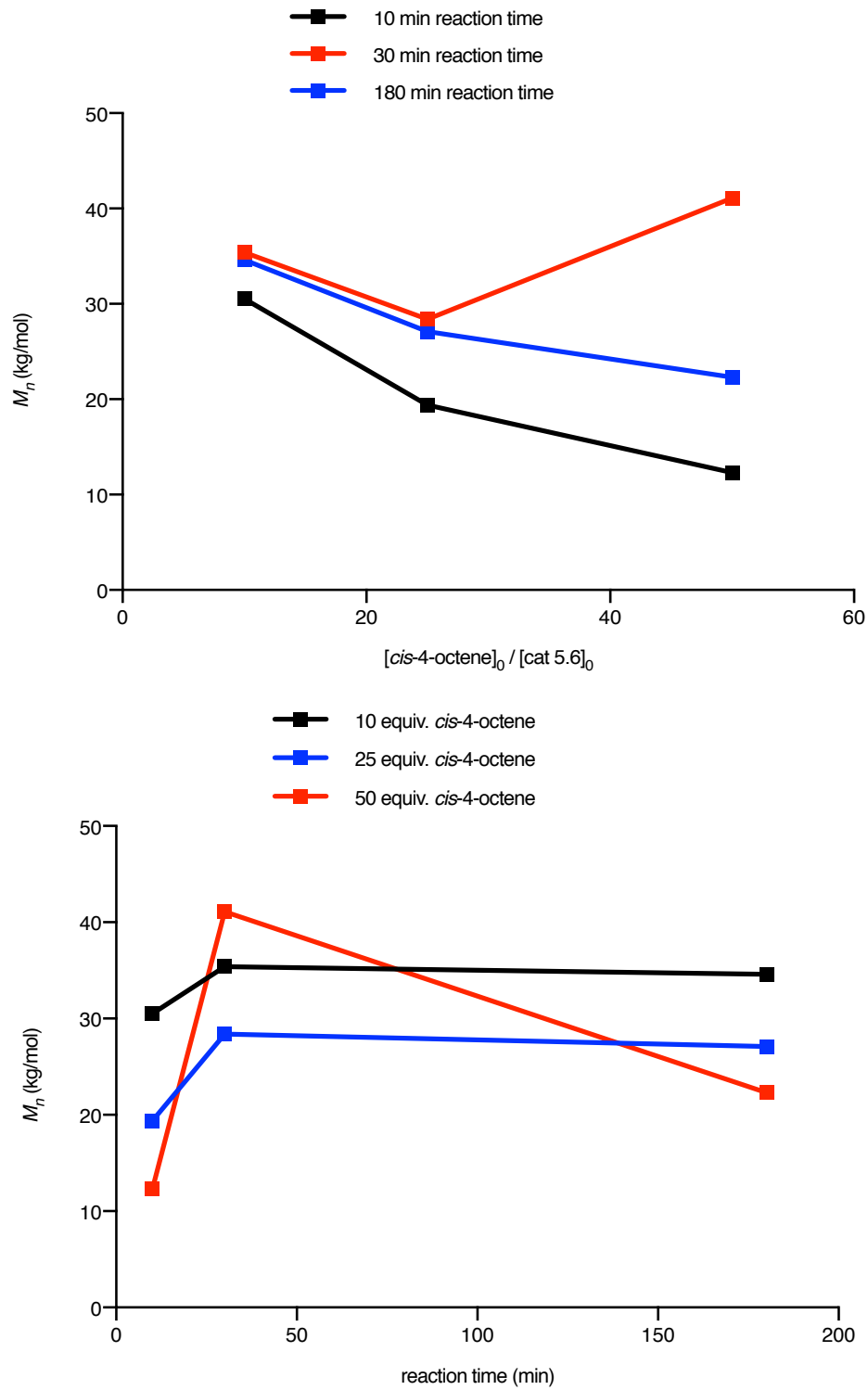


Figure 5.20 | M_n control through $[cis-4-octene]_0$ and reaction time.

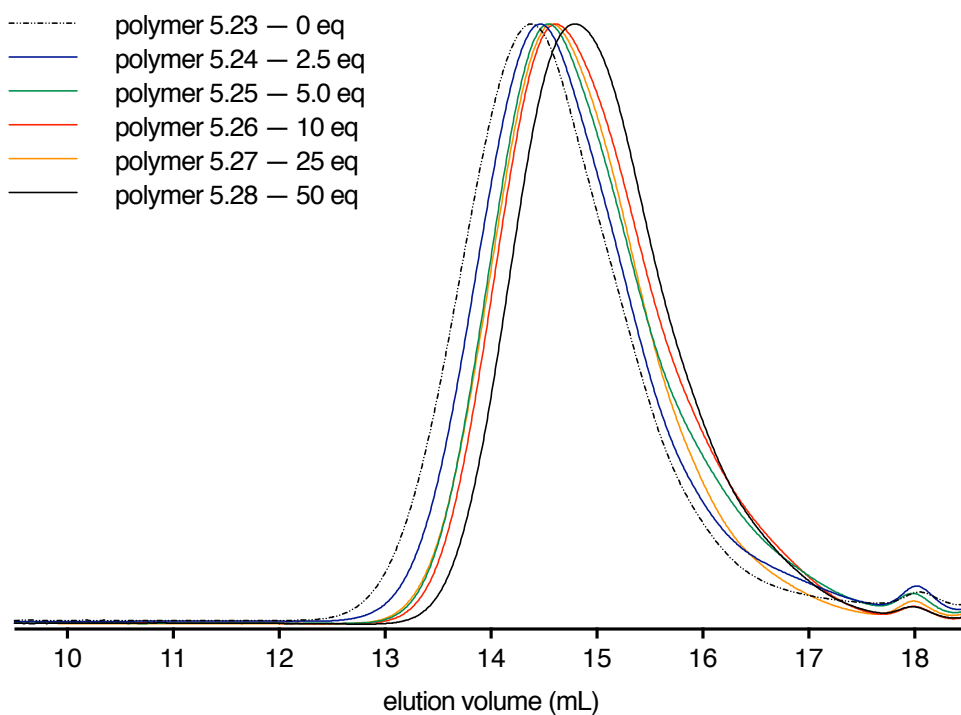
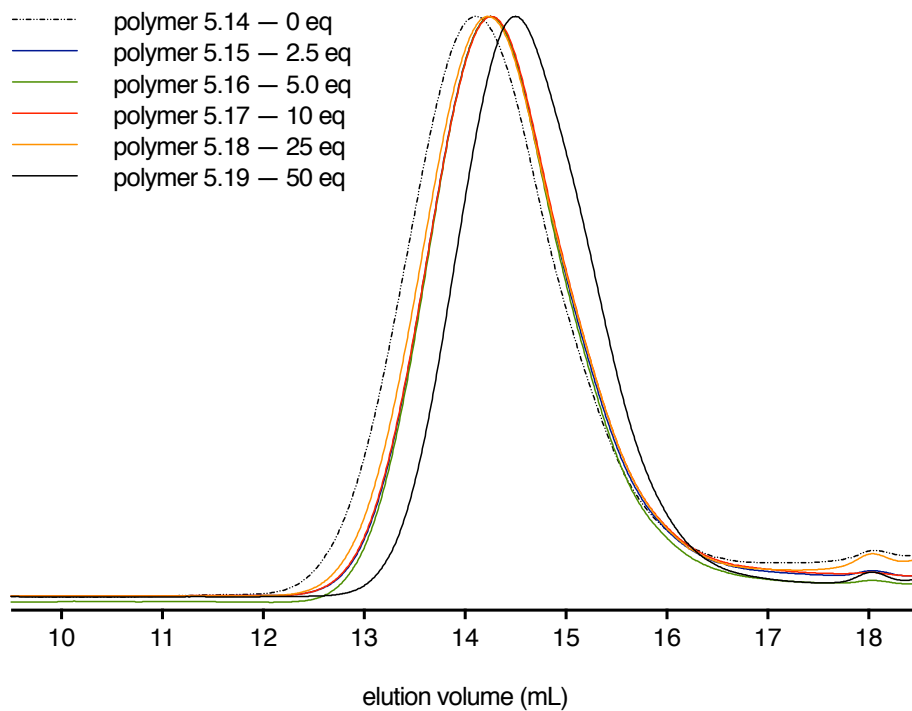


Figure 5.21 | GPC elution profiles of a series of REMP reactions with progressively more eq. of *cis*-4-octene (polymers 5.14 – 5.27 top), and their duplicates (polymers (5.23 – 5.28)).

Effect of REMP Catalyst Tether Lengths

As discussed previously, the means to control MW and microstructure in cyclic PBd would be a significant advance in our efforts to improve our REMP methodology. We suspected the tether lengths from NHC ligand and isopropoxy chelate on our supported molecular REMP catalysts **5.1** – **5.4** could provide some degree of control over material properties. The tether length with the original homogeneous REMP catalysts was shown to greatly affect polymerization profiles.² The distance of the active Ru catalytic site from the SiO₂ surface might affect the rates of monomer incorporation and inter- and intramolecular chain transfer, and thus affect the MW and *cis* content. We investigated this through a series of REMP reactions using catalysts **5.1** – **5.3** polymerize COD at variable concentrations, reaction times, and catalyst loadings (Table 5.3).

Polymers **5.29** – **5.38** (Table 5.3) were characterized using GPC and ¹³C NMR to determine the molecular weight distributions and *cis/trans* isomerism, respectively. The dependence of *cis* content on [COD]₀ was previously observed (Fig 5.3), but we were not able to find this relationship in these experiments. For all concentrations explored (0.5 M, 1.0 M, and 2.0 M), the *cis* content fell between 70% and 78%, unlike the 58% to 82% range we previously observed. Higher concentrations—above 2.0 M—may provide higher *cis* content, but these experiments have not yet been pursued. Polymer **5.32**, however, had a *cis* content far below the others, at 41%. The reaction time (1440 min) and low concentration

(0.5 M) of this reaction led to more instances of chain transfer and *cis*-degradation towards the thermodynamic ratio of 20% *cis*, which is frequently observed for homogeneous metathesis reactions.³⁻⁵ Our previous model of *cis*-selectivity in REMP (Fig 5.4) suggested chain transfer events may have little to no effect on *cis/trans*, but we believe this may not be the case, particularly at lower concentrations. The inherent *cis* selectivity of REMP using catalysts **5.1** – **5.4** may not originate from a steric effect surrounding the ruthenacyclobutane intermediate, but rather, the SiO₂ surface may decrease the frequency of chain transfer events relative to homogeneous catalysts; this phenomenon would be more exaggerated at higher concentrations where diffusion is slower. This is further supported by the elution profiles of polymers **5.29** and **5.32** (Fig 5.24). They were conducted with identical reaction conditions, but **5.32** reacted for 36 times longer. The lower MW region (longer elution time) disappears for **5.32**, likely due to the reincorporation of low MW chains into the active catalyst site, thereby increasing the MW and lowering the D.

Table 5.3 | 15 COD-derived PBd samples prepared under various conditions with catalysts **5.1** – **5.3**. M_w determined by SEC-MALLS and *cis* (%) determined by ^{13}C NMR.

entry	catalyst	catalyst loading (mol %)	[COD] ₀ (mol/L)	reaction time (min)	<i>cis</i> (%)	M_w (kg/mol)	\bar{D} (M_w/M_n)
5.29	5.1	0.01	0.5	40	73	63	3.30
5.30	5.1	0.01	1	40	70	281	1.58
5.31	5.1	0.01	2	40	72	338	1.65
5.32	5.1	0.01	0.5	1440	41	102	1.70
5.33	5.2	0.01	0.5	40	75	35	2.74
5.34	5.2	0.01	1	40	71	301	1.60
5.35	5.2	0.01	2	40	78	428	1.43
5.36	5.3	0.01	0.5	40	74	121	2.13
5.37	5.3	0.01	1	40	72	317	1.47
5.38	5.3	0.01	2	40	74	373	1.52
5.39	5.3	0.025	1.5	120	74	368	1.58
5.40	5.3	0.04	1.5	120	70	272	1.59
5.41	5.3	0.02	1.5	40	73	248	1.42
5.42	5.3	0.0001	5.0	1440	82	483	1.58
5.43	5.3	0.0005	5.0	1080	76	273	1.44

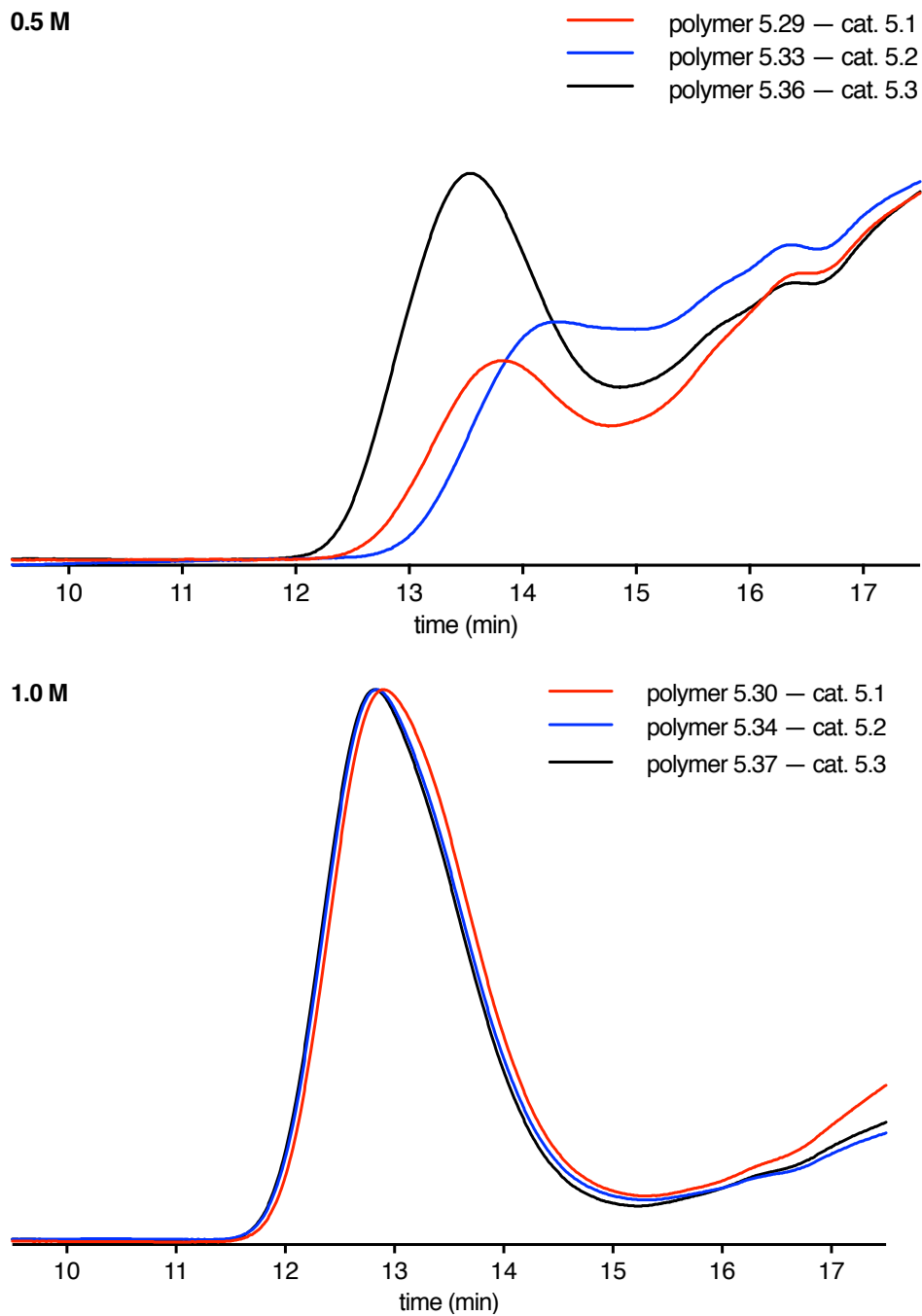


Figure 5.22 | GPC elution profiles of COD REMP using **5.1 – 5.3** at 0.5 M (top), and GPC elution profiles of COD REMP using **5.1 – 5.3** at 1.0 M (bottom).

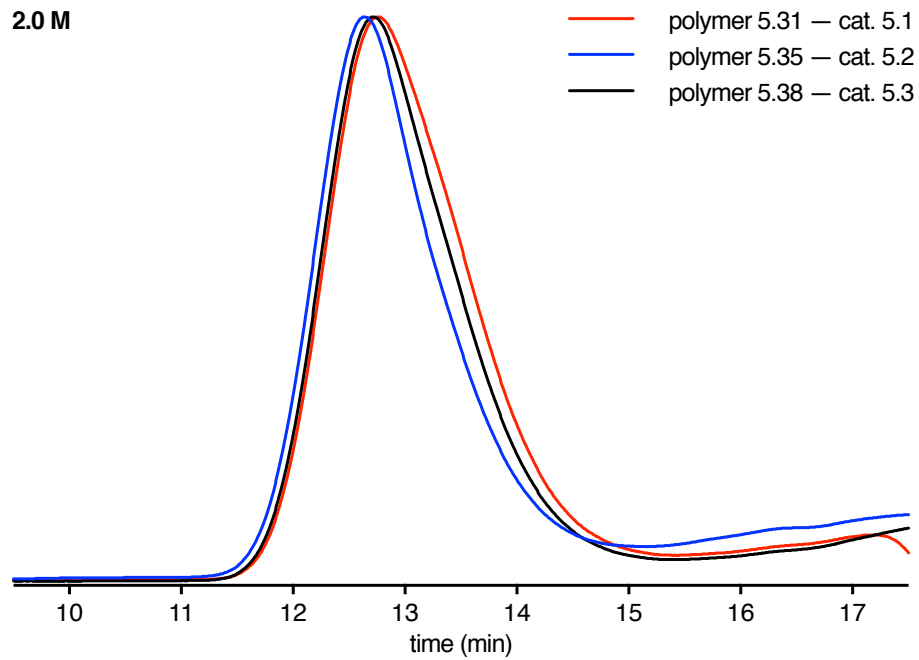


Figure 5.23 | GPC elution profiles of COD REMP using **5.1 – 5.3** at 2.0 M.

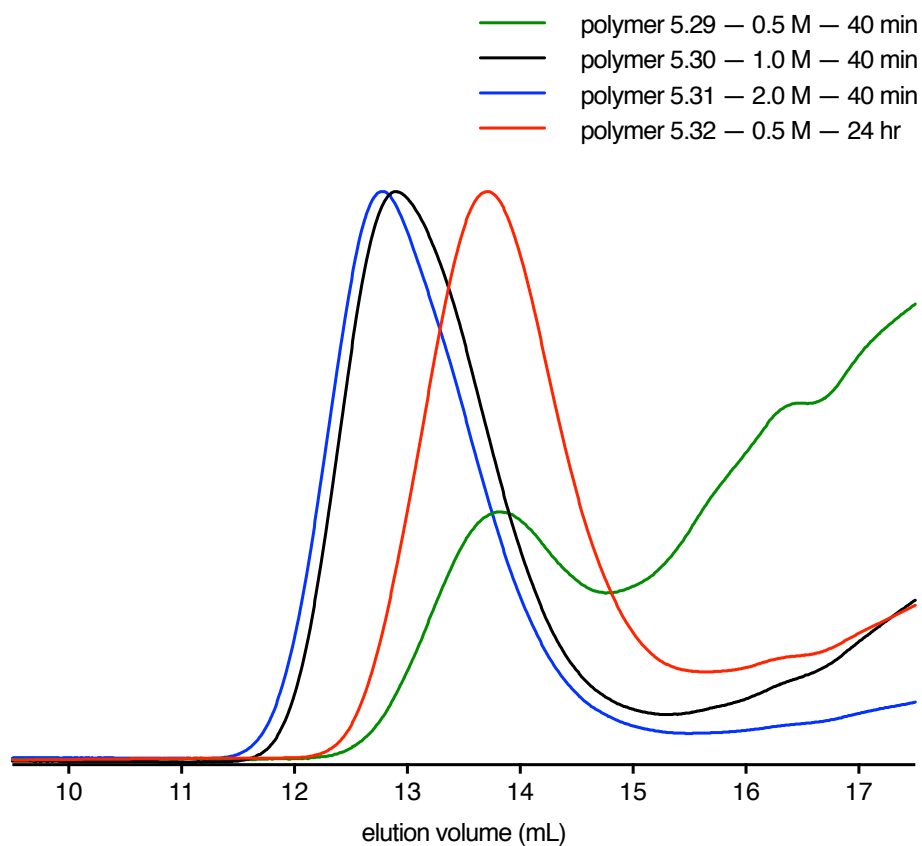


Figure 5.24 | GPC elution profiles of polymers **5.29 – 5.32** prepared with COD and REMP cat. **5.1** at different concentrations and reaction times.

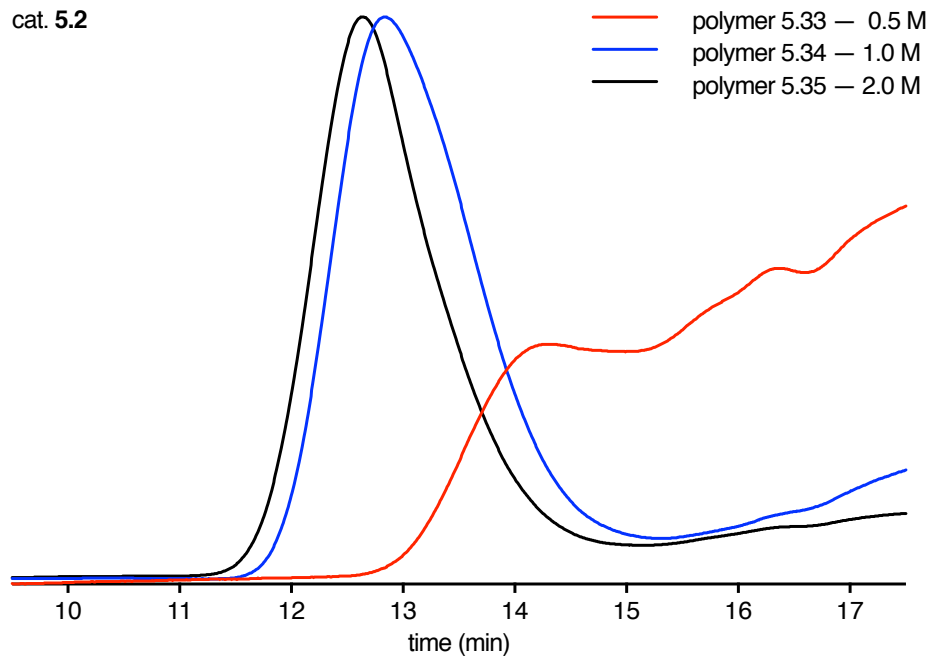


Figure 5.25 | GPC elution profiles of polymers **5.33 – 5.35** prepared with COD and REMP cat. **5.2** at 0.5 M (red), 1.0 M (blue) and 2.0 M (black).

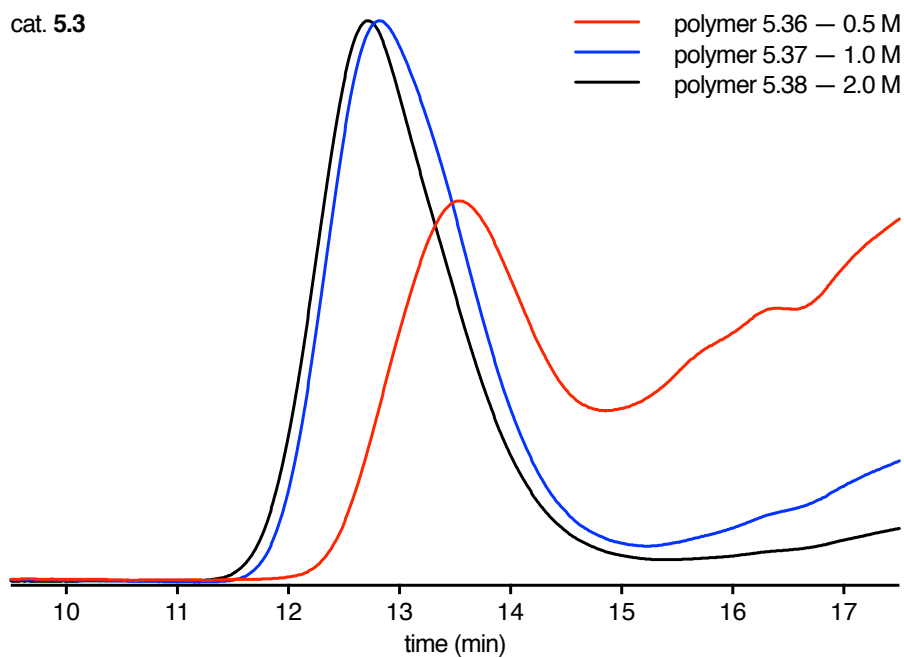


Figure 5.26 | GPC elution profiles of polymers **5.36 – 5.38** prepared with COD and REMP cat. **5.3** at 0.5 M (red), 1.0 M (blue) and 2.0 M (black).

Effects of REMP Catalyst Loading

We further investigated the reactivity and selectivity of REMP catalysts using a broader range of catalyst loading with catalyst **5.3** for COD (Table 5.3, polymers **5.39** – **5.43**). By decreasing catalyst loading, we believed we could decrease the frequency of chain transfer events, and perhaps observe discrepancies in MW and *cis/trans* that we could not observe with higher loadings. Although we did not observe a clear trend with MW vs. catalyst loading as is generally seen with ROMP catalysts,^{Grubbs:2004ct} we did see an excellent GPC elution profile for polymer **5.43**, made using 5.0 ppm catalyst **5.3** (Fig 5.27). It also shows a D value of 1.44, which is among the lowest we have seen for cyclic PBd. Additionally, polymer **5.42**, made using 1.0 ppm catalyst **5.3**, reached a M_w of 483 kDa, which is the highest we have achieved for REMP-derived PBd.

These experiments also provided insight into the nature of *cis* selectivity in REMP. Since we suspect the frequency of secondary metathesis chain transfer events dictates the relative rate of *cis*-degradation, we were interested to find a linear relationship between *cis*(%) and $\log([\text{cat. } \mathbf{5.3}]:[\text{COD}]_0)$ (Fig 5.28). This suggests the rate of chain transfer events is directly proportional to the catalyst loading. We may be able to exploit this phenomenon in the future to control *cis/trans* of PBd and other polyolefins, which would be a powerful addition to the growing array of strategies we have to control reactivity and selectivity during REMP reactions.

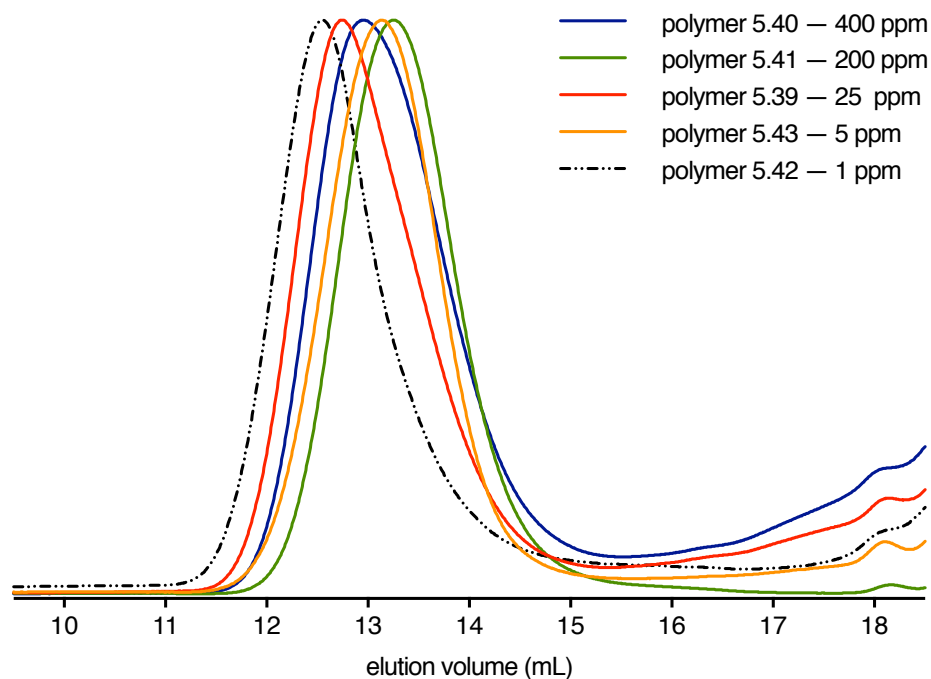


Figure 5.27 | GPC elution profiles of polymers **5.39** – **5.43** prepared with COD and REMP cat. **5.3** using different catalyst loadings ranging from 400 ppm (polymer **5.40**, blue) to 1 ppm (polymer **5.42**, dotted black).

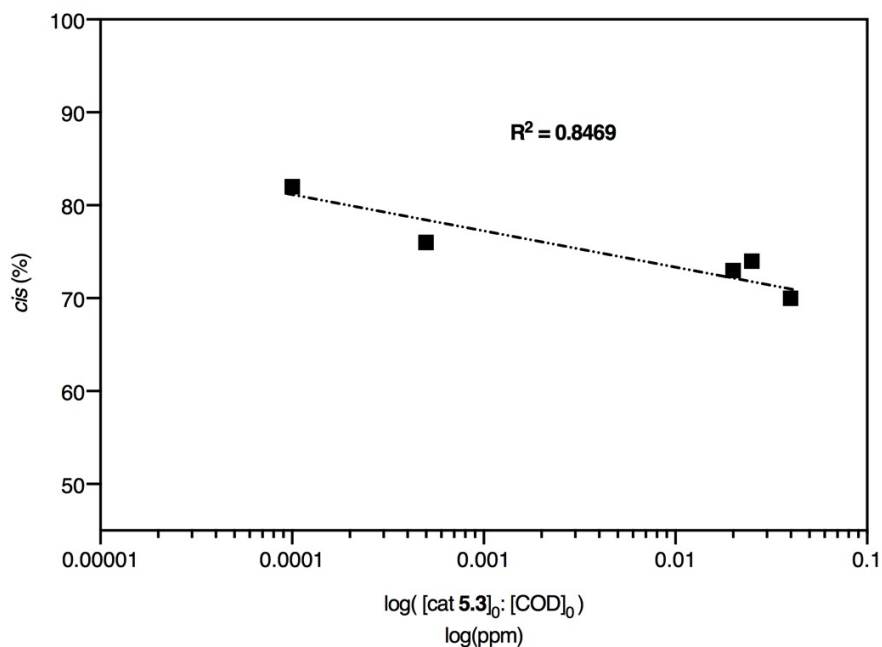


Figure 5.28 | Linear relationship between *cis* and $\log([\text{cat. } 5.3]:[\text{COD}]_0)$ for REMP of COD using catalyst **5.3**.

5.3 – Conclusions and Future Outlook

The investigations into selectivity in REMP reactions discussed in this chapter elucidated the relationship between catalyst loading, *cis/trans* isomerism, MW, D, and reaction time. Experimentally determined reaction parameters allowed us to control the material properties of PBd more than was previously possible. CTAs were shown to reduce the MW of PBd during ROMP and REMP reactions with homogeneous and supported catalysts, respectively. Further studies will be required to reveal any selectivities or reactivities unique to any of the 4 supported molecular REMP catalysts based on their tether lengths to the surface of the SiO₂ support.

5.4 – Experimental

General Information

All reactions were carried out in glassware flame-dried in vacuo (100 mTorr) unless otherwise specified. Reactions were performed using air-free Schlenk technique (100 mTorr vacuum and UHP grade 5.0 argon gas) on the benchtop or in a Vacuum Atmospheres glovebox (N₂-filled, O₂ concentration < 0.25 ppm) unless otherwise specified. All solvents were purchased from Sigma-Aldrich (anhydrous, 99.9%) and further purified by passage through solvent purification columns, sparged with argon, and then stored over 4 Å molecular sieves in Strauss flasks, unless otherwise specified.¹⁷ All homogeneous Grubbs catalyst (**3.1** – **3.6**, Fig 3.1) were received as a generous gift by Materia, Inc. (Pasadena, CA) and used without further purification. All other reagents were purchased from Sigma-Aldrich and used as received unless otherwise stated. Room temperature was 18-20 °C for all syntheses described herein.

Size-exclusion chromatography (SEC) data was obtained with an HPLC system consisting of two two Agilent PLgel MIXED-B 300×7.5 mm columns with 10 µm beads, and an Agilent 1260 Series pump and autosampler; the columns were connected in series with a Wyatt 18-angle DAWN HELEOS multi-angle laser light scattering detector and Optilab rEX differential refractive index detector. The mobile phase was either pure THF or stabilized THF (50-150 ppm butylated hydroxytoluene (BHT)).

Orbital agitation of REMP reactions was performed using an IKA KS 260 basic flat orbital shaker with a swivel motion (no z-axis motion). Orbital agitation rate varied between 200 and 400 rot/min.

5.4 – References

- (1) Brandt, H. D.; Nentwig, W.; Rooney, N.; LaFlair, R. T.; Wolf, U. U.; Duffy, J.; Puskas, J. E.; Kaszas, G.; Drewitt, M.; Glander, S. *Ullmann's Encyclopedia of Industrial Chemistry*, 1, 2nd ed.; Wiley-VCH: Weinheim, Germany, 2000; Vol. 39, pp 30–32.
- (2) Xia, Y.; Boydston, A. J.; Yao, Y.; Kornfield, J. A.; Gorodetskaya, I. A.; Spiess, H. W.; Grubbs, R. H. *J. Am. Chem. Soc.* **2009**, *131* (7), 2670–2677.
- (3) Marx, V. M.; Sullivan, A. H.; Melaimi, M.; Virgil, S. C.; Keitz, B. K.; Weinberger, D. S.; Bertrand, G.; Grubbs, R. H. *Angew. Chem. Int. Ed.* **2015**, *54* (6), 1919–1923.
- (4) Endo, K.; Grubbs, R. H. *J. Am. Chem. Soc.* **2011**, *133* (22), 8525–8527.
- (5) Cannon, J. S.; Grubbs, R. H. *Angew. Chem. Int. Ed.* **2013**, *52* (34), 9001–9004.

Appendix 1

NMR Spectra Relevant to Chapter 2

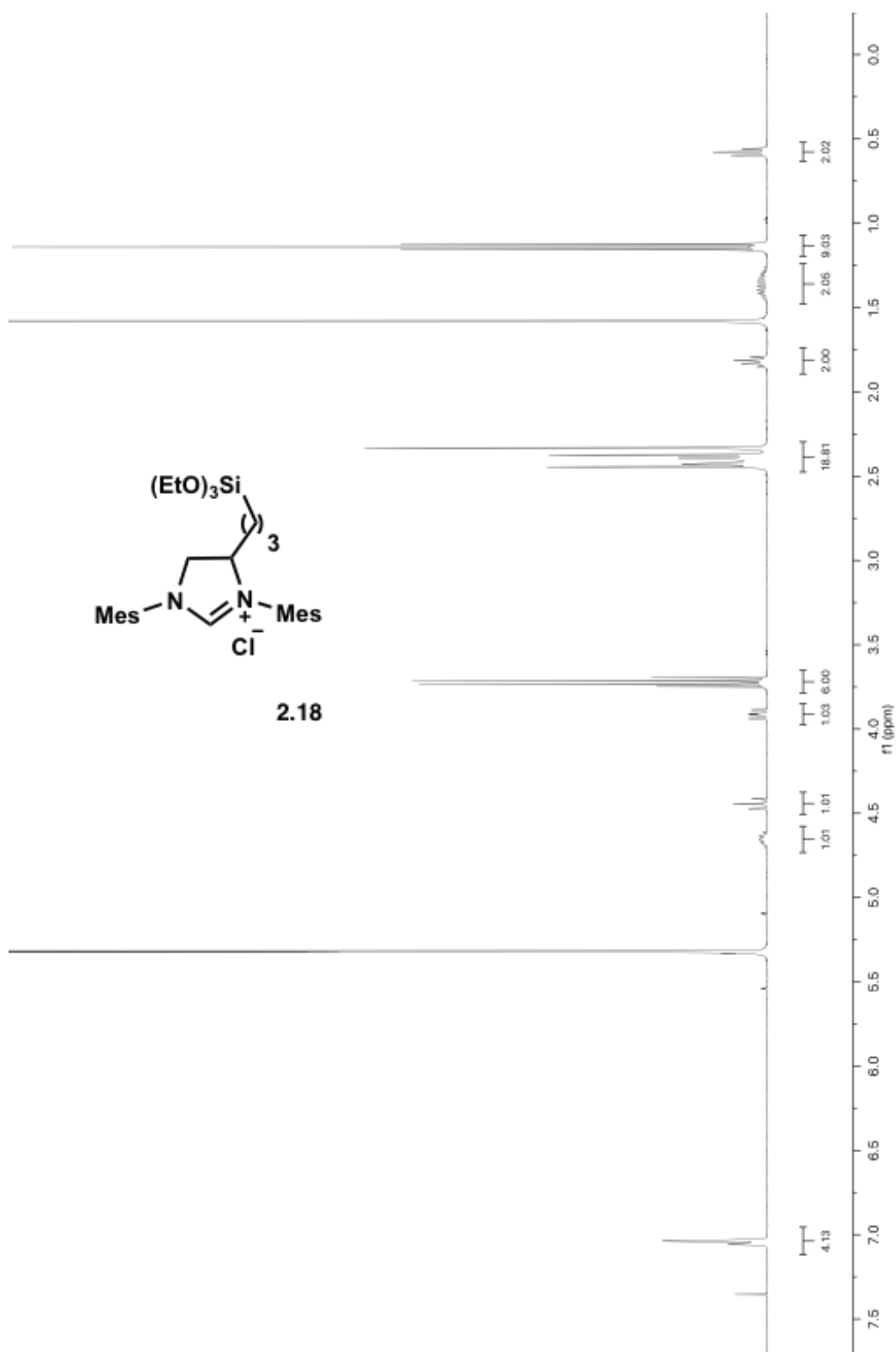


Figure A.1 | ^1H NMR spectrum for **2.18**

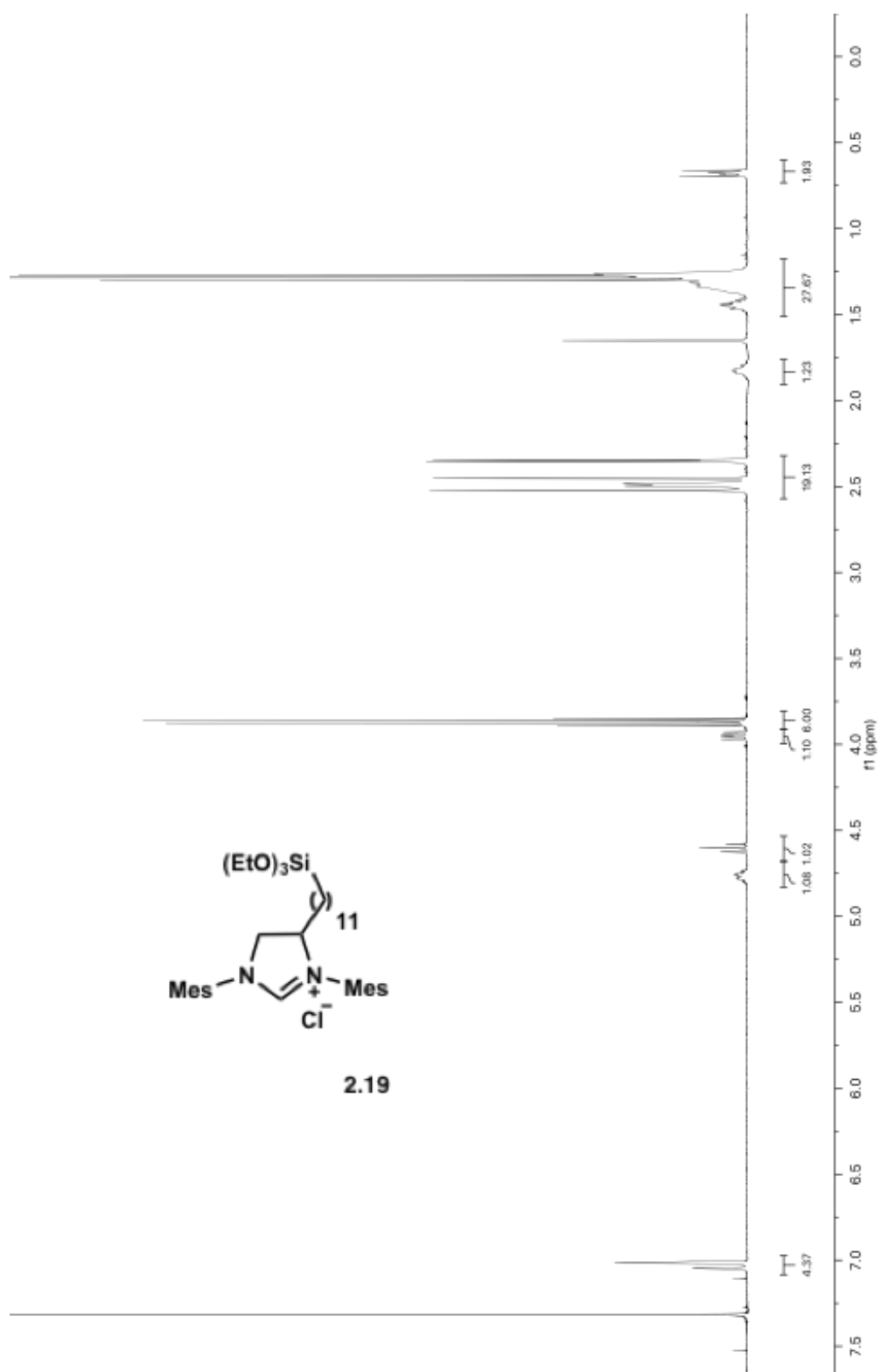


Figure A.2 | ^1H NMR spectrum for **2.19**

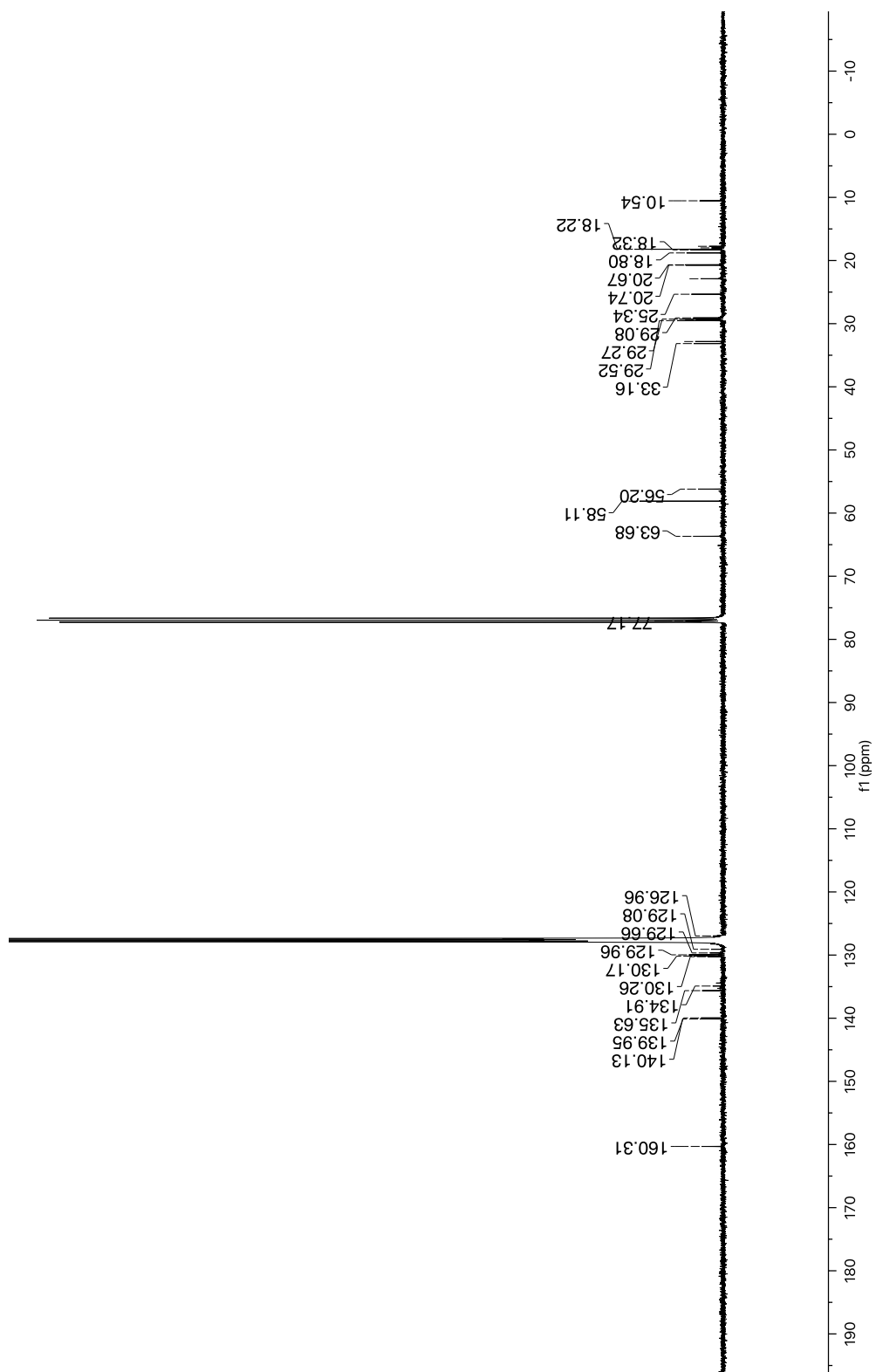
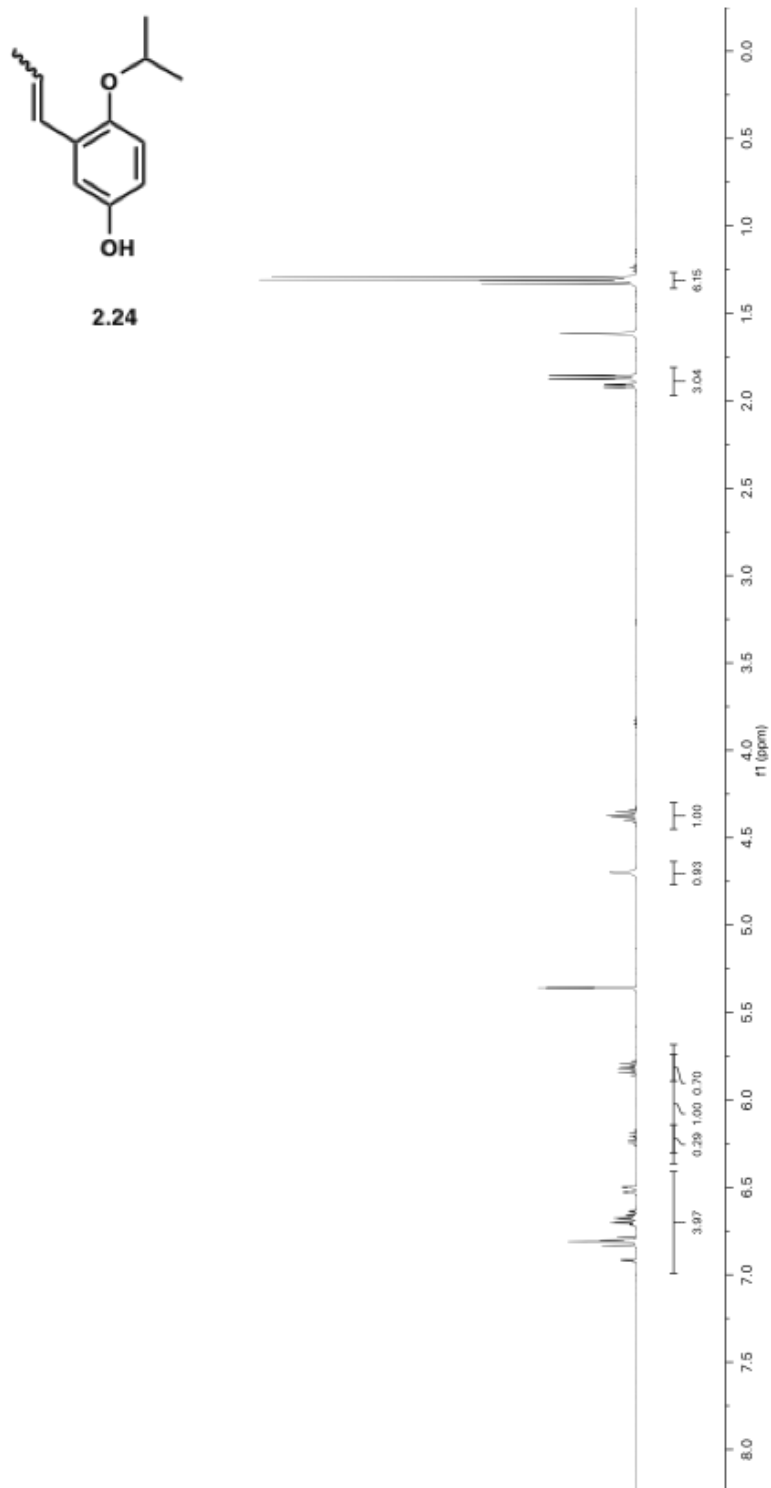


Figure A.3 | ¹³C NMR spectrum for 2.19



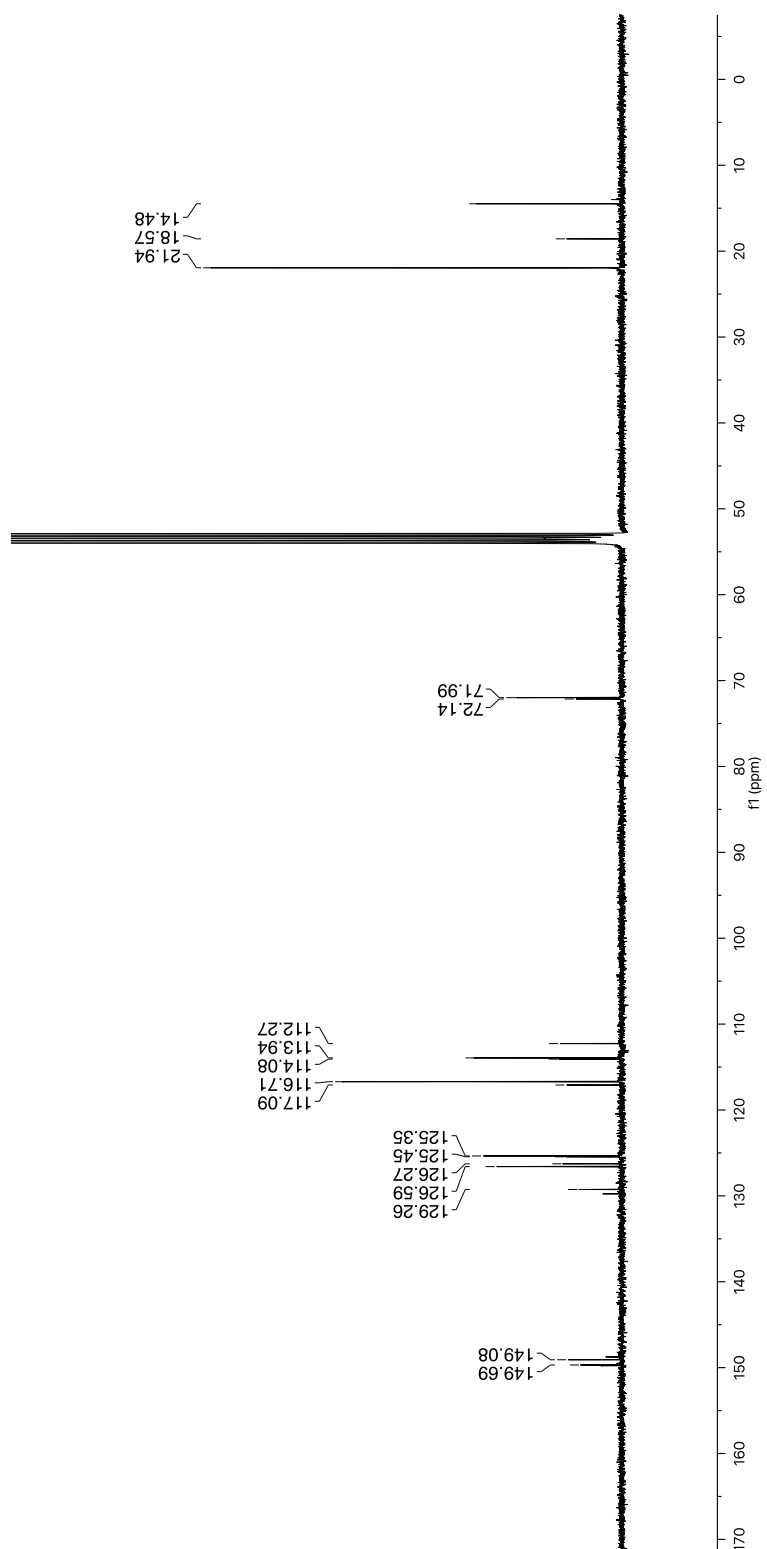


Figure A.5 | ^{13}C NMR Spectrum of 2.24

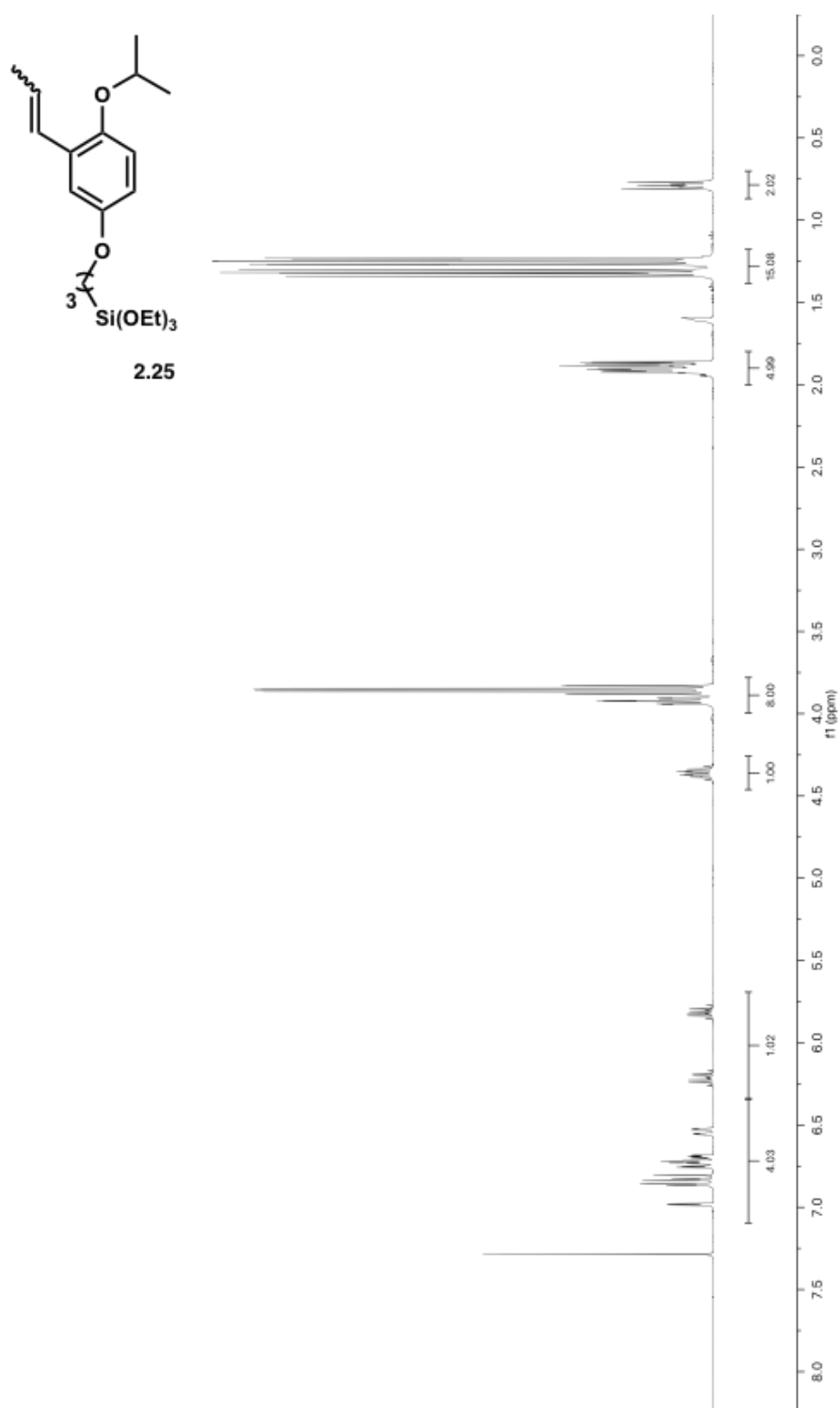


Figure A.6 | ^1H NMR Spectrum of 2.25

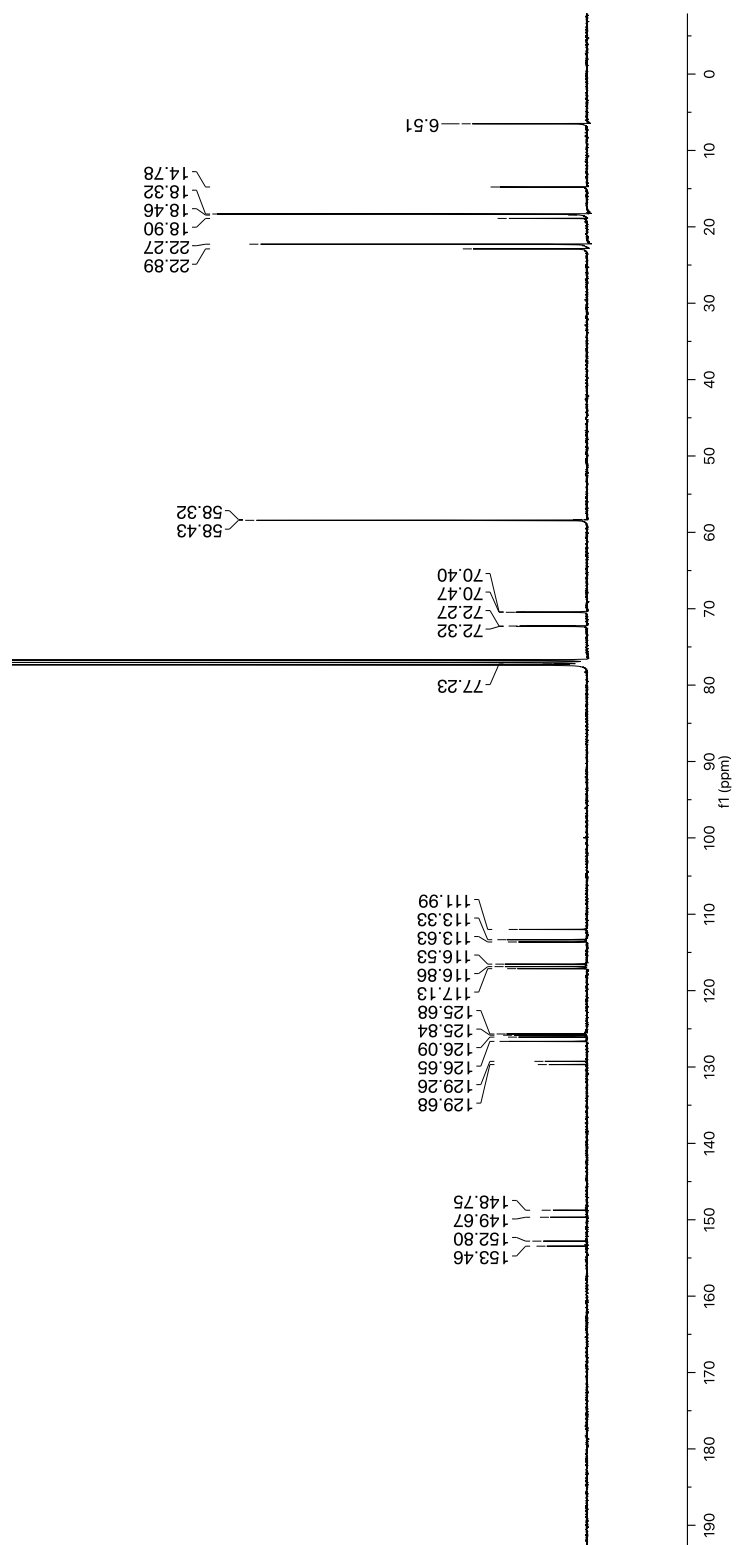
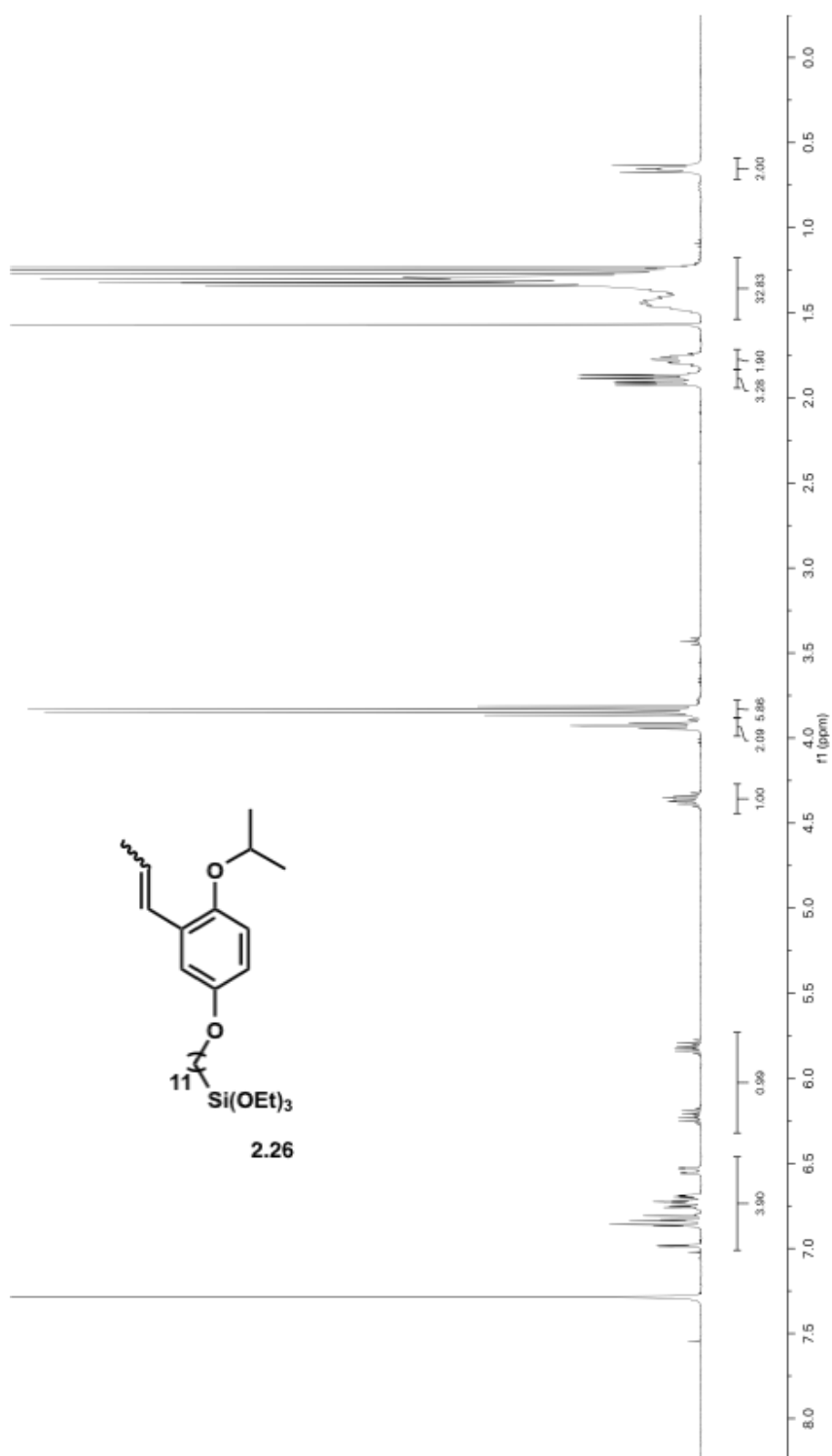


Figure A.7 | ^{13}C NMR Spectrum of 2.25

Figure A.8 | ^1H NMR Spectrum of **2.26**

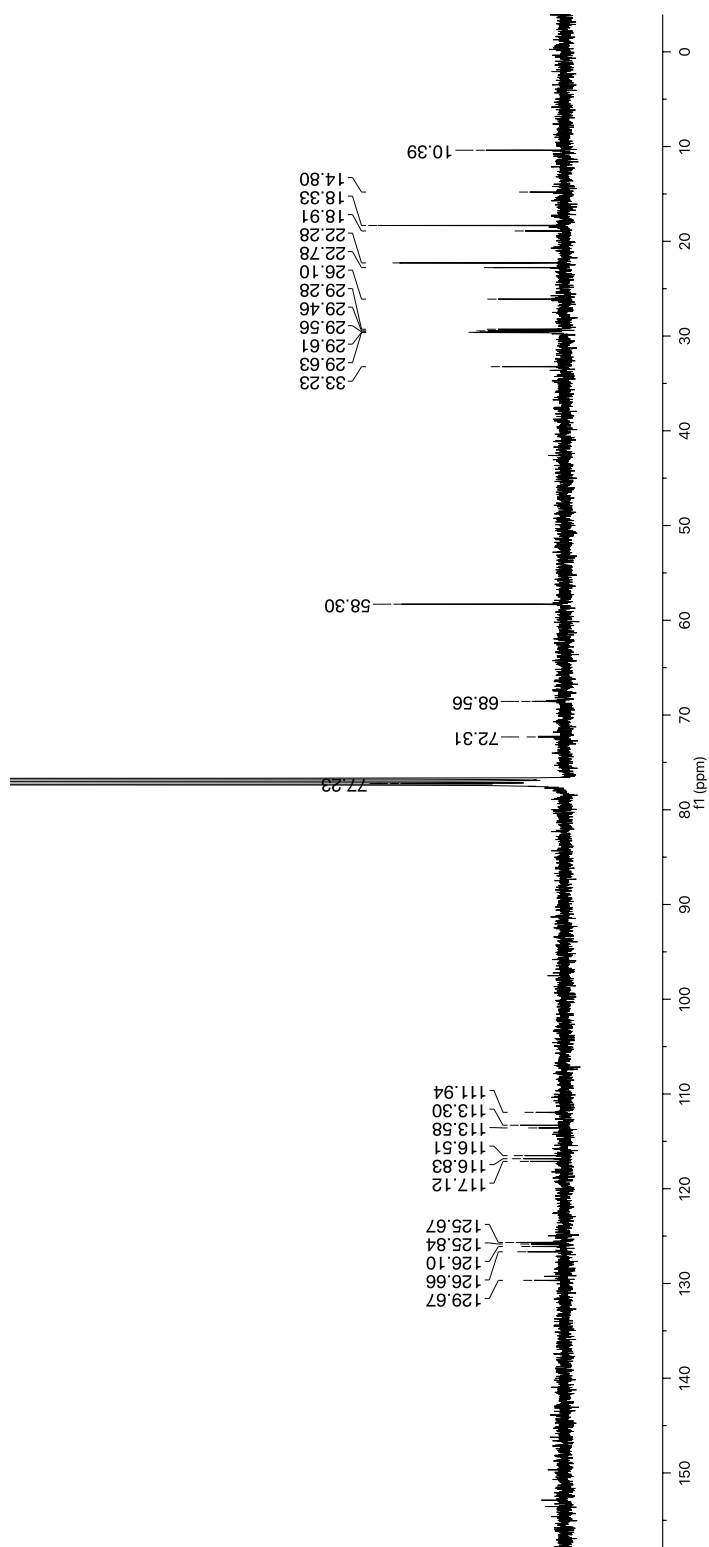


Figure A.9 | ^{13}C NMR Spectrum of 2.26

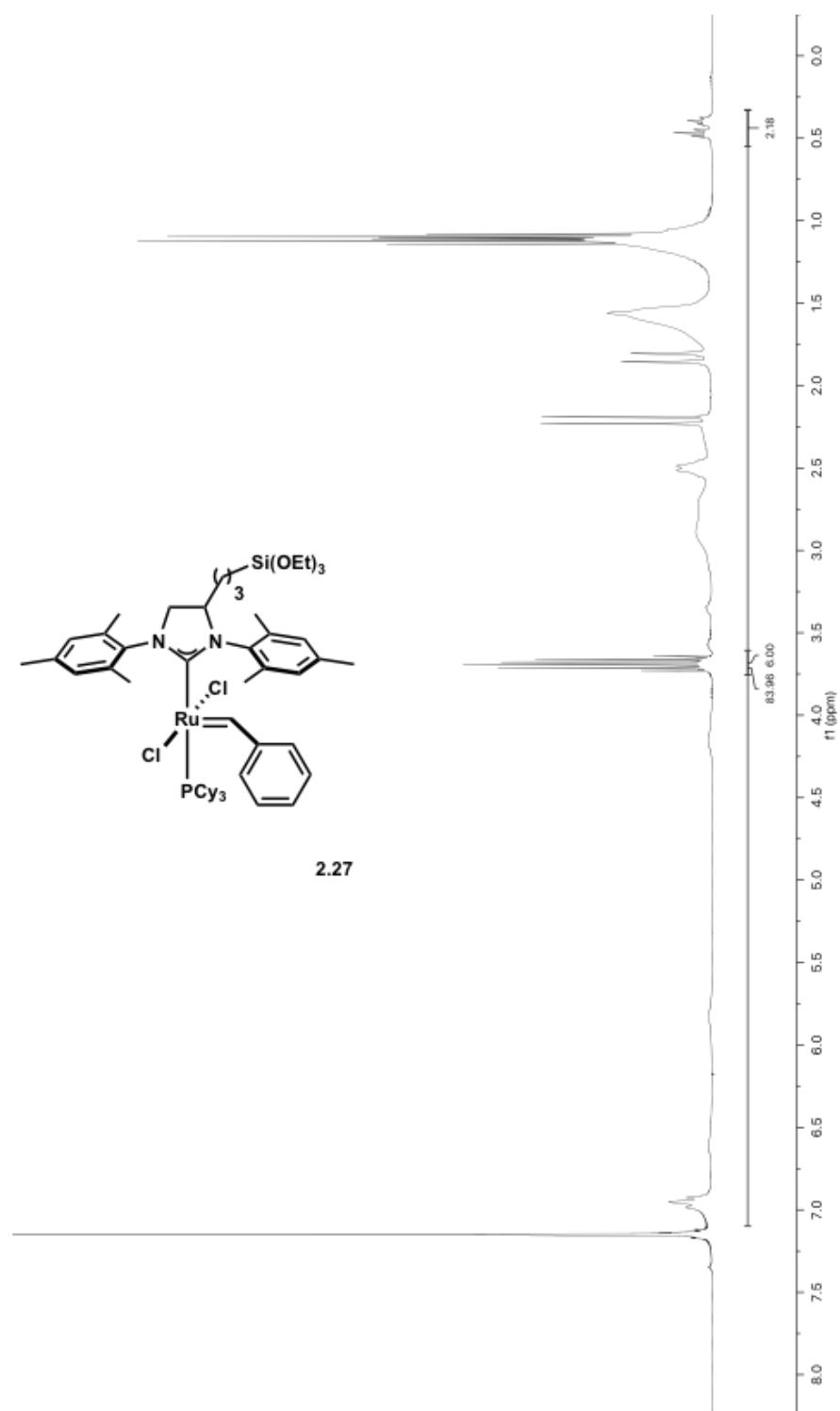


Figure A.10 | ^1H NMR Spectrum of **2.27**

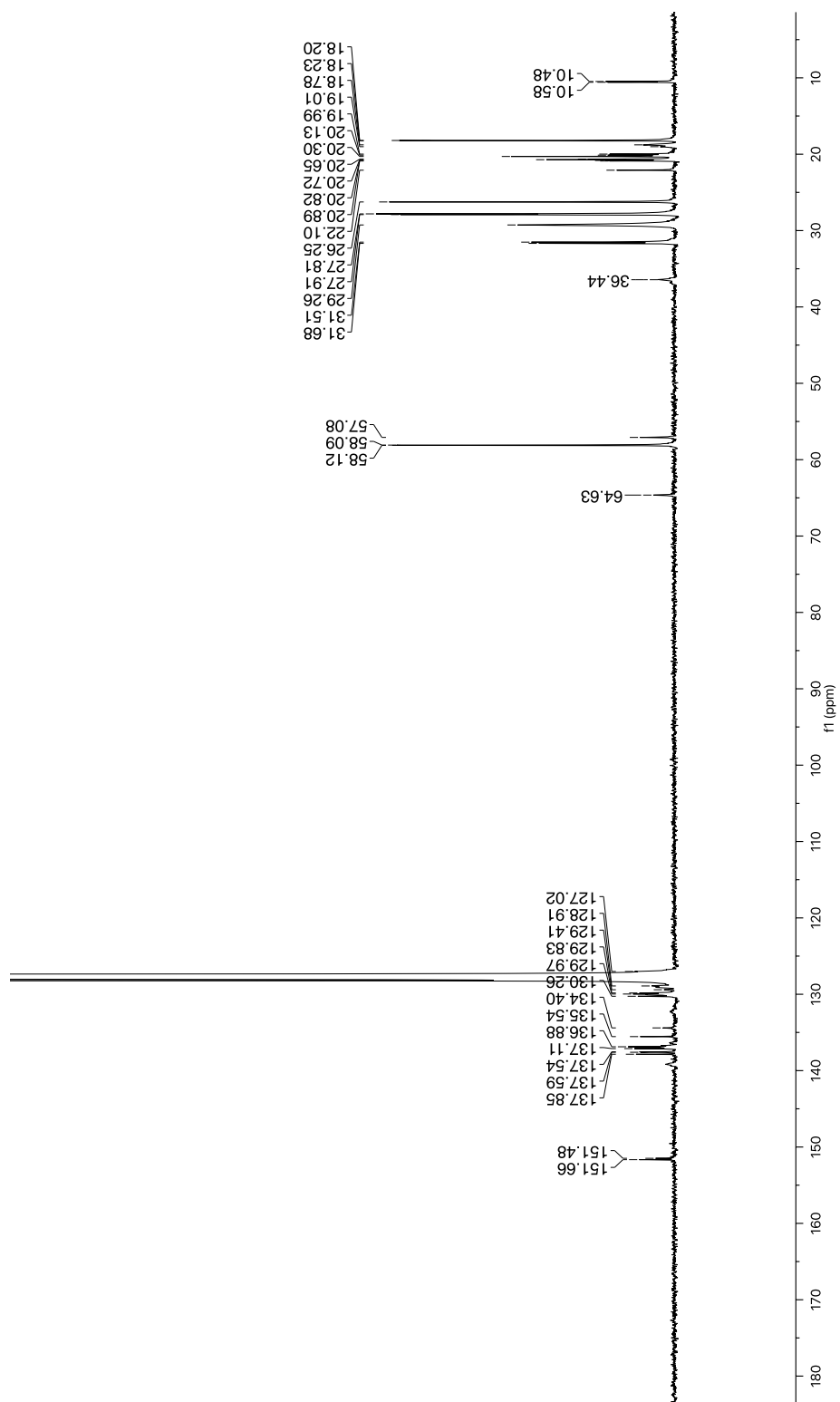


Figure A.11 | ^{13}C NMR Spectrum of 2.27

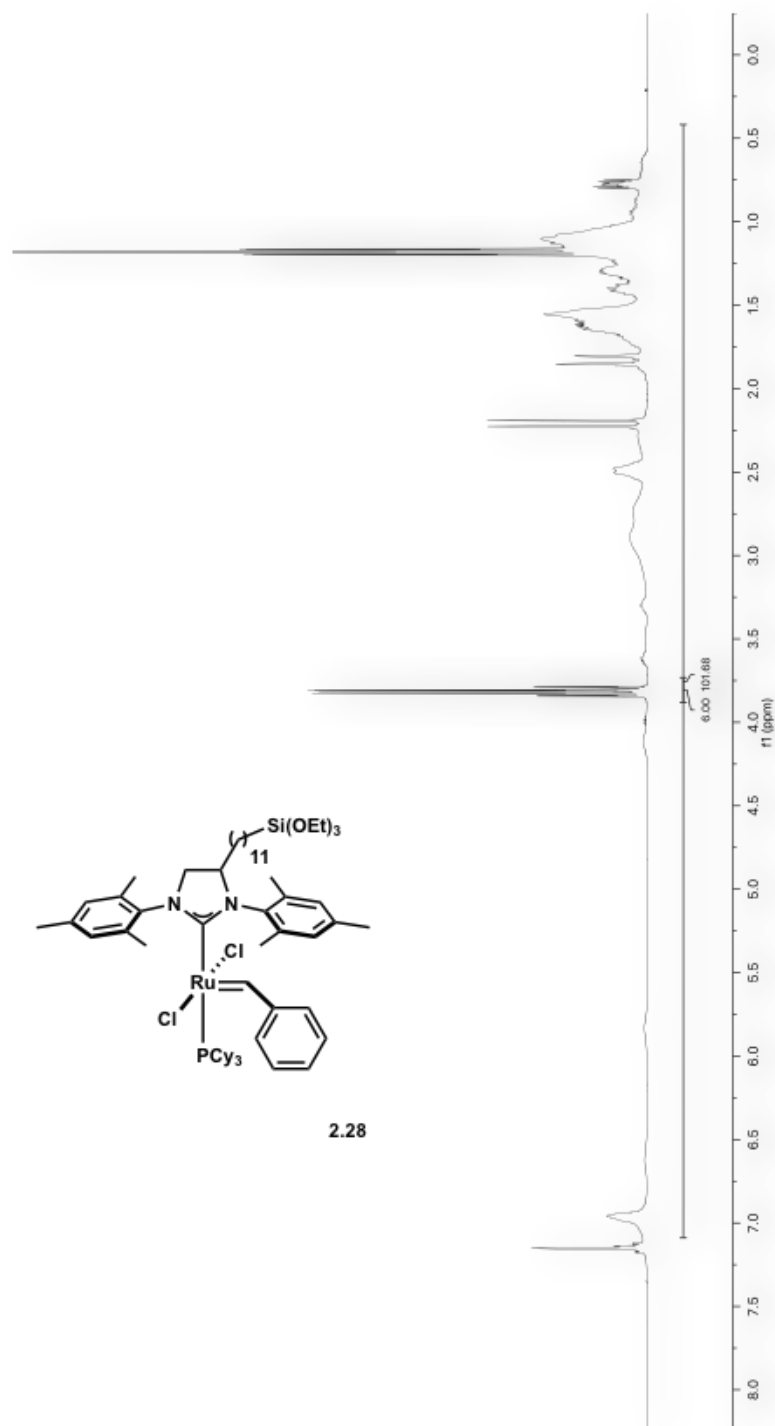


Figure A.12 | ^1H NMR Spectrum of **2.28**

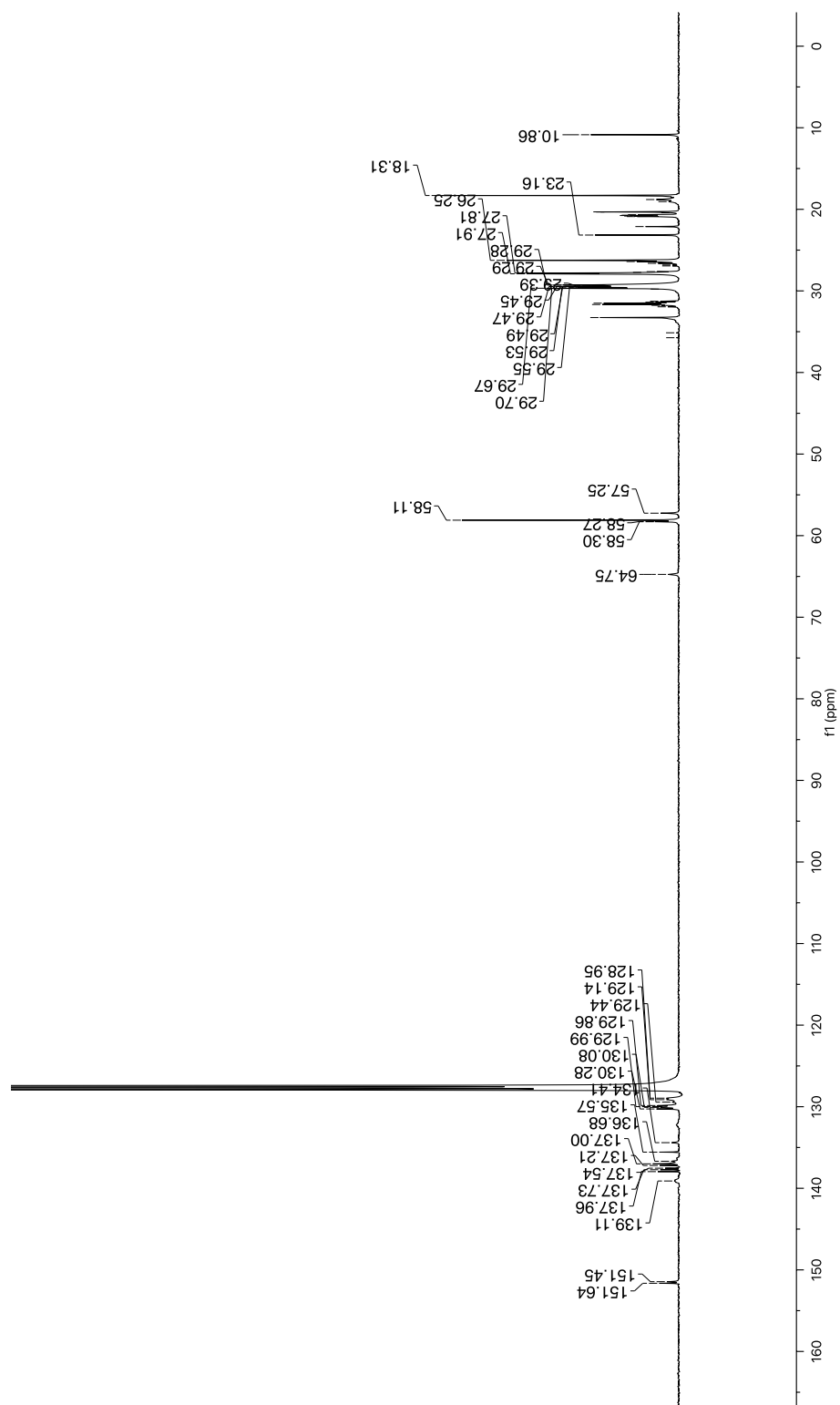


Figure A.13 | ^{13}C NMR Spectrum of 2.28

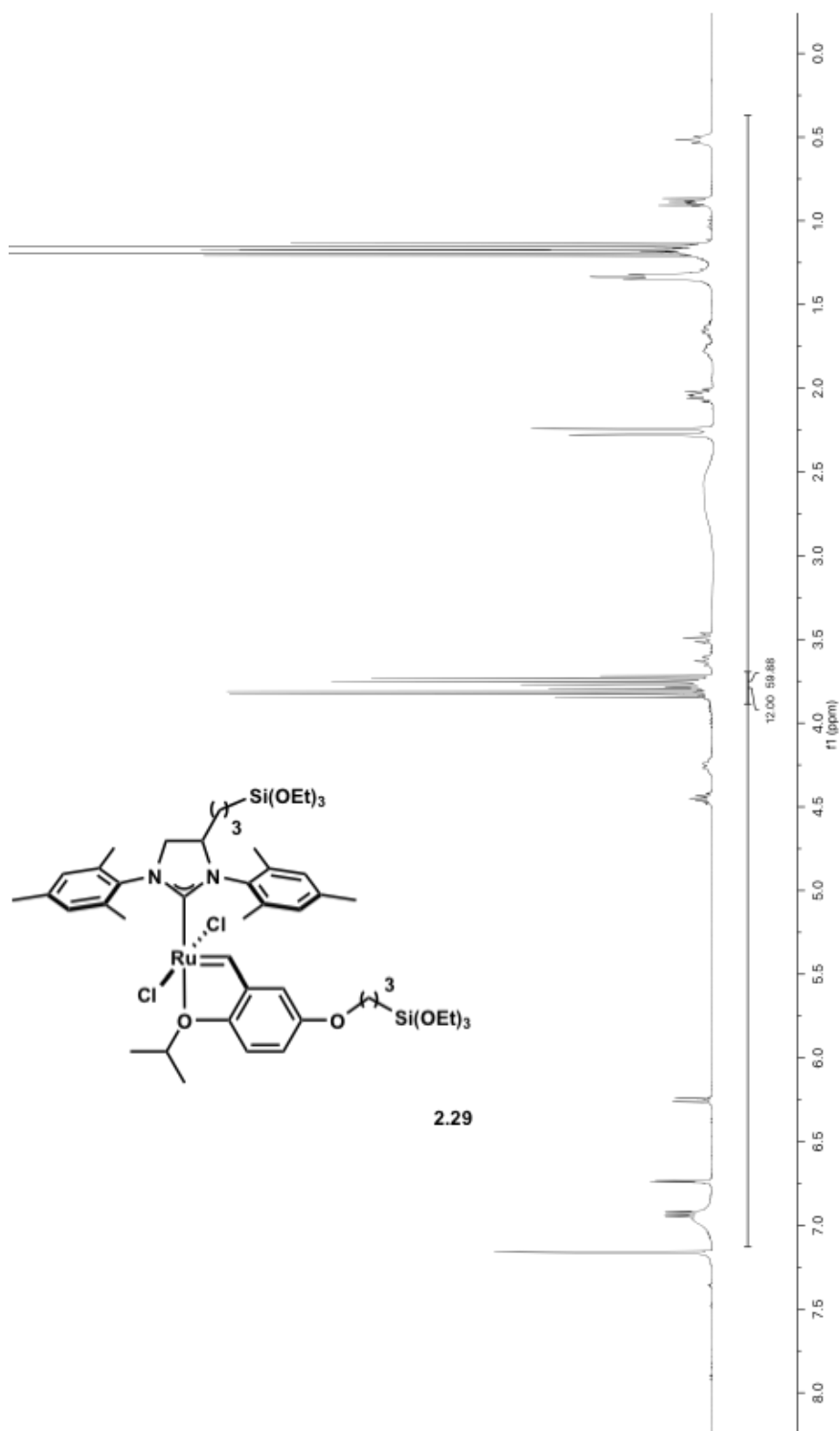


Figure A.14 | ^1H NMR Spectrum of **2.29**

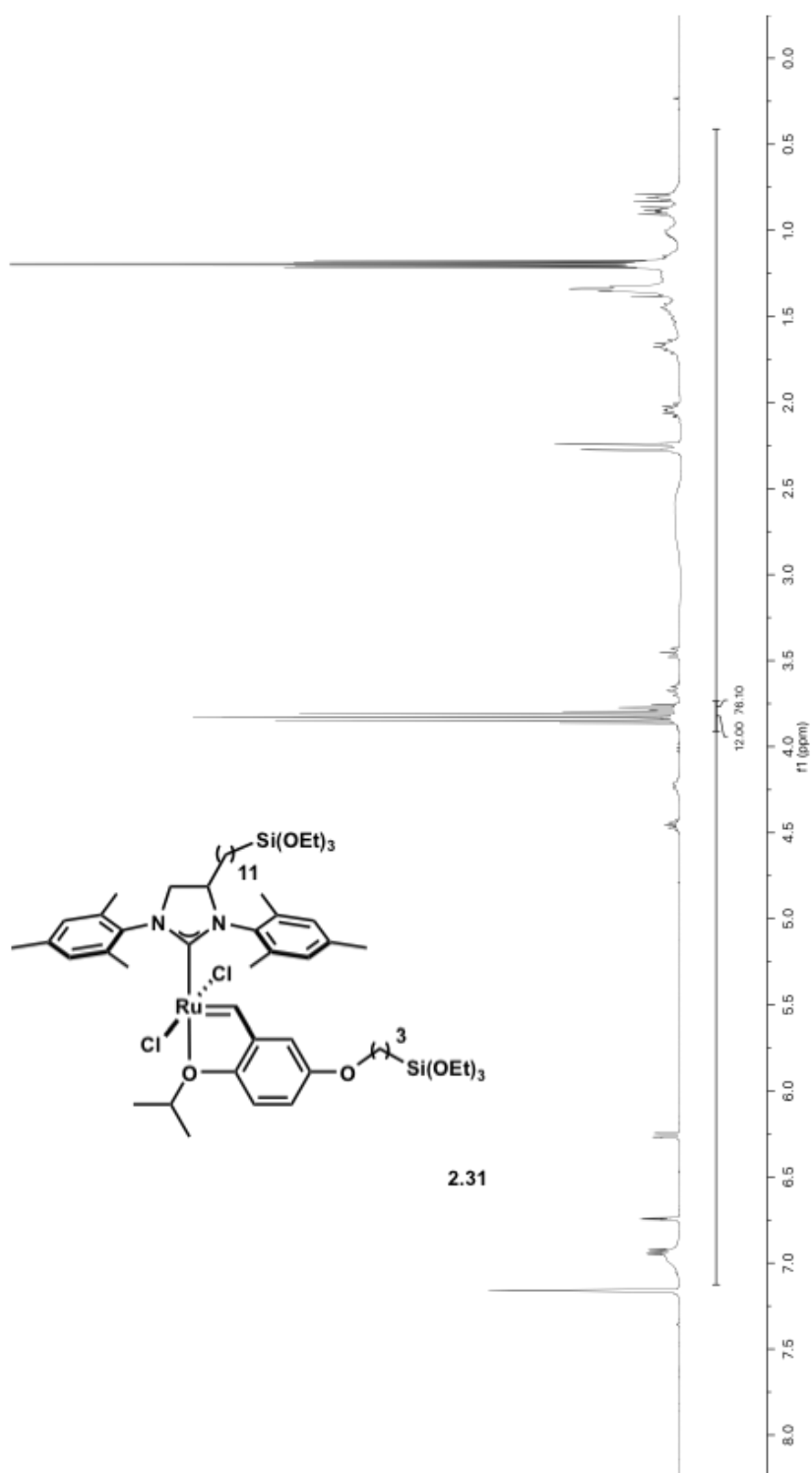
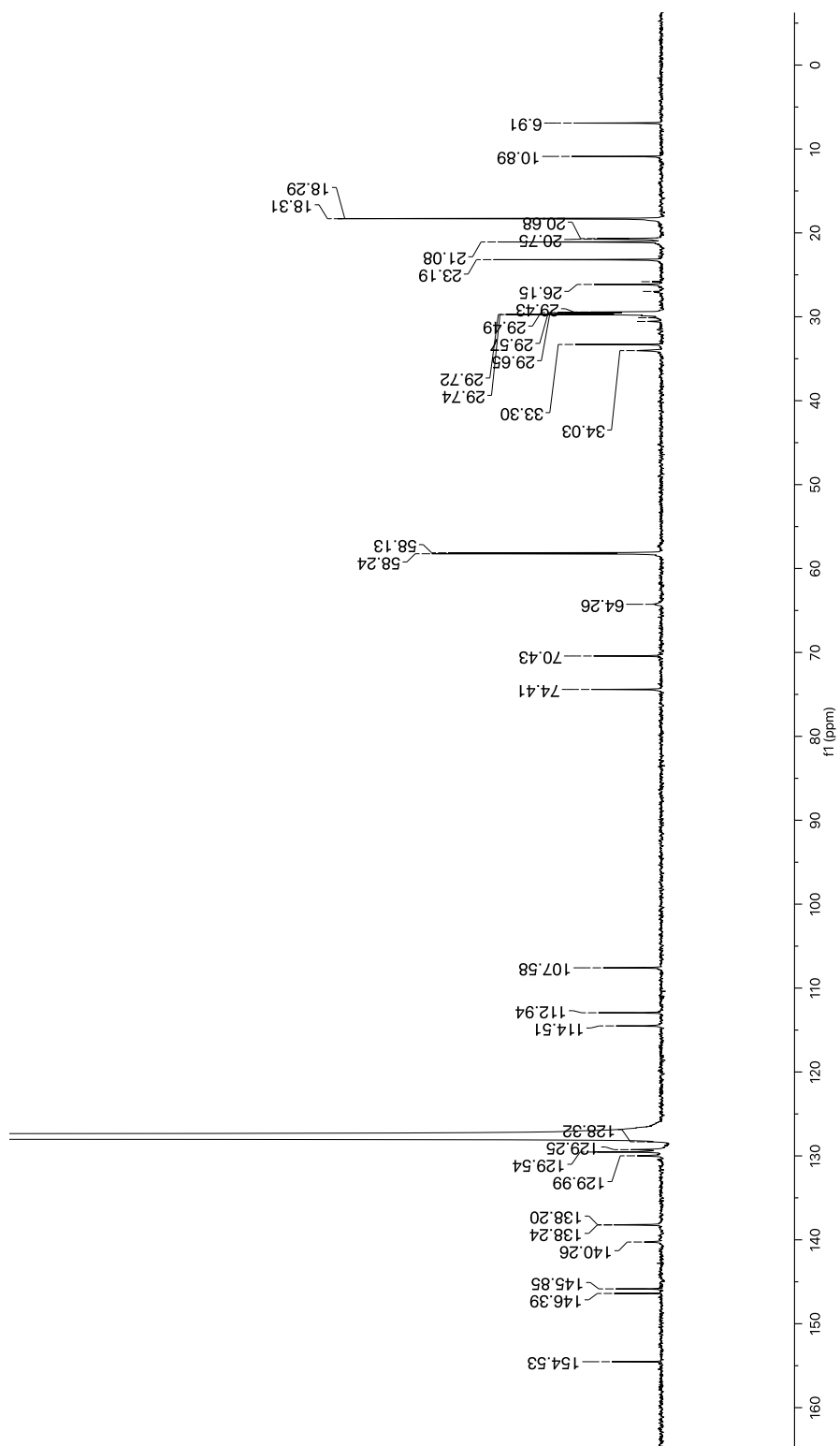


Figure A.15 | ^1H NMR Spectrum of **2.31**

Figure A.16 | ^{13}C NMR Spectrum of 2.31

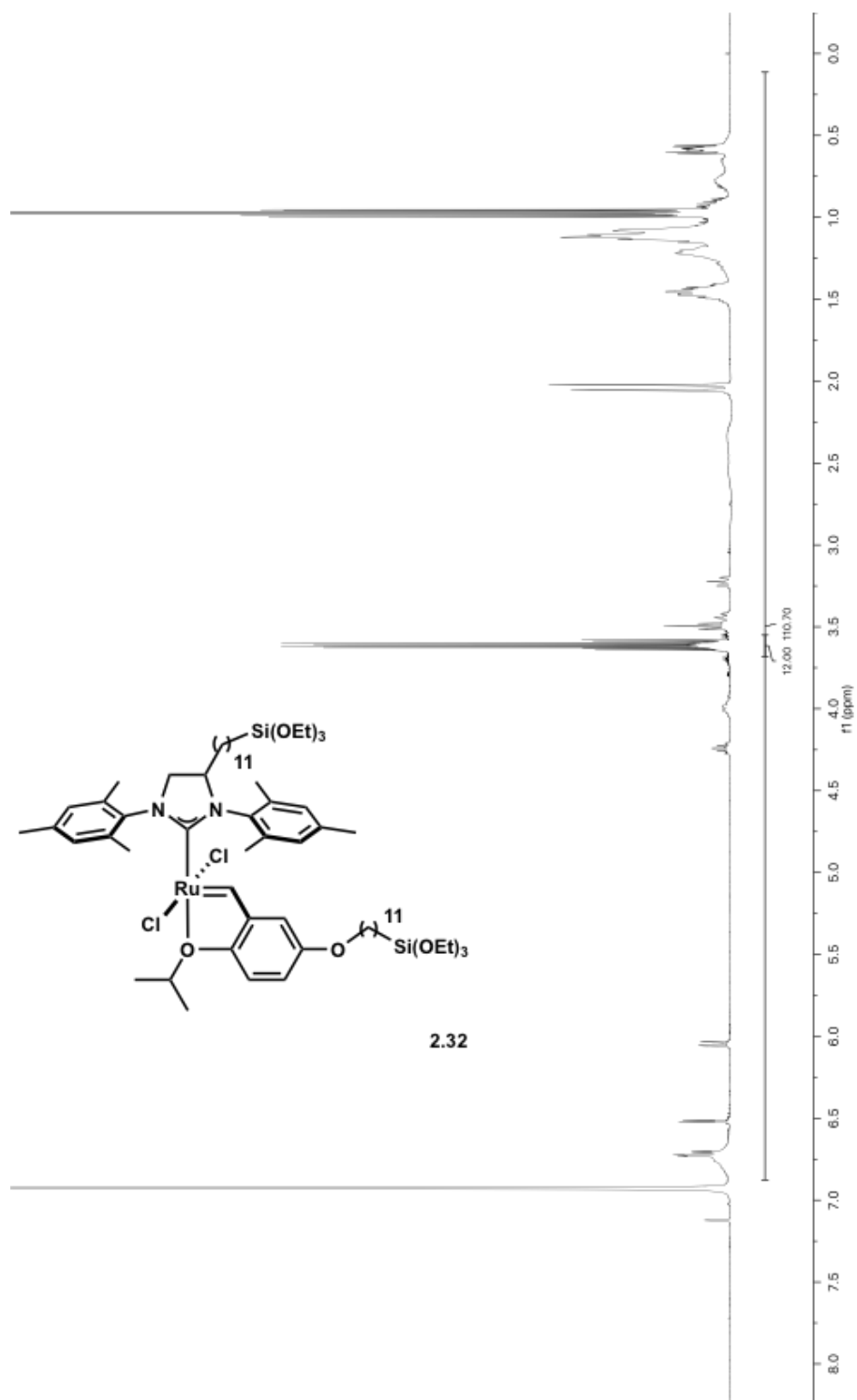


Figure A.17 | ^1H NMR Spectrum of **2.32**

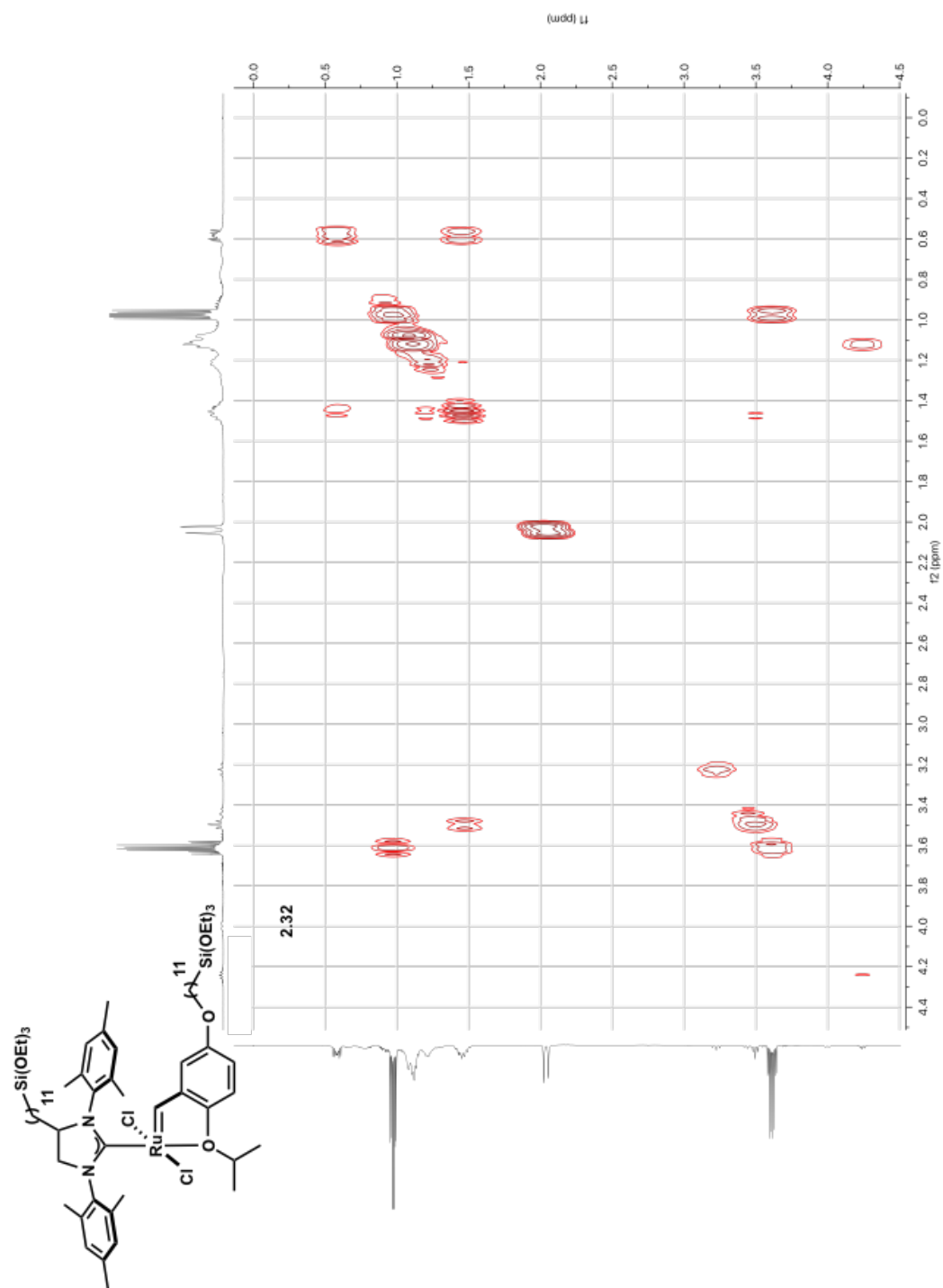


Figure A.18 | COSY NMR Spectrum of 2.32

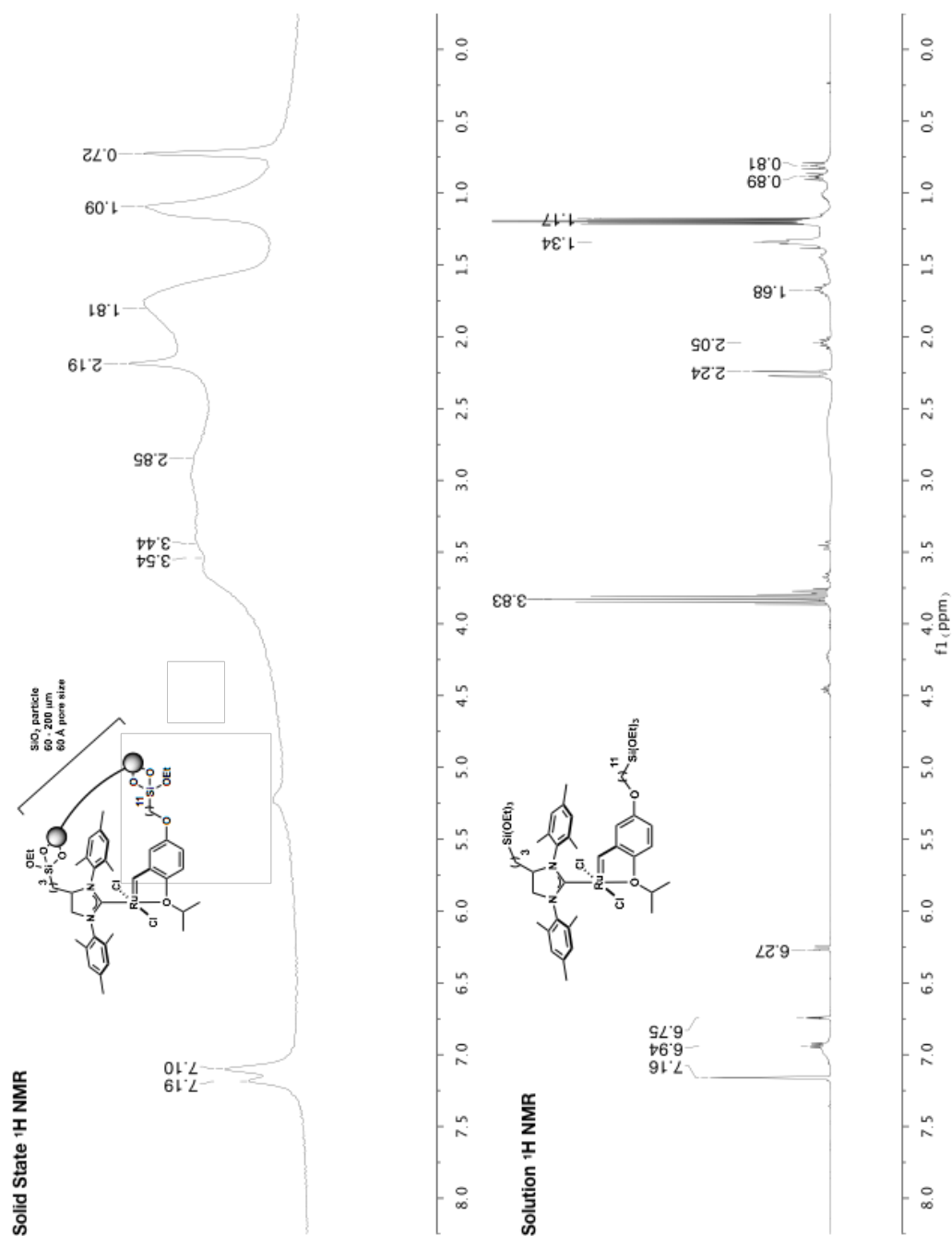


Figure A.19 | Comparison of solution ^1H NMR of homogeneous pre-catalyst and solid state ^1H NMR after attachment to silica support.

Appendix B

ICP-MS Characterization of REMP Catalysts

Appendix B Acknowledgments

Quan Gan

ICP-MS Measurements

Approximately 30 mg of supported molecular REMP catalysts **B.1** – **B.3** were precisely weighed in plastic vials using a Sartorius BP110S balance, digested with 1 mL distilled 68% nitric acid at 20 °C overnight on a IKA KS 260 shaker with a shaking speed of 100 motion/minute. After digestion, samples were diluted with 50 mL deionized water purified by Milli-Q system to a final acid concentration of about 2%. Samples were analyzed using an Agilent 8800 Triple Quadrupole inductively coupled plasma mass spectrometer (ICP-MS). The intensities of ruthenium isotopes 99, 100, 101, 102 and 104 were measured, and the intensity of pure 2% nitric acid was subtracted to give the net intensities. The net intensities were compared with that of ruthenium standard solutions obtained by diluting a ruthenium standard (99.60 ppm ruthenium in 2% HCl, purchased from VeriSpec) with 2% nitric acid. The numbers provided indicate the average concentration of the five isotopes measured (Table B.1).

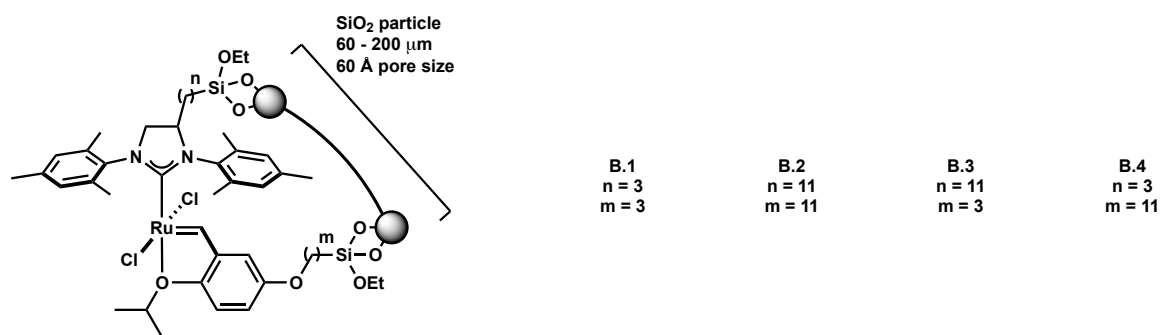


Figure B.1 | Supported molecular REMP catalysts used in this dissertation.

Table B.1 | Ruthenium content for catalysts B.1 – B.3

Entry	Target Ru ($\mu\text{mol/g SiO}_2$)	Actual Ru ($\mu\text{mol/g SiO}_2$)
B.1	20	3.22 \pm 0.11
B.2	20	3.79 \pm 0.24
B.3	20	2.74 \pm 0.11
B.4	20	-

These are the correct values for the actual Ru content in catalysts B.1 – B.3 used for all experiments described in this dissertation. This data was acquired three days before the submission deadline and there was insufficient time to correct the preceding chapters. The actual catalyst loading for all REMP catalysts was actually more than 5x lower than is reported throughout this dissertation; e.g.: "0.01 mol% **B.3** loading" should read "0.00137 mol % **B.3** loading" throughout this dissertation. Future discussions of this research will use the corrected values shown above (Table B.1). Insufficient supply of **B.4** at the time of these measurements precluded quantification of actual Ru content.